Politecnico di Milano

Facoltà di Ingegneria dei Processi Industriali

sede di milano leonardo

Corso di Laurea Specialistica
in Ingegneria Nucleare

Preliminary Analysis of the MSRE Dynamic Behaviour

Relatore

Prof. Antonio Cammi

Correlatore

Dr. Carlo Fiorina

Tesi di laurea di:

Benedetto Spinelli

matr. 720899

Anno Accademico 2009-2010

Contents

List of Tables

List of Figures

Estratto in lingua italiana

Il MSR (Molten Salt Reactor) è uno dei concetti innovativi di reattori nucleari scelti dal Generation IV International Forum (GIF). Questi sistemi innovativi sono sviluppati al fine di ottenere una tecnologia sostenibile e sicura che produca energia a costi non elevati. Tra le peculiarità di questo reattore vi è il fatto che il combustibile è disciolto nel sale, generando potenza direttamente nel termovettore. Essendo il combustibile circolante, parte dei precursori, responsabili dell'emissione di neutroni ritardati, decadono durante il ricircolo e quindi all'esterno del nocciolo, causando una perdita netta di reattività. Il comportamento dinamico del reattore è fortemente influenzato da queste caratteristiche e richiede la messa a punto di appositi strumenti. Questo lavoro di tesi ha dunque come obiettivo quello di elaborare un modello numerico in grado di riprodurre la dinamica di un reattore a sali fusi, per quel che riguarda sia il nocciolo che il sistema di raffreddamento. Come riferimento è stato scelto il MSRE (Molten Salt Reactor Experiment), un reattore sperimentale progettato e costruito negli anni '60 agli Oak Ridge National Laboratories, negli Stati Uniti. E' stato scelto poichè sono disponibili non solo i dati di progetto di tutto l'impianto ma anche molti dati sperimentali [1].

Il MSRE è un reattore di bassa potenza (8 MW), che non prevede la conversione di potenza da termica ad elettrica. Si tratta di un reattore termico moderato a grafite, il cui combustibile è disciolto in un sale che circola attraverso la struttura di grafite. Uno schema semplificato dell'impianto è riportato in figura 1. La generazione di potenza avviene per la maggior parte nel sale e per il resto nella grafite. La potenza generata viene trasferita tramite uno scambiatore di calore dal sale contenente il combustibile, circolante nel primario, ad un sale contenuto nel circuito secondario. Quest'ultimo viene poi raffredato tramite un aerotermo, che dissipa la potenza termica nell'ambiente.

Nel primo capitolo è stato fatta un'introduzione generale sulla tecnologia dei sali fusi, dando anche una descrizione dei criteri che hanno portato a far sì che essa fosse inserita tra i sistemi innovativi scelti dal GIF. Le principali peculiarità di questa tecnologia e le caratteristiche che la qualificano per sviluppi futuri sono state illustrate. Infine sono stati discussi i principali vantaggi e svantaggi della tecnologia a sali fusi

[1] Questo reattore è anche stato utlizzato nell'ambito dell'odierno progetto di ricerca europeo sui sali fusi (MOST, Molten Salt Reactor Technologies) per la definizione di un benchmark comune per tutti gli enti che vi partecipano

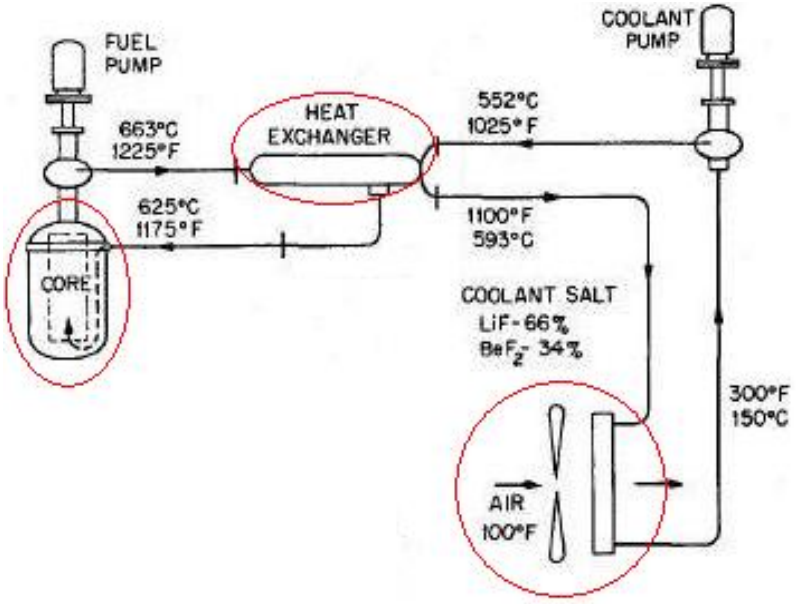

Figura 1: Layout semplificato del MSRE

in base alle valutazioni fatte sia nei report riguardanti il MSRE che nella letteratura riguardante il *Molten Salt concept*. Ad esempio, il fatto che il combustibile sia disciolto all'interno di un fluido circolante permette non solo di aggiungere nuovo combustibile senza dover fermare l'impianto, ma anche di rimuovere i prodotti di fissione in modo continuo. Tutto ciò contribuisce ad evitare di dover avere un ampio margine di reattività ad inizio vita, cosa che invece risulta necessaria in un rattore dove il combustibile è solido e chiuso all'interno di barrette. Inoltre, è possibile scegliere il ciclo di combustibile da utilizzare. Per esempio, il MSRE è stato esercito con due tipi di combustibile: uno a base di ^{235}U, ed un'altro in cui erano presenti sia una parte di ^{235}U, sia una di ^{233}U e sia una di ^{232}Th, sottoposto a breeding.

L'obiettivo del secondo capitolo è quello di ottenere una caratterizzazione del reattore in stato stazionario a tutti i livelli di potenza. Partendo dalla lettura dei vari report sono stati descritti tutti i componenti del sistema riportandone i dati di progetto. Inoltre, sono state discusse e documentate le caratterstiche dei vari tipi di combustibile utilizzati, del circuito primario e del circuito secondario. In seguito, sono stati ricavati i bilanci stazionari a potenza nominale per potere ricavare tutte le temperature del circuito e verificarne la correttezza e la coerenza. Nel fare questo, è stata riscontrata nei dati di design un'ampia sovrastima di alcune proprietà fisiche (in particolare la conducibilità termica). Questo problema fu affrontato anche dai progettisti del reattore, che dovettero, non appena i dati sperimentali riguardanti le proprietà fisiche dei

sali furono disponibili, abbassare da 10 a 8 MW la potenza termica nominale perchè fossero rispettati i limiti di design sulle temperature. Anche il dato di design riguardante il coefficiente di scambio termico nello scambiatore di calore tra sale primario e secondario risultava sovrastimato. In questo capitolo, basandosi su un diverso metodo (ϵ-NTU, effectiveness- Net Tranfer Units) sono stati ricalcolati i coefficienti di scambio termico totali sia dello scambiatore primario che del radiatore (il valore del coefficiente di scambio dul radiatore risulta invece confrontabile con quello di progetto). Infine, è stata data una descrizione della strategia di controllo del reattore: i coefficienti di retroazione sono negativi sia per quanto riguarda la temperatura della grafite che quella del sale, e quindi contribuiscono alla stabilità del sistema dato che nel momento in cui le temperature si alzano una retroazione negativa sulla reattività tende a riportare il rattore in una condizione di stazionarietà. L'alta capacità di autoregolarsi di questo reattore permise di esercirlo tramite un controllo del tipo reattore segue. Infatti il reattore era normalmente gestito tramite la regolazione del flusso d'aria e della superficie di scambio al radiatore[2]. Se si aumenta il flusso d'aria, la temperatura del sale secondario si abbassa così come quella del sale primario: ne consegue una retroazione positiva sulla reattività e quindi un aumento di potenza. Il processo è lo stesso ma in senso opposto nel caso si desideri dimnuire la potenza. In base alla strategia di controllo si sono potuti calcolare i valori della portata d'aria e del coefficiente di scambio termico totale al radiatore necessari a mantenere il reattore stazionario ai vari livelli di potenza.

Il terzo capitolo è stato dedicato allo sviluppo di modelli numerici per studiare la dinamica dell'impianto. La neutronica è stata modellizzata adottando una cinetica puntiforme. Per quanto riguarda la termoidraulica, partendo dalla legge di conservazione dell'energia, sono stati seguiti diversi approcci, aumentando il grado di complessità del modello. Inizialmente si è adottato un modello zero-dimensionale basato sulle temperature medie dei sali (primario e secondario) calcolate come media aritmetica tra temperature in ingresso ed in uscita in un determinato componente (core, scambiatore e radiatore). Tuttavia questo modello presenta alcuni difetti, come ad esempio il fatto che cambiando la temperatura d'ingresso a gradino la temperature in uscita cambia in senso opposto a ciò che succede fisicamente. Un difetto del genere risulta molto penalizzante in un modello che si propone di riprodurre l'andamento di potenze e temperature, perchè si hanno delle oscillazioni non fisiche. Perciò si è introdotta una discretizzazione in senso assiale dell'equazione di conservazione dell'energia mono-dimensionale nella regione del nocciolo. Con questo accorgimento si è potuto riprodurre anche il trasporto convettivo del sale. La discretizzazione è stata fatta tramite il metodo upwind. Per accrescerne la generalità è stato anche implementato il Θ-metodo. Nel modello può essere fissato il numero di nodi in cui viene discretizzato assialmente il nocciolo. In questo approccio la potenza termica, calcolata come proporzionale alla densità neutronica, può essere distribuita assialmente, associando una certa potenza all'i-esimo nodo. Infine, volendo includere nel modello anche il trasporto

[2]Sotto il livello di potenza pari a 1 MW, il reattore era controllato a potenza imposta

convettivo dei precursori, anche l'equazione differenziale che descrive la popolazione di precursori è stata discretizzata tramite il metodo upwind. Tutti i vari modelli sono stati implementati in MATLAB® e risolti tramite Simulink [25], uno strumento in grado di gestire e risolvere (anche graficamente) le equazioni differenziali ordinarie. Lo schema generale del modello implementato in Simulink è qui riportato.

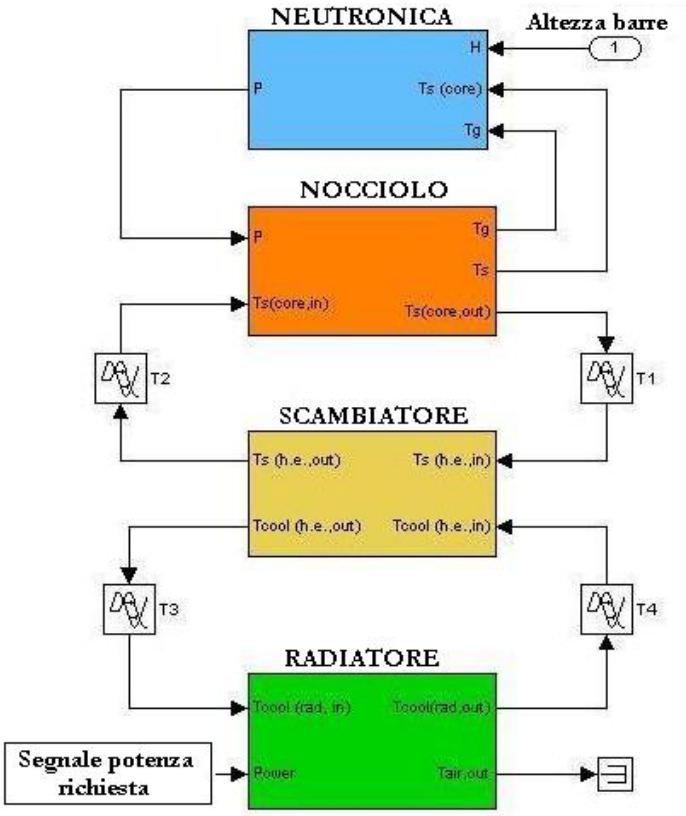

Figura 2: Schema generale del modello Simulink

Si può osservare che i due possibili ingressi sono l'altezza (o meglio la variazione di altezza) delle barre di controllo, data in ingresso al blocco NEUTRONICS, e un segnale di potenza, mandato al blocco RADIATOR. Quest'ultimo regola la portata d'aria e la superficie di scambio (tramite apertura/chiusura di un portale) necessarie ad ottenere la potenza desiderata. Come accennato precedentemente, la normale regolazione della potenza veniva svolta tramite uno schema del tipo *reattore segue*, ovvero aumentando o diminuendo il flusso d'aria al radiatore e quindi il calore asportato dal circuito secondario. Il modello sviluppato permette di svolgere un ampio spettro di simulazioni per studiare la dinamica dell'impianto sia in condizioni normali che in alcune condizioni incidentali.

Nell'ultimo capitolo sono stati presentati e discussi i risultati ottenuti. Innanzitutto è stato effettuato lo studio in frequenza del sistema per ottenere alcune indicazione sul comportamento dinamico dell'impianto a diverse potenze. Risposta in modulo e fase a diverse potenze sono stati confrontati con i dati disponibili nei report.

Per esempio, in figura 3 si può osservare l'andamento della risposta ad un inserzione

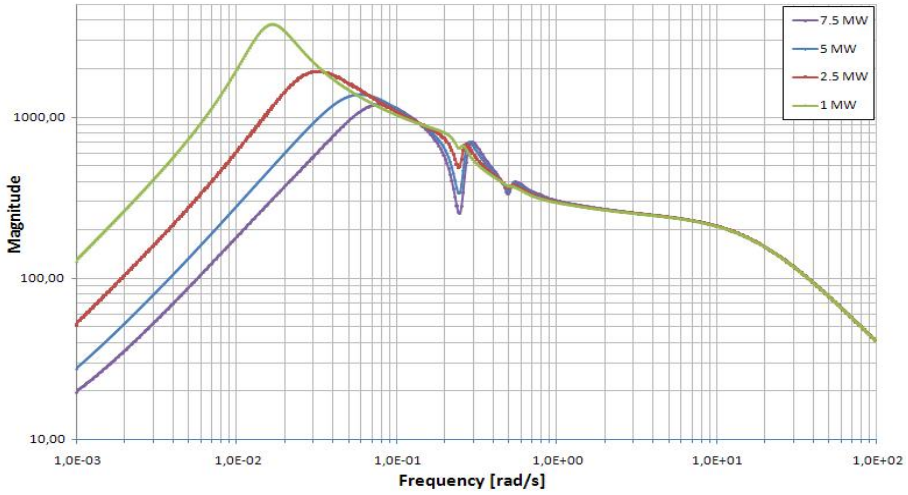

Figura 3: Risposta in frequenza (grafico del modulo) a diversi livelli di potenza del modello discretizzato assialmente

di reattività (graficata per vari livelli di potenza). Si nota che il picco si sposta in alto e a sinistra all'abbassarsi della potenza. Questo indica, come lecito attendersi, che la risposta sarà meno smorzata alle basse potenze. Si può inoltre osservare una risonanza ad un certo valore di pulsazione (0.25 rad/s), valore legato al tempo di ricircolo del sale nel cicuito primario (25 secondi).

Successivamente, sono stati calcolati i risultati per il reattore in condizioni stazionarie: è stato trovato il livello di reattività di compensazione (necessaria a mantenere il reattore critico), è stato presentato l'andamento delle temperature caratteristiche dell'impianto (sale primario, sale secondario, aria) in funzione della potenza ed è stato discusso il tempo di risposta complessivo del sistema, che dipende dalla potenza a cui sta lavorando.

Tra i risultati trovati, di particolare interesse è il fatto che, utilizzando un modello completamente zero-dimensionale per la popolazione dei precursori (e quindi non modellizzandone il trasporto convettivo dovuto al moto del sale), si ottiene un valore di reattività di compensazione diverso da quello che si ottiene considerando la distribuzione assiale dei precursori all'interno del nocciolo. Ad esempio, con il modello zero-dimensionale si calcola, in caso di reattore funzionante con ^{235}U, un valore di reattività di compensazione ρ_0=246 pcm, mentre utilizzando un modello che tenga conto della distribuzione di precursori si ottengono risultati diversi a seconda del numero di

nodi in cui viene discretizzata la regione del nocciolo (con 2 nodi si ottiene ρ_0=265 pcm, con 10 nodi ρ_0=272 pcm e con 200 nodi ρ_0=273 pcm). Questa differenza è dovuta al fatto che, passando dal modello 0D a quello 1D, e poi aumentando il numero di nodi, viene riprodotta più fedelmente la distribuzione di precursori all'interno del nocciolo. In questo caso, avere un accumulo dei precursori a causa del trasporto convettivo nella regione più alta del nocciolo si traduce in un maggior numero di precursori che escono dal nocciolo prima di decadere.

Si è poi passati ad analizzare i risultati dei transitori, dividendoli in transitori in condizioni normali e transitori in condizioni incidentali. Per quanto riguarda i transitori in condizioni normali sono stati simulati le inserzioni di reattività a diversi livelli di potenza e i cambiamenti del livello di potenza realizzati tramite un cambiamento delle condizioni al radiatore. Anche in questo caso i risultati sono stati confrontati con i dati presenti nei report. Per quanto riguarda i transitori incidentali sono stati simulati, sempre partendo da condizioni di lavoro nominali: inserzione veloce di tutte le barre di controllo, espulsione delle stesse, perdita della capacità di circolazione del sale primario (rottura della pompa), perdita istantanea della capacità di raffreddamento al radiatore, e rientro del sale primario sovra-raffreddato (overcooling). Dalle simulazioni

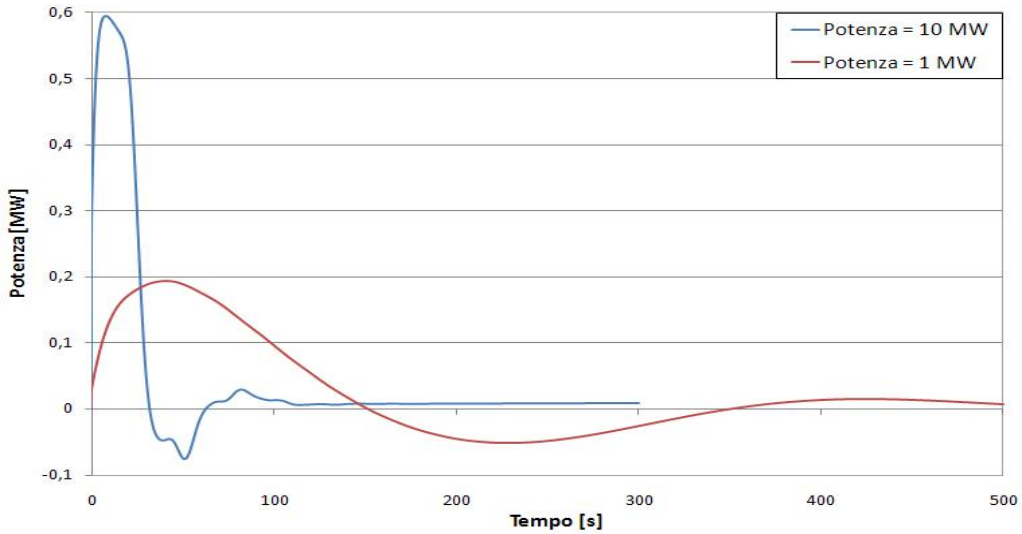

Figura 4: Andamento della potenza (reattore funzionante con ^{235}U) in risposta ad un gradino di reattività di 10 pcm

sono state ottenute diverse indicazioni riguardo al comportamento dinamico del reattore. Ad esempio, grazie al fatto che nel modello non solo il nocciolo ma tutto l'impianto è stato riprodotto, si osserva che il sistema è in grado di auto-regolarsi ad ogni livello di potenza (vedi figura 4) e che il controllo del tipo *reattore segue* è assolutamente conveniente, in quanto il movimento delle barre di controllo porta, a fine transitorio, a variazioni di potenza molto basse, per via degli alti coefficienti di retroazione. Inoltre,

a parità di inserzione di reattività la risposta del sistema cambia molto a seconda del combustibile utilizzato, dato che in caso di ^{233}U si è più vicini alla pronto-criticità del reattore.

Infine, dai risultati ottenuti si sono potute ricavare diverse considerazioni riguardo al modello elaborato, ad eventuali futuri sviluppi dello stesso o in generale ad indicazioni di ricerca in questo campo. Si è visto che il modello elaborato risulta essere completo (riproduce tutto l'impianto) ed è in grado di riprodurre transitori in condizioni normali e di dare indicazioni su quelli incidentali, Da sottolineare è il fatto che esso richiede basse capacità computazionali e quindi porta a termine le simulazioni velocemente. Si è trovato che la distribuzione di precursori ha una notevole influenza sulla risposta del reattore, e che è necessario tenerne conto se si vogliono riprodurre gli andamenti dei dati: deve essere quindi inclusa nel modello per ottenere transitori più significativi.

La più rilevante discrepanza tra il modello elaborato ed i dati di confronto trovati sui report riguarda la potenza di picco a seguire un'inserzione di reattività (in questo caso positiva). In effetti, si trova che il valore di picco restituito dal modello è sempre più alto, di circa una volta e mezzo, rispetto ai dati forniti dagli ORNL. Per spiegare questa discrepanza sono stati individuati alcuni motivi plausibili:

- il modello elaborato risulta mancante della distribuzione radiale della potenza e della portata;
- non è stata modellizzata la diffusione neutronica; tuttavia, anche non volendo complicare eccessivamente il modello, sono necessari ulteriori studi di neutronica, poichè la valutazione di un coefficiente di retroazione medio su tutto il nocciolo da moltiplicare per una temperatura mediata su tutto il nocciolo non tiene conto dell'importanza neutronica delle varie zone del nocciolo;

In sintesi, si può affermare che il lavoro svolto fornisce un contributo allo sviluppo di un tool di simulazione in grado di riprodurre la dinamica di un reattore a sali fusi. Il modello realizzato è infatti in grado di calcolare i valori della potenza e delle temperature di tutto l'impianto, di simulare l'andamento di questi parametri durante i transitori operativi e anche durante alcuni transitori incidentali. Da non trascurare è anche il fatto che questo modello richiede capacità computazionali minime (è in grado di simulare diversi tipi di transitori in brevi tempi di calcolo). Ciò permette, ad esmpio, di svolgere rapide analisi di sensitività al variare del parametro scelto.

Da questo lavoro si possono trarre indicazioni importanti per quanto riguarda l'eventuale sviluppo di un tool completo per studiare la dinamica dei reattori a sali fusi. Per prima cosa, all'aumentare del grado di complessità dei vari modelli sviluppati si sono individuati i fenomeni di maggiore importanza nella dinamica di tali reattori. Inoltre, confrontando i risultati ottenuti dalle simulazioni con quelli dati dai report, si sono ricavate alcune indicazioni riguardo quali ulteriori migliorie è necessario apportare per ottenere risposte dotate di un maggior grado di affidabilità.

Introduction

In the recent years there has been a growing interest in the Molten Salt Reactor (MSR) [1]. Actually, the MSR meets many of the future goals of nuclear technology, in particular for what concerns an improved sustainability and unique characteristics in term of actinide burning. Thanks to its favorable features, this reactor has been considered in the framework of the Generation IV International Forum [2]. The objective of this thesis is to realize a numerical model of a molten salt reactor. The developed model should allow a preliminary, general analysis of the dynamic behaviour of the plant, being capable of handling many of the peculiar dynamic features of a molten salt reactor. Indeed, the MSR is a fluid-fuel system, where the molten salt plays both the role of coolant and fuel, thus creating a complex and highly coupled physical environment. The fluid-fuel implies that power is generated directly in the heat-carrier and that part of precursors leaves the core before decaying so emitting delayed neutrons out of the core region, causing therefore a net loss of reactivity that has to be necessarily compensated in order to hold the chain reaction.

For what concerns the system, the MSRE (Molten Salt Reactor Experiment), an experimental reactor built and operated in the '60s, was chosen as reference since many experimental data are available. Moreover, other models are available for comparison because, when the MOST [3] group decided to attempt a benchmark exercise among some participants to assess the adequateness of the computational tools available for the physical evaluation of a fluid-fuel system, the experimental data reported for the MSRE were used as reference for the benchmark of these codes (developed for the neutronic analysis of molten salt reactors) [3].

In the first chapter, a description of essential features of the MS concept is reported, discussing the general advantages and disadvantages that issue from this technlogy, with particular regard to the MSR dynamic behaviour.

In the second chapter a description of the MSRE is given and the characteristics of each component are pointed out. Indeed, the model has to be comprehensive of the whole power plant: core, primary circuit loop, heat exchanger and secondary circuit loop, including the removal of thermal power. An overview of the adopted control strategy is given. Further on, a thermal characterization of the plant in steady-state

[3] The MOST (MOlten Salt reactor Technology) Project started within the 5th European Framework Program to assess the state of the art in the field of molten salts, in all its different aspects.

conditions is developed, inorder to be able to realize a model capable of working at any power level.

Building a coherent, performing model is the issue faced in the third chapter and is the main goal of the thesis work. Different numerical approaches to the problem are described and attention is focused in the modelling of the primary loop, which shows the major challenges. Starting with a zero-dimensional lumped model, the degree of complexity is increased where necessary. Each developed model is analysed in order to find whether and where the model fails in reproducing the plant dynamic behaviour. With the purpose of circumvent these defects, different modelling solutions are taken in consideration and implemented.

In the last chapter, the response of the various developed models are compared. The best available model is used to simulate some significative transients, both in operating and abnormal or accidental conditions. On the basis of the simulation results, the dynamic behaviour of MSRE is discussed. Where experimental data are available in ORNL reports, the obtained results are compared to them. Finally, analysing the model response, some indications regarding an eventual future development and extension of the present work are given.

Chapter 1

The molten salt concept

First of all in this chapter it is given a brief overview of Generation IV nuclear energy systems. Objectives of the program, goals of the selected systems and a summary of main characteristics of these systems are presented.

Subsequently, a preliminary description of the molten salt concept is given and the peculiar features of this technology are pointed out, starting from molten salt reactors realized in the past, focusing on the MSRE (Molten Salt Reactor Experiment, built in the '60s), up to more recent studies.

1.1 Generation IV nuclear energy systems

Taking into account the expected increase in energy demand worldwide and the growing awareness about sustainable development, nuclear energy will probably be needed to meet future global energy demand. Nuclear power plant technology has been classified according to the design generations: current operating reactors belong to the Second Generation. Third Generation reactors ($\sim$2000 and on) are now undergoing the licensing process and some are already under construction (such as EPR in France and Finland or AP1000 in China).

Fourth Generation reactors are new and advanced systems, which are being developed by the GIF (Generation IV International Forum) and should be operating from 2030 and beyond. Moreover, they are intended to meet the goals listed below [1].

1. Sustainability

    - Gen IV nuclear energy systems will provide sustainable energy generation that meets clean air objectives and provides long-term availability of systems and effective fuel utilization for worldwide energy production.
    - Gen IV nuclear energy systems will minimize and manage their nuclear waste and notably reduce the long-term waste storage, thereby improving protection for the public health and the environment.

2. Economics

    - Gen IV nuclear energy systems will have a clear life-cycle cost advantage over other energy sources.
    - Gen IV nuclear energy systems will have a level of financial risk comparable to other enegy projects.

3. Safety and Reliability

    - Gen IV nuclear energy systems operations will excel in safety and reliability.
    - Gen IV nuclear energy systems will have a very low likelihood and degree of reactor core damage.
    - Gen IV nuclear energy systems will eliminate the need for offsite emergency response.

4. Proliferation resistance and Physical Protection

    - Gen IV nuclear energy systems will increase the assurance that they will be very unattractive and the least desirable route for diversion or theft of weapons-usable materials, and provide increased physical protection against acts of terrorism.

The systems should also offer a true potential for new applications compatible with an expanded use of nuclear energy, in particular in the fields of hydrogen or synthetic hydrocarbon production, sea water desalination and process heat production. It has been recognized that the above-mentioned objectives, widely and officially shared by a large number of countries, should be at the basis of an internationally shared R&D program, which allows keeping open and consolidating the technical options, and avoiding any early premature down selection.

The Generation IV Technology Roadmap [2], prepared by GIF member countries, identified six promising reactor systems and fuel cycle concepts. The six selected systems employ a variety of reactor, energy conversion and fuel cycle technologies. Their designs feature thermal and fast neutron spectra, closed and open fuel cycles and a wide range of reactor sizes from very small to very large.

All Generation IV systems have features aiming at performance improvement, new applications of nuclear energy, and/or more sustainable approaches to the management of nuclear materials. High temperature systems offer the possibility of efficient process heat applications and eventually hydrogen production. Enhanced sustainability is achieved primarily through adoption of a closed fuel cycle with reprocessing and recycling of plutonium, uranium and minor actinides using fast reactors; this approach provides significant reduction in waste generation and uranium resource requirements [2].

The following table (Tab. 1.1) summarizes the main characteristics of the six Generation IV systems.

System	Neutron spectrum	Coolant	Temp. [°C]	Fuel cycle	Size [MWe]
VHTR (Very High Temp. Reactor)	thermal	helium	900-1000	open	250-300
SFR (Sodium-cooled Fast Reactor)	fast	sodium	550	closed	30-150, 300-1500, 1000-2000
SCWR (SuperCritical Water Reactor)	thermal/ fast	water	510-625	open/ closed	300-700, 1000-1500
GFR (Gas-cooled Fast Reactor)	fast	helium	850	closed	1200
LFR (Lead-cooled Fast Reactor)	fast	lead	480-800	closed	20-180, 300-1200, 600-1000
MSR (Molten Salt Reactor)	epithermal	fluoride salts	700-800	closed	1000

Table 1.1: Overview of Generation IV systems [2]

The following section will deal with the last of Gen IV reactor system, the Molten Salt Reactor. Its features will be considered and discussed, mostly in light of dynamical aspects.

1.2 The Molten Salt concept

Molten salt reactors are liquid-fueled reactors that can be used for production of electricity, actinide burning, production of hydrogen, and production of fissile fuels. Fissile, fertile, and fission isotopes are dissolved in a high-temperature molten fluoride salt [1] with a very high boiling point (1400 °C) that is both the reactor fuel and the coolant.

The near-atmospheric-pressure molten fuel salt flows through the reactor core that contains graphite moderator. In the core, fission occurs within the flowing fuel salt (that is heated to ∼700 °C) which then flows into a primary heat exchanger where the heat is transferred to a secondary molten salt coolant. The fuel salt then flows back to the reactor core.

The use of a liquid fuel, versus the solid fuels of the other Generation IV concepts, creates potentially unique capabilities that are not achievable with solid-fuel reactors, but it also implies a different set of technical challenges with respect to other Generation IV concepts. The three main properties that qualify MSR for the avdance utilization are [4]:

1. Inherent safety.
2. Excellent neutron economy.
3. *In situ* (continuous or in-batch) reprocessing possibility.

Generation IV MSRs are thought to convert thermal power into electrical power through a high-temperature Brayton cycle [2]. The Brayton cycle (with or without steam bottoming cycle) may use either nitrogen or helium as a working gas (see Figure 1.1).

However, the MSR is an old concept. Two experimental MSRs built at Oak Ridge National Laboratory (ORNL) established the basic technology for the MSR. The first reactor was the 2.5 MW_t Aircraft Reactor Experiment (ARE) that in 1954 demonstrated peak operating temperatures up to 860°C. This was part of an effort to build a nuclear-powered military aircraft with the jet engines receiving heat from the MSR via an intermediate heat transport loop. The specific objective of the ARE was to build and operate an high-temperature low-power circulating-fuel reactor of materials which would be suitable for a high-power reactor [5]. The ARE was followed in the 1960s by the Molten Salt Reactor Experiment, an 8 MW_t reactor, to demonstrate key features required for a Molten Salt Breeder Reactor (MSBR), thought for electricity production. A detailed description of MSRE is given in section 2.1.

Here below an overview of pros and cons of MSR concept is reported, in the light of ORNL experience and GIF decision to include this nuclear systems in the "nuclear systems of the future".

[1] Chloride salts are being studied for these applications, too.

[2] The Rankine cycle may also be employed, altough it would reduce the thermal efficiency

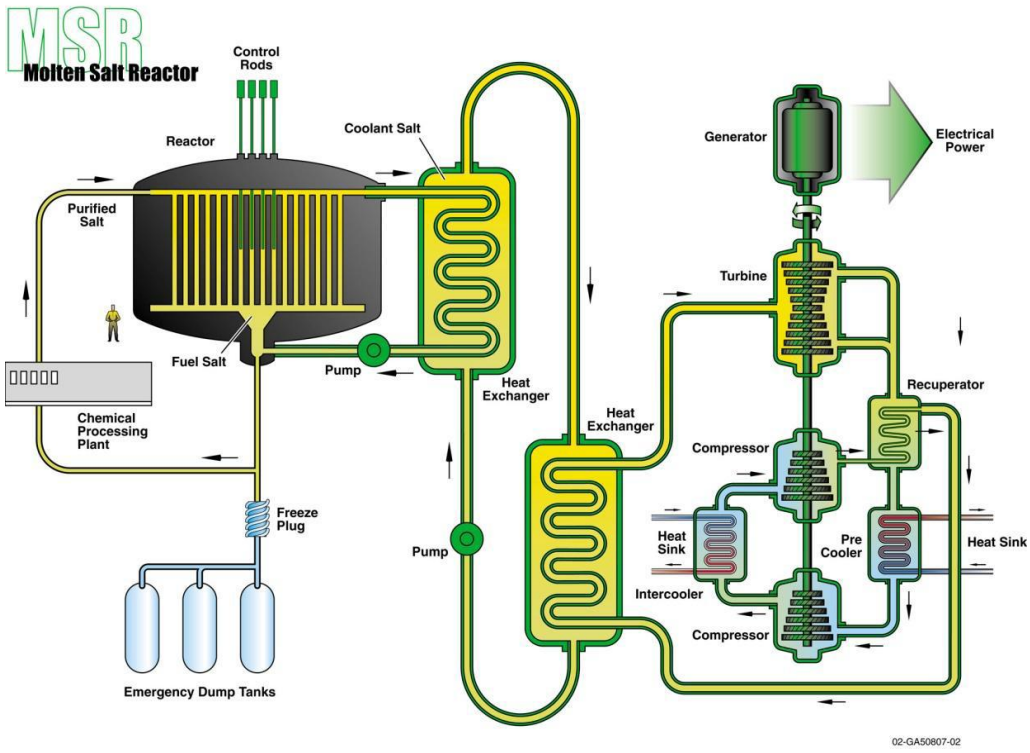

Figure 1.1: Generation IV MSR layout

1.2.1 Attractive features of the MSR concept

1. The fuel is fluid, thus eliminating the extra costs associated with the fabrication, handling, and reprocessing of solid fuel elements. Burnup in the fuel is not limited by radiation damage or reactivity loss, since the fuel can be reprocessed continuously in a side stream for removal of fission products, and new fissionable material can be added while the reactor is in operation [6].

2. Destruction of long-lived radionuclides without the need to fabricate solid fuels can be achieved. Moreover, a wider choice of fuel cycles (once through, waste burning, fissile fuel production through breeding) is possible without major changes in the reactor design [7].

3. Molten-salt reactors can operate at high temperatures to achieve good thermal efficiencies in the heat-power cycle [6].

4. The negative temperature coefficient of the reactor and the low excess of reactivity are such that the nuclear safety is not primarily dependent upon fast-acting control rods [6].

5. The fuel salt has a low cross section for the parasitic absorption of neutrons. Very good neutron economies can be achieved [6].

6. The fluoride salts used as the fluid fuel mixture have good thermal stability, since solubility of heavy metals increases with temperature [6]. They are also stable to radiation stability and do not undergo violent chemical reaction either with water or with air. They are compatible with the graphite moderator and can be contained in specially developed high-nickel alloys [6].

7. Very low fissile fuel inventory relative to other reactor concepts (fissile inventory may be as low as a tenth of a fast reactor per kW_e) that may create alternative safeguard strategies [7].

8. Use of relatively high circulation rates and temperature differences result in high mean power density, high specific power, and low fuel inventory [6].

9. Low capital costs are promoted by the following characteristics [8].

    - Fuel and blanket salts have vapor pressure below 1 atm up to 2600°F (1625°C), and they have good heat-transfer and fluid-flow properties. Thus, molten salts, are low-pressure, high-temperature heat sources, and units can be designed to supply steam to one or more turbine-generator sets. The salts do not undergo violent chemical reactions with air or with a variety of coolants. Volatile fission products can be purged continuously. Because of these characteristics *the containment can be semplified.*
    - The good solubility of uranium, thorium and plutonium in fluoride salts together with the thermal and radiation stability of the solution, made *not necessary to provide equipment for recombining decomposition products.*
    - The fuel solutions generally have a high negative temperature coefficients of reactivity. The Xenon-135 (and other mobile fission products) can be removed continuously. Fuel can be added while the reactor is at full power by means of relatively simple equipment, therefore only a small amount of excess reactivity must be controlled. These attributes should lead to *simplified nuclear control and safety systems.*
    - Full passive safety in very large reactors. (Under accident conditions, the fuel is drained to passively cooled, critically safe storage tanks.)

10. Low fuel costs are promoted by several characteristics [8].

    - The good radiation stability permits long burnup where desirable.
    - There are not fuel elements to fabricate.
    - Bred materials and fission products can be removed on short cycle and good breeding ratios at low cost can be obtained.

1.2.2 Disadvantages of the MSR concept

1. The fuel salt mixture melts at a temperature in the range 450 to 510°C, so means must be provided for maintaining all salt-containing portions of the system above this temperature [6].

2. The fluoride salts react with oxygen to precipitate fuel constituents as oxides. Although zirconium tetrafluoride is included in the salt mixture so that ZrO_2 will precipitate in preference to UO_2, care must be taken to prevent the fuel from being contaminated with air, water, or other oxygen-containing materials [6].

3. The radioactivity in any fluid-fuel system is in a mobile form, and special provisions must be taken for containment and maintenance [6].

4. Some characteristics of the salt systems tend to make the cost high [8].

   - Since the salts melt at 450 to 510°C, provision must be made for preheating the reactor equipment to a high temperature before the salts are admitted and also for *preventing the salts from freezing.*
   - If electric power is produced through a classical Rankine cycle, *an intereemediate heat-transfer system must be provided* (or a specially designed heat generator) to keep water from coming in contact with the salt and to isolate the reactor prymary system from high pressure in the event of a leak. The chemical reaction on mixing is not violent, but hydrogen fluoride is generated and it is corrosive. Also, zirconium and uranium oxides precipitate from the salts in contact with moisture.
   - High-nickel alloys are to be preferred to stainless steel and Inconel at high temperatures (over 650 °C). It is more performing but also more expensive.
   - The graphite must be specially processed in order to achieve low permeability to salts and to gaseous fission products.
   - Isotope ^{7}Li must be separated from lithium element (often used in the salt) since a low parasitic absorption of neutrons is required to be employed as a constituent of fuel and blanket salts.
   - Since the reactors involve the handling of large quantities of mobile fission products, some special precautions must be taken in the containment. Also, the equipment in the circulating systems become radioactive and must be serviced by remote maintenance methods.

The contemporary research is based on the revision of the older knowledges and reopens the discussion about the advantages and disadvantages of the technology.

Chapter 2

Characterization and calibration of MSRE steady state functioning

This chapter deals with MSRE design features. First of all, a general description of the MSRE project is reported, including most relevant characteristics of the plant. Also, an overview of all main components is given.

Later on, it is faced the issue of describing the MSRE operation when working in steady-state condition at different power levels. The analysis will be constitued of two parts: in the first one, the design data at nominal power are taken and it is verified whether they are coherent with each other through two different ways of proceeding (thermal power is imposed or fuel temperature is imposed). In the second one, the actual data found during operation (which partly differ from the design ones) are considered. The mismatch between design and actual data is discussed.

Finally, the characterization of steady state functioning of the plant is carried outfor different power levels. This calculation is developed for all power levels, starting from 1 MW up to the nominal power (below 1 MW heat losses are relatively significant [1] and a "power imposed" control strategy is adopted, instead of a "outlet temperature imposed").

2.1 Description of MSRE plant and goals of the project

Molten-salt reactors were first investigated as a means of providing a compact high-temperature reactor for nuclear powered aircrafts. In 1954 an Aircraft Reactor Experiment (ARE) was constructed at Oak Ridge National Laboratory (ORNL) which demonstrated the feasibility of a molten-salt-fueled reactor at high temperature. Fuel entered the ARE core at 650 °C and left at 815 °C when the reactor power level was 2.5 MW. Immediately after the successful operation of the ARE, the Aircraft Reactor Test (ART) was started at ORNL as part of the Aircraft Nuclear Propulsion Program

[1] In the models developed in this work heat losse are not considered.

(ANP). This test was discontinued in 1957 when the ANP was revised, but the high promise of molten-salt reactor type for achieving low electric power generating costs in central power stations led ORNL to continue parts of the basic study program [6].

In the framework of the Molten-Salt Reactor Program (MSRP) it was designed and deveoped the Molten-Salt Reactor Experiment (MSRE), which was undertaken by the ORNL. The goal of the MSRP was the development of large, fluid-fuel reactors having good neutron economy and producing low cost electricity.

2.1.1 Goals of the MSRE project

The main goal of the Molten-Salt Reactor Experiment was to demonstrate that the desirable features of the molten-salt concept could have been embodied in a practical reactor for electricity generation.

An important objective was to provide the first large-scale, long-term, high-temperature test in a molten-salt reactor. A particular emphasis was indeed in testing the compatibility of materials (fluoride salts, graphite, and structural materials), the performance of key components, and the reliability and maintainability of the plant. It was decided that a reactor of 10 MW thermal output would have fulfilled all these purposes. Conversion of the 10 MW of heat to useful electricity was not considered to be necessary to demonstrate the concept, so it was decided that heat would have been dissipated to the atmosphere.

In the course of the 5 years of testing and operation of the MSRE (1964 - 1969), a considerable experience with components and systems of the reactor plant was accumulated [9]. The MSRE was a very successful experiment, in that it answered many questions and posed but a few new ones. The most important results were:

1. the conclusion that it was quite a practical reactor. It ran for long periods of time, and when maintenance was required, it was accomplished safely and without excessive delay.

2. Also, it demonstrated the expected flexibility and ease of handling the fuel. It was the first reactor in the world to operate with U-233 as the sole fuel (the highly radioactive U-233 used would have been extremely difficult to handle if it had to to be incorporated into solid fuel elements).

Three problems requiring further development turned up during the construction and operation of the MSRE [10]:

1. The first was that the Hastelloy N used for the MSRE was subject to a *radiation hardening*, due to accumulation of helium at grain boundaries. Later, it was found that modified alloys that had fine carbide precipitates within the grains would hold the helium and restrain this migration to the grain boundaries.

2. The second problem concerned the tritium produced by neutron reactions with lithium. At high temperatures the radioactive tritium, which is chemically like

hydrogen, penetrates metals quite readily, and unless captured in some way, would appear in the steam generators and reach the atmosphere. After considerable development work, it was found that an intermediate salt coolant made of a mixture of sodium fluoride and sodium fluoroborate, would have capture the tritium which could have been removed and isolated in the gas purge system.

3. The third problem came from the discovery of tiny cracks on the inside surface of the Hastelloy N piping for the MSRE. It was found that these cracks were caused by the fission product tellurium. It was shown that that this tellurium attack could be chemically controlled by keeping the fuel on the reducing side.

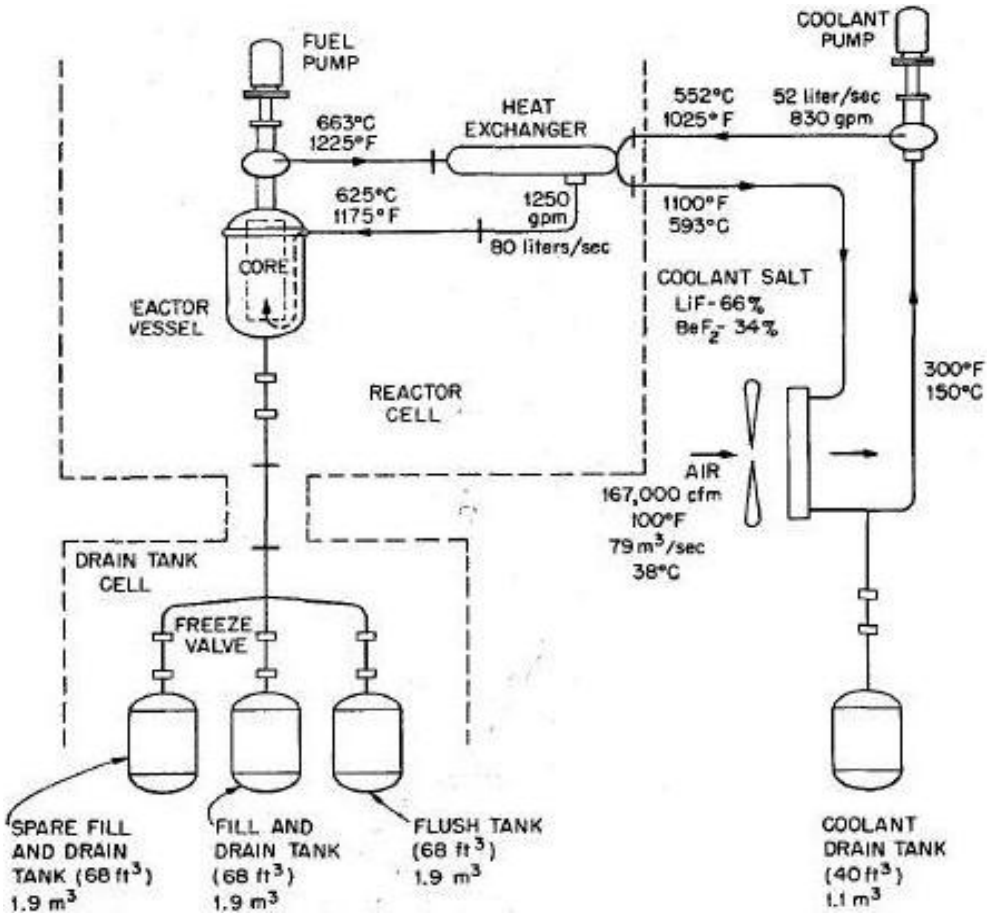

Figure 2.1: General layout of MSRE

2.2 Design data of the plant

All data collected in this section are extracted from Oak Ridge National Laboratory reports, see [6] and [9]. The MSRE was a single fluid, circulating molten-salt fuel, graphite-moderated reactor designed for a heat generation of 10 MW. The fuel employs a molten mixture of lithium, beryllium, and zirconium fluoride salts as a solvent for uranium and/or thorium fluorides. Heat generation occurs as the fuel flows through machined passages in the graphite core, and the heat is trasferred from the fuel salt to a similar coolant salt in a shell and tubes heat exchanger. Finally, the heat is dissipated to air in an air blast radiator. Since power production is not an objective of this experiment, no electric power generation equipment is utilized.

It is intended in this section to give a generale description of the design of MSRE systems, pointing out the most important features and presenting data of general interest. The general arrangement of MSRE plant is shown in Fig. 2.1.

2.2.1 Fuel and coolant salt

The compositions of fuel and coolant salts are shown in Table 2.1, while physical properties of the salts are given further on (see Table 2.8). Three different types of fuel salts are reported: they have been all employed through MSRE life. Favorable neutron absorption and chemical and physical properties were important requirements for the composition selected. Beryllium fluoride is used to obtain a low melting point. Lithium fluoride (99.99% Li^7 in both fuel and coolant salts) imparts good fluid flow properties to the mixure. Zirconium fluoride protects the fuel salt against precipitation of UO_2 from contamination by air and moisture, because Zr precipitates as an oxide preferably to uranium, thorium and plutonium [6].

The first experiments in the MSRE have been run with partially enriched uranium because there were uncertanties concerning the chemical behaviour of that fuel. Later the reactor has been operated with the highly enriched uranium fuel and with the thorium-uranium fuel.

2.2.2 Fuel circulating system

The fuel circulating system consists of the reactor vessel, the fuel pump, the heat exchanger, interconnecting piping and auxiliaries and services. The major components of this system were contained in the reactor hot cell, which provided safety against salt freezing.

The reactor vessel is a 1.52 m diameter, 2.44 m height tank, containing a 1.44 m diameter by 1.63 m high graphite core structure. When filled, the core, having a nominal volume of 2.55 m^3, contains 0.57 m^3 of fuel salt and 1.98 m^3 of graphite. The normal operating temperature was about 650 °C. When the reactor was not in operation, the salt was drained to one (or both) of the fuel drain tanks. Interconnecting salt piping and freeze valves permit filling the reactor or transferring salt between

Fuel type	Fuel Salt			Coolant Salt
	A Thorium-Uranium	B Highly Enriched Uranium	C Partially Enriched Uranium	
Salt Composition (mole %)				
LiF	70	66.8	65	66
BeF_2	23.7	29	29.2	34
ZrF_4	5	4	5	-
ThF_4	1	0	0	-
UF_4	0.3	0.2	0.8	-
Uranium Composition (at. %)				
^{234}U	1	1	0.3	-
^{235}U	93	93	35	-
^{236}U	1	1	0.3	-
^{238}U	5	5	64.4	-

Table 2.1: Composition of fuel salts and coolant salt

tanks.

The adopted structural material was INOR 8. It is a nickel alloy containing 17% molybdenum, 7% chromium, and 4% iron, specifically developed to have good strenght and to contain reactor fuel and blanket salts with little corrosion at high temperature [6]. INOR-8 physical properties are shown in Table 2.2.

INOR-8		
Density	8774.5	kg/m^3
Melting point	1355 - 1400	°C
Thermal conductivity	20.4	W/(m· °C)
Specific heat at 700 °C	577.8	J/(kg ·°C)
Mean coefficient of thermal expansion, 20-700°C	25.2 $\times 10^{-6}$	°C^{-1}

Table 2.2: Physical properties of INOR-8 [6]

At the design power of 10 MW, with no fuel absorption by the graphite, 1.4 MW of heat is generated in the fuel outside the nominal core volume, 0.6 MW is generated in the graphite and 8.0 MW is generated in the fuel within the core, giving an average power density of 14 MW/m^3 in the nominal core volume [8]. Nevertheless, in this analysis and successive modelling, the whole power generated in the fuel will always be assumed fully generated within the core. Design data for the core vessel and the core container are reported in Table 2.3 and 2.4.

Core vessel		
Construction material	INOR-8	
Inlet nozzle	12.7	cm
Outlet nozzle	12.7	cm
Outer Diameter	150.18	cm
Inner Diameter	147.32	cm
Wall thickness	1.43	cm
Overall height	2.56	m
Head thickness	2.54	cm
Design pressure	345×10^3	Pa
Design temperature	700	°C
Cooling annulus ID	142.24	cm
Cooling annulus OD	147.32	cm
Inlet Pipe Diameter	15.2	cm
Outlet Pipe Diameter	20.3	cm
Fuel inlet temperature	635	°C
Fuel outlet temperature	663	°C

Table 2.3: Core vessel design data and dimensions

Core container		
Inner Diameter	140.97	cm
Outer Diamter	142.24	cm
Wall thickness	0.635	cm
Height	172.72	cm

Table 2.4: Core container design data [6]

The graphite core matrix is sufficiently unrestrained so that on a temperature rise the induced stresses due to the expansion of the graphite will be minimized. The coefficient of expansion for the graphite is 2.35 to 3.05×10^{-6} °C^{-1} whereas for INOR-8 it is 14×10^{-6} °C^{-1} (in the 20-650°C range). This difference causes the core barrel to move 0.48 cm radially away from the graphite core blocks on heatup of the reactor. To prevent an excessive amount of salt flow in the annular space thus created, an INOR-8 ring surrounds the bundle of the graphite outer rods at the bottom. Use of unclad graphite in the MSRE required the graphite to be compatible with the fuel salt, fisson products and INOR-8. Also, its thermal conductivity should not decrease too much with time. Another important characteristic is that the penetration of salt into the voids of graphite should be minimum, since the degree of salt permeation affects the graphite temperature both during operation and after shutdown. The extent of absorption of fission-product gases is of concern in that the ^{135}Xe contributes significantly to the poison fraction. Properties of MSRE core graphite are shown in Table 2.5.

Bulk density	1860	kg/m^3
Thermal conductivity		
With grain at 20°C	200	W/(m ·°C)
Normal to grain at 20 °C	110	W/(m ·°C)
Temperature coefficient of expansion		
With grain at 20 °C	1×10^{-6}	1/°C
Normal to grain at 20 °C	3×10^{-6}	1/°C
Specific heat		
-20 °C	585	J/(kg ·°C)
90 °C	920	J/(kg ·°C)
315 °C	1380	J/(kg ·°C)
540 °C	1630	J/(kg ·°C)
650 °C	1760	J/(kg ·°C)

Table 2.5: Properties of MSRE core graphite [6]

The fuel pump is a centrifugal type pump with an overflow tank. The drive motor is directly coupled to the shaft, and the complete assembly is about 2.44 m high. The fuel pump bowl is at the highest elevation in the primary circulating system and serves as an expansion volume for the salt. The level of the molten-salt interface in the bowl is an indication of the inventory of the salt in the system.

The primary heat exchanger is used to transfer heat from the fuel salt to the coolant salt. The heat exchanger is a horizontal, shell and U-tube type, with the fuel salt circulating in the shell and the coolant salt in the tubes, fabricated with INOR-8. The overall dimensions and design data are given in Table 2.6.

The shell has a 40.6 cm outer diameter, and a lenght of about 2.44 m, including

the coolant salt header. The shell is 1.27 cm thick in both the cylindrical portion and the heads. To prevent vibration at the higher flow rates due to the clearance between the tubes and the baffle plates, INOR-8 rods were inserted between the tubes. There were 159 tubes, 1.27 cm outer diameter with 0.107 cm wall thickness, affording a total heat transfer surface of ≈ 23.6 m^2. The tubes were arranged on a 1.97 cm equilateral triangular configuration.

The heat exchanger is installed horizontally, pitching toward the fuel-salt outlet at a slope of about 3°. Each U-tube is oriented so that the coolant salt will also drain. The shell is surrounded by electric heating units. In normal operation, the coolant-salt pressure will be maintained at a slightly higher value than the fuel the fuel-salt pressure so that coolant salt will flow into the fuel system if a leak develops.

The heat exchanger was designed for low holdup of salts, simplicity of construction, and quite high performance. The space limitations within the containment cell required a fairly compact unit. A U-tube configuration best satisfied this requirement and also minimized the thermal-expansion problems.

From the heat transfer standpoint, it was better to have the fuel salt passing through the shell and the coolant-salt through the tubes, since the fuel-salt volume flow was larger. A further consideration in this direction was that the fuel-salt system operates at a slightly lower pressure than the coolant-salt system and there was a small savings in the required shell thickness. Also, there was some savings in the required tubes thickness, since they felt an internal pressure rather than external.

2.2.3 Drain tank system

Four tanks were provided for safe storage of the salt mixtures when they were not in use in the fuel-salt and coolant-salt circulating systems. Among these four tanks, three tanks were connected to the reactor by means of the fill and drain line. Fuel drain tanks were provided with a cooling system capable of removing 100 kW of fission product decay heat. The fourth tank was provided for the coolant salt. Moreover, the fuel dump tank was provided with heat for keeping the clean fuel molten. The tank was provided with electric heaters similar to those on other parts of the salt circuits, in order to avoid freezing of the salt.

The molten salt in both primary and secondary circuits was sealed off from the respective drain tanks by means of the freeze plugs in the drain lines. Moreover, the tanks were provided with devices capable of indicating high and low liquid levels and also with weight cell indicating the weight of the tanks and their contents [11].

2.2.4 Coolant circulating system

The coolant-salt system transported reactor heat from the fuel salt heat exchanger to the air-cooled radiator where the energy was dissipated to the environment by the discharge of warm air from the stack. The coolant system (also referred as secondary system) circulated a lithium and beryllium salt, similar in physical properties to the

Shell & Tube Heat Exchanger		
Construction material	INOR-8	
Heat load	10	MW
Shell-side fluid	Fuel salt	
Tube-side fluid	Coolant salt	
Layout	25% cut, cross-baffled shell with U-tubes	
Baffle pitch	30.48	cm
Tube pitch (triangular)	1.97	cm
Active shell lenght	≈ 1.8	m
Overall shell lenght	2.44	m
Shell diameter	40.64	cm
Shell thickness	1.27	cm
Average tube lenght	4.27	m
Number of U-tubes	159	
Tube OD	1.27	cm
Tube thickness	0.107	cm
Heat transfer surface	≈ 23.6	m^2
Design temperature: shell side	705	°C
Design temperature: tube side	705	°C
Design pressure: shell side	4.8×10^5	Pa
Design pressure: tube side	7.2×10^5	Pa
Terminal temperature: fuel salt	635 inlet, 663 outlet	°C
Terminal temperature: coolant salt	551 inlet, 593 outlet	°C
Effective log mean ΔT	73.9	°C
Pressure drop: shell side	1.65×10^5	Pa
Pressure drop: tube side	2.00×10^5	Pa
Fuel salt flow rate	75.7	l/s
Coolant salt flow rate	53.6	l/s

Table 2.6: Design data for primary heat exchanger [6]

fuel salt but without fissionable materials. Coolant salt composition is given in Table 2.1.

The main components in the system were the fuel heat exchanger, located in the reactor cell, the coolant-salt circulating pump and the radiator, both located in the coolant salt cell. In accidental conditions all parts of coolant-salt circulating system could have been maintained above the liquidus temperature of the salt, about 450 °C, by means of electric heaters. The coolant-salt circulating pump was very similar to the fuel salt pump, besides that it was not provided of the overflow tank. The coolant-salt circulating pump bowl was located at the highest point in the colant salt system and served as an expansion volume.

The radiator had 120 tubes, 1.9 cm outer diameter $\times$ 9.14 m lenght, arranged in serpentine coils to provide $\approx$ 75.6 m^2 of heat transfer surface [6]. A drawing of the radiator coil configuration is shown in Fig. 2.2. The salt should moved downward

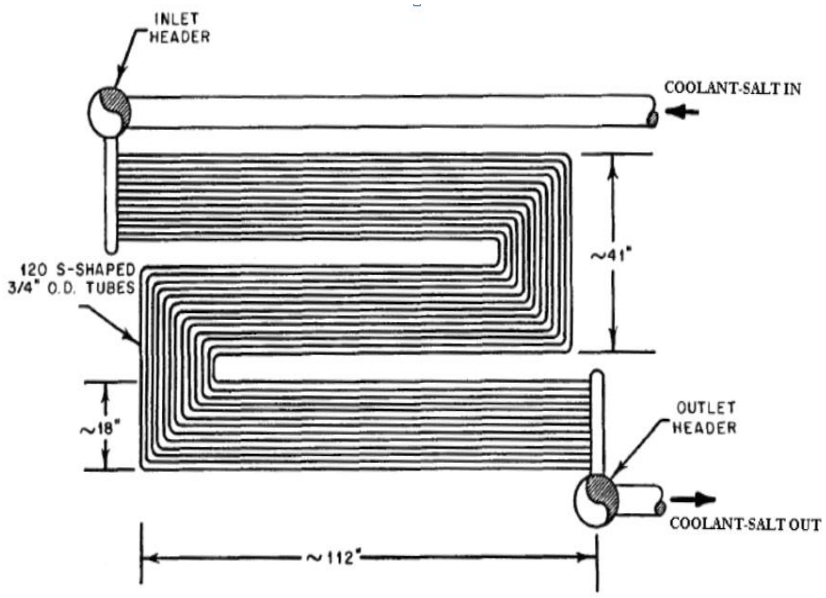

Figure 2.2: Radiator coil configuration

through the radiator as it is cooled. The cooling air was supplied by two axial blowers having a combined capacity of about 80 m^3/s.

One of the chief considerations in designing the MSRE radiator was that it had to be protected from freezing of the coolant salt in the tubes in the event of sudden loss of reactor power. To guard against freezing of the coolant salt in the radiator tubes quick-closing doors were provided for the radiator to close off the air flow, and the radiator assembly included electric heaters inside the enclosure. When the doors were in the up (open) position, a counter-weight is held down by three magnets, any

Radiator		
Construction material	INOR-8	
Duty	10	MW
Number of tubes	120	
Tube matrix	12 tubes per row; 10 rows deep	
Tube spacing	3.8	cm
Row spacing	3.8	cm
Tube OD	1.9	cm
Tube thickness	0.18	cm
Tube lenght	9.14	m
Heat transfer surface	$\approx$65.6	m^2
Design temperature	675	°C
Operating pressure at design point	5.2×10^5	Pa
Terminal temperature: coolant salt	551 inlet, 593 outlet	°C
Terminal temperature: air	38 inlet, 149 outlet	°C
Effective log mean ΔT	479	°C
Overall heat transfer coefficient	58.5	W /($m^2 \cdot$ °C)
Pressure drop: salt side	1.4×10^5	Pa
Pressure drop: air side	2.4×10^3	Pa
Coolant salt flow rate	53.6	l/s
Air flow rate	80	m^3/s

Table 2.7: Radiator design data

two of which are capable of holding this weight. In event of power failure or reactor scram, the magnets released the counter-weight and the doors were allowed to fall freely. Instead, during operating conditions, the doors will be lowered by an electric motor. The radiator design data are summarized in Table 2.7.

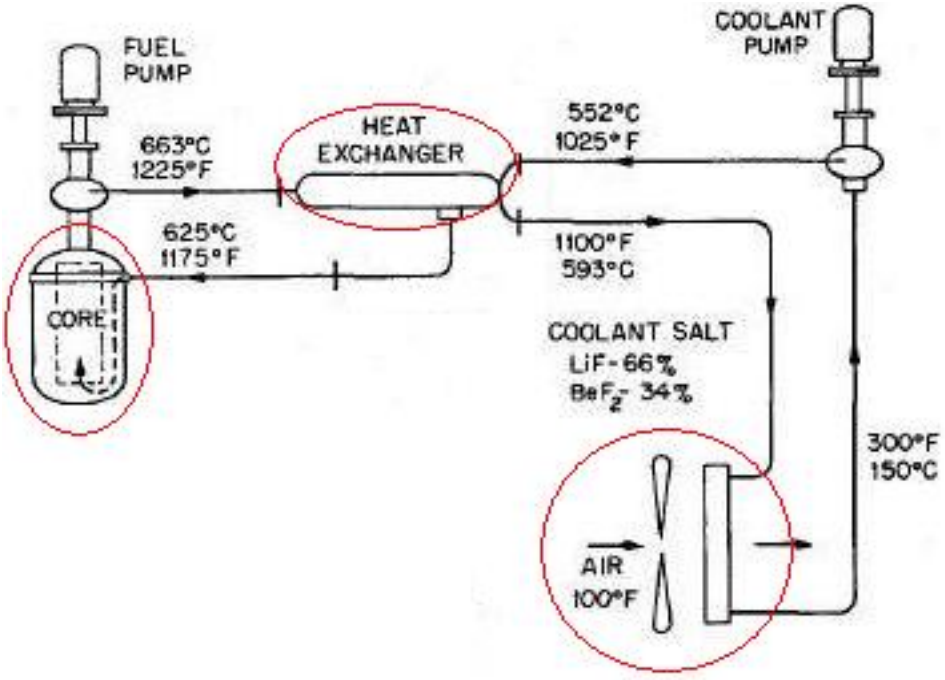

Figure 2.3: Simplified layout of MSRE

2.3 MSRE steady-state energy balances from design data

In this section, nominal values of power and temperatures given by official reports (written before the reactor has been operated), taken from reports [6], [8], [12] and [13], will be compared with values calculated through a model run in Matlab® [14]. The model will work for steady-state only. Two different ways of calculating the power and temperatures values will be developed (see page 31 and following). Further on, heat exchanger and radiator performances will be evaluated, since the in ORNL reports, as it will be seen, unaccetable errors on estimations of heat transfer coefficents are present.

Heat losses will not be considered, neither in tubelines connecting the main components, nor within main components themselves. Pressure drops will also not be considered and pumps contribute to heat balances will not be taken into account, either. The topic of this section is to give an overview of nominal data of MSRE and to reproduce heat balances on core, heat exchanger and radiator and to compare them with each other and with balances given by ORNL reports.

The goal is to verify whether data pertaining to fuel flow, coolant flow, air flow, and also physical properties, heat exchange coefficients and thermal power are coherent with each other. A simplified draw of the reactor, relative to the parts analysed in this section, is shown in Figure 2.3.

It has to be mentioned that the behaviour of the molten salt as a heat transfer fluid had been investigated before designing the MSRE. First af all, physical properties of fuel and coolant salt were estimated: values of physical properties are given in Table 2.8. Starting from these physical properties, knowing nominal values of fuel-salt

Salts Physical Properties			
	Fuel-salt	Coolant-salt	
Thermal conductivity	4.75	6.05	W/(m $\cdot$°C)
Viscosity	0.0074	0.0083	Pa $\cdot$ s
Density	2472	1922	kg/m^3
Specific Heat	1.93 $\times 10^3$	2.39 $\times 10^3$	J/(kg $\cdot$°C)

Table 2.8: Physical properties of fuel and coolant salts used in MSRE heat exchanger design and evaluation

flow and coolant-salt flow, missing data and coefficients have been calculated using the following formulas:

- Logarithmic mean ΔT, calculated with the following formula:

$$\Delta T_{lm} = \frac{(T_{in}^{hot} - T_{out}^{cold}) - (T_{out}^{hot} - T_{in}^{cold})}{\frac{(T_{in}^{hot} - T_{out}^{cold})}{(T_{out}^{hot} - T_{in}^{cold})}} \tag{2.1}$$

- Effective logarithmic mean ΔT, calculated with the following formula:

$$\Delta T_{lm-eff} = F \cdot \Delta T_{lm} \tag{2.2}$$

  where F is is a correction factor, applied to include the effect of a single-pass shell.

- Power exchanged calculated with:

$$P = U \cdot A \cdot \Delta T_{lm-eff} \tag{2.3}$$

  where U is an overall heat transfer coefficient in W/(m$^2\cdot$ °C), A is the heat transfer surface and P is the exchanged thermal power.

- Power exchanged calculated with:

$$P = \Gamma \cdot c_p \cdot \Delta T_{in-out} \tag{2.4}$$

  where Γ is the mass flow in kg/s, c_p is the specific heat in J/(kg $\cdot$ °C), P the power released or absorbed by the fluid between inlet and outlet and ΔT_{in-out} is the fluid temperature difference between inlet and outlet.

In the following paragraphs, reactor core, heat exchanger and radiator are investigated. A brief overview over MSRE neutronics is now given. The MSRE neutron spectrum is thermal. Indeed, this reactor is graphite moderated. The fact that the fuel circulates through the MSRE core has a definite effect on some of the nuclear properties, such as the effective fraction of delayed neutrons. Since the transit time through the active region of the core is only about one-third of the loop transit time, a portion of the delayed neutrons (from decaying of long-living precursors are emitted outside the core) where they are lost to the chain reaction. Calculation will be made to evaluate this loss under steady state operating conditions (see chapter 4).

Two types of fuel will be considered when the model will be implemented and run: the first one is fuel type C, the second one (enriched with thorium) is fuel type A (see Table 2.1). Neutronics main features and parameters are shown in Table 2.9 and 2.10 for the two fuel types. Data regarding neutronics of fuel B were not given in reports.

U-235 fuel (fuel type C)			
Fuel	-8.71		pcm/°C
Graphite	-6.66	pcm/°C	
Neutron Prompt Lifetime, Λ	2.4×10^{-4}		s
Total Delayed Neutron Fraction, β	666		pcm
Density (at 650 °C)	2290		kg/m^3
Approximation with 6 Groups of Precursors			
Group	Decay constant	Half-life	Delayed neutron fraction
i	λ_i	$T_i^{1/2}$ [s]	β_i
1	0.0124	55.9	22.3×10^{-5}
2	0.0305	22.73	145.7×10^{-5}
3	0.111	6.24	130.7×10^{-5}
4	0.301	2.3	262.8×10^{-5}
5	1.14	0.61	76.6×10^{-5}
6	3.014	0.23	28×10^{-5}

Table 2.9: Neutronic main features of U-235 fuel

2.3.1 Reactor core

The basic concept of MSRE is a cylindrical vessel containing a graphite matrix for neutron moderation through which a molten salt fuel is circulated. The core dimensions were set after that preliminary calculations showed that, in this region, the critical mass was relatively insensitive to core size [8]. A fuel volume fraction of 0.225 was chosen because it was close to the minimum critical concentration of uranium and had a favorably low reactivity effect due to fuel permeation of the graphite [8].

U-233 fuel (fuel type A)			
Fuel	-11.3		pcm/°C
Graphite	-5.81		pcm/°C
Neutron Prompt Lifetime, Λ	4.0×10^{-4}		s
Total Delayed Neutron Fraction, β	264		pcm
Density (at 650 °C)	2310		kg/m^3
Approximation with 6 Groups of Precursors			
Group	Decay constant	Half-Life	Delayed neutron fraction
i	λ_i	$T_i^{1/2}$ [s]	β_i
1	0.0126	55.01	22.8×10^{-5}
2	0.0337	20.57	78.8×10^{-5}
3	0.139	4.99	66.4×10^{-5}
4	0.325	2.13	73.6×10^{-5}
5	1.13	0.61	13.6×10^{-5}
6	2.50	0.28	8.8×10^{-5}

Table 2.10: Neutronic main features of U-233fuel

Fuel entered the vessel at an annular volute around the top of the cylinder and passed down between the graphite and the vessel wall. A dished head at the bottom reverses the flow and directs it up through rectangular passages in the graphite matrix into a dished head at the top, from which it goes to the suction line of a sump-type pump mounted directly above and concentric with the reactor vessel (see Figure 2.1). Flow through the reactor is nearly laminar, and the passage width is narrow enough to prevent an excessive *Poppendiek effect* [2].

The specified channel configuration is the result of intensive studies into the temperature effects associated with the relative slow flow through the core (about 0.4 m/s [6]). On the contrary, turbulent flow is desirable in the annulus in order to minimize the Poppendiek effect [11]. The arrengement of typical fuel channels in the core is reported in Figure 2.4, and core design data (significative geometrical characteristics and heat exchange parameters) are given in Table 2.11.

Moreover, it is noteworthy that approximately 14% of the reactor power is produced in, or transferred to, the fuel as it flows through the peripheral regions. This results in a 4 °C temperature rise out of the core region [8]. However, this phenomenon will be neglected when modelling the reactor core (as it was neglected in the model implemented at ORNL to predict/reproduce the dynamical behaviour of the MSRE).

The MSRE contains three control rods whose centers are located at three corners of a 10 cm square around the axis of the core. The poison elements are hollow cylinders,

[2]The Poppendiek effect contributes to the fuel near the wall of a channel to be hotter than the mean for the channel. The rise in temperature of fluid near the wall is associated with internal heat generation and relatively low fluid flow in the boundary layer [15].

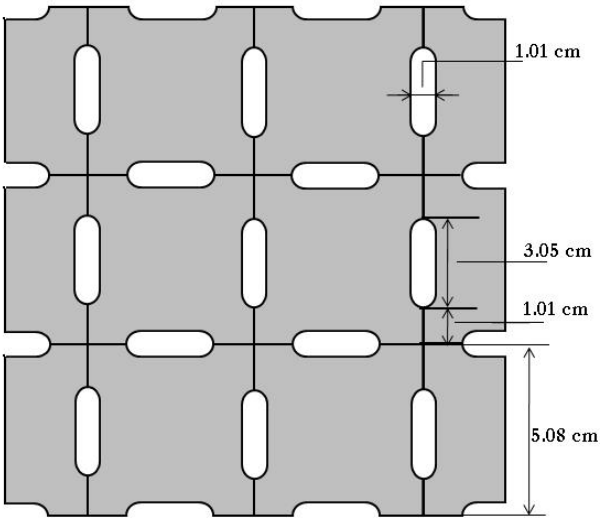

Figure 2.4: Typical fuel channels arrangement of MSRE core

containing 30%wt of Al_2O_3 and 70%wt of Gd_2O_3. Thirty-six such elements, each clad in Inconel, are used for each control rod [8].

Heat produced in the graphite by absorption of beta and gamma radiation and the elastic scattering of fast neutrons amounts to about 7% of the total heat produced in the reactor. Since this heat has to be transferred to the fuel for removal, the temperature of the graphite is, in general[3], higher than that of the fuel in the adjacent channels.

The heat transfer coefficient k_{eq} is a core overall coefficient, which links graphite average temperature to fuel salt bulk temperature. The temperature difference between the mean graphite and fuel temperatures within an individual cell can, in general, be broken down in two parts [15]:

1. the difference between the average temperature in a graphite block and the temperature at the interface, since heat produced in the graphite needs to be removed (it is conveyed to the surface through heat conduction);

2. the temperature drop across the graphite-fuel interface, resulting from heat flow out of the graphite, including the Poppendiek effect, which causes the fuel near the wall of a channel to be hotter than the mean for the channel.

[3]During transients following a power rise it can happen that fuel salt temperature is higher than graphite temperature, see chapter 4.

Graphite core		
Diameter	140.34	cm
Graphite core blocks	$5.1 \times 5.1 \times 170$	cm
Number of fuel channels (equivalent)	1140	
Fuel channel width	1.01	cm
Fuel channel lenght	3.05	cm
Effective reactor lenght	≈165	cm
Heat exchange in the core - nominal data		
Fuel salt heat capacity	7.56	MJ/°C
Graphite heat capacity	6.48	MJ/°C
Bulk grahite - Fuel salt heat transfer coefficient, k_{eq}	0.036	MW/°C
Fraction of power generated in the graphite, γ_g	0.07	
Fraction of power generated in the fuel, γ_f	0.93	

Table 2.11: MSRE graphite core design data

2.3.2 Heat exchanger

An evaluation of heat exchanger performance has been carried through with Equations from 2.1 to 2.4. As mentioned, results obtained are based on design full power values of parameters. They are shown in Table 2.12.

Looking at last two rows of Table 2.12, it is clearly observable that power changes whether calculation is based on the difference between inlet and outlet fuel-salt temperature, or on the difference between inlet and outlet coolant-salt temperature, or on the mean logarithmic ΔT_{lm} between the two fluids.

At a more careful analysis, it can be seen that errors on power calculations based on inlet-outlet temperature variation (see Equations of type 2.4) are probably due to the appoximation made assuming specific heat to be constant. In this case, the errors found in power calculations equal at most at 2.5% of nominal full power.

It is not quite immediate to understand what kind of error causes a power overestimate when Equation 2.3 is used in evaluating thermal power Presuming nominal data (such as ΔT_{lm}, heat transfer area and overall heat exchange coefficient) are correct, this discordance remains so far unesplicable. Anyway, because of this inconsistency of nominal data with each other, it has been decided to adjust, as a preliminary guess, the value of the product $U_{s,cool} \cdot A$ so that calculation of exchanged power with Eqn. 2.3 gives the desired result, i.e. the nominal power of 10 MW. This new value of $U_{s,cool}$ is obtained solving:

$$U_{s,cool} \cdot A = \frac{P}{\Delta T_{lm}}$$

Heat Exchanger			
	Fuel salt Shell side	Coolant salt Tube side	
Volumetric flow	75.7	53.6	l/s
Density	2472	1922	kg/m^3
Mass flow	187.12	103.08	kg/s
Velocity	–	3.69	m/s
Reynolds Number	13000	9000	–
Prandtl Number	2.994	3.256	–
Film coefficient	18170	27820	$W/(m^2 \cdot °C)$
Overall heat transfer coefficient	6734		$W/(m^2 \cdot °C)$
Heat transfer area	23.6		m^2
Nominal h.e.-inlet temperature	662.8	551.7	°C
Nominal h.e.-outlet temperature	635.0	593.3	°C
ΔT log mean, see Eqn. 2.1	76.2		°C
ΔT log mean, given in [6]	76.1		°C
Correction coefficient F	0.96		–
Effective ΔT log mean, see Eqn. 2.2	73.9		°C
U ·A	158900		W/°C
Exchanged power, see Eqn. 2.3	11.74		MW
Exchanged power, see Eqn. 2.4	10.01	10.25	MW

Table 2.12: Heat exchanger parameters

2.3.3 Radiator

An evaluation of radiator performance has been carried out with Equations from 2.1 to 2.4. Results obtained are based on nominal full power values of parameters. They are shown in Table 2.13.

It can be observed that evaluation of exchanged power (last three rows of Table 2.13) gives results which are quite coherent with each other. Yet, some errors are present, but they are probably due to the approximation made assuming specific heats of coolant-salt and air to be constant. Also, the main error is on power dumped by coolant salt to the radiator, and not, as it was in the case of the primary heat exchanger, on power calculated through Equation 2.3, that is by using ΔT_{lm} on the radiator. This consideration implies that nominal values of temperatures, temperature deltas, overall heat transfer coefficient, heat transfer area and other radiator parameters, are correct and coeherent with each other. Another method has been used to proof consistency of this values and same conclusions have been found (see page 37).

Radiator		
Coolant-Salt Flow	53.6	l/s
Air Flow (at nominal power)	79.3	m^3/s
Air Density at blowers inlet	1.1165	kg/m^3
Air Mass flow	88	kg/s
Overall heat transfer coefficient	316.8	$W/(m^2 \cdot °C)$
Heat transfer area	65.6	m^2
Nominal coolant-salt inlet temperature	593.3	°C
Nominal coolant-salt outlet temperature	551.7	°C
Nominal air inlet temperature	≈ 38	°C
Nominal air outlet temperature	≈ 150	°C
ΔT log mean, [6], page 296	478.9	°C
ΔT log mean, see Eqn. 2.1	478.3	°C
U ·A	20800	W/°C
Exchanged power, see Eqn. 2.3	9.95	MW
Power Dumped by Coolant-salt, see Eqn. 2.4	10.25	MW
Power Absorbed by Air, see Eqn. 2.4	9.92	MW

Table 2.13: Radiator parameters

2.4 Model for MSRE steady-state assessment

In orded to assess the coherence of nominal data with each other it has been decided to build a model of plant principal components, see Equations from 2.6 to 2.19.

The model will be used to verify whether, at nominal power, the temperatures values respect their nominal values given in ORNL reports or not. Once the cause of the discordance found in nominal power calculation will be cleared, the model will be upgraded so that it will be capable to calculate temperatures for steady state conditions at all power levels.

The model describes the reactor working in a steady state. The model is constitued of N equations, and it describes a system with N+3 unknown variables. So three of these variables need to be fixed. Of course one of these three variables will be the air inlet temperature, which does not depend on reactor parameters but only on envinronment conditions. Attention is required in choosing the two other variables which have to be fixed, because the system has to be linear in order to be solved by the Matlab code. Therefore, the two variables to be fixed will be chosen among the ones that initially make the system not linear (see Eqn. 2.19). Among all combinations of fixable variables two cases will be chosen and taken in exam (see page 30).

The simple model, constitued of the following equation system, has been elaborated and then run in Matlab® .

$$\mathbf{P} \cdot \gamma_g = k_{eq} \cdot (\mathbf{T_g} - \mathbf{T_s^{core}}) \tag{2.5}$$

$$P \cdot \gamma_s + k_{eq} \cdot (T_g - T_s^{core}) = \Gamma_s \cdot c_s \cdot (\mathbf{T_s^{core,out}} - \mathbf{T_s^{core,in}}) \quad (2.6)$$

$$T_s^{core} = \frac{T_s^{core,out} + T_s^{core,in}}{2} \quad (2.7)$$

$$T_s^{core,out} = \mathbf{T_s^{h.e.,in}} \quad (2.8)$$

$$T_s^{core,in} = \mathbf{T_s^{h.e.,out}} \quad (2.9)$$

$$U_{s,cool} \cdot (\mathbf{T_s^{h.e.}} - \mathbf{T_{cool}^{h.e.}}) = \Gamma_s \cdot c_s \cdot (T_s^{h.e.,in} - T_s^{h.e.,out}) \quad (2.10)$$

$$T_s^{h.e.} = \frac{T_s^{h.e.,out} + T_s^{h.e.,in}}{2} \quad (2.11)$$

$$U_{s,cool} \cdot (T_s^{h.e.} - T_{cool}^{h.e.}) = \Gamma_{cool} \cdot c_{cool} \cdot (\mathbf{T_{cool}^{h.e.,out}} - \mathbf{T_{cool}^{h.e.,in}}) \quad (2.12)$$

$$T_{cool}^{h.e.} = \frac{T_{cool}^{h.e.,out} + T_{cool}^{h.e.,in}}{2} \quad (2.13)$$

$$T_{cool}^{h.e.,out} = \mathbf{T_{cool}^{rad,in}} \quad (2.14)$$

$$T_{cool}^{h.e.,in} = \mathbf{T_{cool}^{rad,out}} \quad (2.15)$$

$$U_{cool,air} \cdot (\mathbf{T_{cool}^{rad}} - \mathbf{T_{air}}) = \Gamma_{cool} \cdot c_{cool} \cdot (T_{cool}^{rad,in} - T_{cool}^{rad,out}) \quad (2.16)$$

$$T_{cool}^{rad} = \frac{T_{cool}^{rad,out} + T_{cool}^{rad,in}}{2} \quad (2.17)$$

$$U_{cool,air} \cdot (T_{cool}^{rad} - T_{air}) = \mathbf{\Gamma_{air}} \cdot c_{air} \cdot (\mathbf{T_{air}^{rad,out}} - \mathbf{T_{air}^{rad,in}}) \quad (2.18)$$

$$T_{air} = \frac{T_{air}^{rad,out} + T_{air}^{rad,in}}{2} \quad (2.19)$$

where subscript g is used to indicate *graphite*, subscript s is used to indicate *fuel-salt*, subscript *cool* is used to indicate *coolant-salt*, subscript *air* is used to indicate *air*, superscript *out* is used to indicate *outlet*, superscript *in* is used to indicate *inlet*, superscript *core* is used to indicate *core*, superscript *h.e.* is used to indicate *heat exchanger*, superscript *rad* is used to indicate *radiator*. Also, P is the total thermal power, γ_g is the fraction of power generated in the graphite, γ_s is the fraction of power generated in the fuel salt, k_{eq} is a fictitious heat transfer coefficient (see page 25) between fuel-salt and graphite $U_{s,cool}$ is the global heat exchanger coefficient on heat tranfer between fuel-salt and coolant-salt $U_{cool,air}$ is a global radiator coefficient on heat transfer between coolant-salt and air. Finally, T is to indicate *temperature*, Γ_s stands for fuel-salt mass flow, Γ_{cool} stands for coolant-salt mass flow, Γ_{air} stands for air mass flow, c_s is the fuel-salt specific heat, c_{cool} is the coolant-salt specific heat and c_{air} is the air specific heat.

In this model, representative temperatures of fuel-salt, coolant-salt and air in any component are described as the arithmetic mean between inlet and outlet temperature in that component.

It must be to point out that this model presents a significative fault in some equations, precisely in Equations 2.11, 2.13, 2.17 and 2.19. Indeed, in order to obtain a linear model, thermal power exchanged over heat exchanger or radiator is accounted as a global heat transfer coefficient times the difference between average temperatures of

the two flowing fluids, instead of being calculated with logarithmic mean temperature difference.

In the following paragraphs the model is solved with Matlab® . As previously explained, the model, in order to be solvable, needs three variables to be fixed. One of them will be always the radiator inlet temperature of the air. The other two will be fixed in the following way (keeping in mind that they have to be chosen in order the system to result linear and therefore solvable by the code):

1. In the first case power is fixed at 10 MW. Radiator outlet air temperature is fixed and equals 150 °C.

2. In the second case air flow is fixed at 88 kg/s, which is the nominal value given in report [6]. Core outlet fuel-salt temperature is fixed and equals 663 °C.

Radiator inlet air temperature is always fixed and it is assumed to be always equal to 38 °C. In both case the program is run twice, the first one with nominal the value of $U_{s,cool} * A$ given in Table 2.12, and the second time with a fictitious value of $U_{s,cool} \cdot A$, found inverting Equation 2.3 so that nominal power and nominal ΔT_{lm} were respected.

Equations constituiting the model are inserted according to the following scheme:

$$\underline{\underline{A}} \cdot \underline{X} = \underline{B} \cdot \underline{U} \tag{2.20}$$

where $\underline{\underline{A}}$ is the matrix of coefficients, $\underline{X}$ is the unknown variables vector, $\underline{B}$ is the vector of fixed variables coefficients and $\underline{U}$ is the vector of fixed vaiables. Solution is obtained by $\underline{X} = \underline{\underline{A}}^{-1} \cdot (\underline{B} \cdot \underline{U})$. Being radiator inlet air temperature always fixed and already known (38 °C) in all tested cases, its value is not given in tables of results. Matrixes of coefficients and vectors of known and unknown variables are shown for each of the four cases.

First Case - Power Imposed

Power is fixed at 10 MW. Radiator outlet air temperature is fixed and equals 150 °C. Solution for vector of unknown variables is given in Table 2.14. The matrix product to be solved is the following one:

$$
\begin{pmatrix}
k_{eq} & -k_{eq} & \Gamma_s \cdot c_s & \Gamma_s \cdot c_s & 0 & 0 & 0 & 0 & 0 & \\
0 & 1 & -1/2 & -1/2 & 0 & 0 & 0 & 0 & 0 & \\
0 & 0 & 1 & 0 & 0 & -1 & 0 & 0 & 0 & \\
0 & 0 & 0 & 1 & 0 & 0 & -1 & 0 & 0 & \\
0 & 0 & 0 & 0 & U_{s,cool} & -\Gamma_s \cdot c_s & \Gamma_s \cdot c_s & -U_{s,cool} & 0 & \\
0 & 0 & 0 & 0 & 1 & -1/2 & -1/2 & 0 & 0 & \\
0 & 0 & 0 & 0 & U_{s,cool} & 0 & 0 & -U_{s,cool} & -\Gamma_{cool} \cdot c_{cool} & \\
0 & 0 & 0 & 0 & 0 & 0 & 0 & 1 & -1/2 & \cdots \\
0 & 0 & 0 & 0 & 0 & 0 & 0 & 0 & -1 & \\
0 & 0 & 0 & 0 & 0 & 0 & 0 & 0 & 0 & \\
0 & 0 & 0 & 0 & 0 & 0 & 0 & 0 & 0 & \\
0 & 0 & 0 & 0 & 0 & 0 & 0 & 0 & 0 & \\
0 & 0 & 0 & 0 & 0 & 0 & 0 & 0 & 0 & \\
0 & 0 & 0 & 0 & 0 & 0 & 0 & 0 & 0 &
\end{pmatrix}
$$

$$
\begin{pmatrix}
0 & 0 & 0 & 0 & 0 & 0 \\
0 & 0 & 0 & 0 & 0 & 0 \\
0 & 0 & 0 & 0 & 0 & 0 \\
0 & 0 & 0 & 0 & 0 & 0 \\
0 & 0 & 0 & 0 & 0 & 0 \\
0 & 0 & 0 & 0 & 0 & 0 \\
\Gamma_{cool} \cdot c_{cool} & 0 & 0 & 0 & 0 & 0 \\
\cdots \quad 1/2 & 0 & 0 & 0 & 0 & 0 \\
0 & 0 & 0 & 1 & 0 & 0 \\
1 & 0 & -1 & 0 & 0 & 0 \\
0 & U_{cool,air} & \Gamma_{cool} \cdot c_{cool} & -\Gamma_{cool} \cdot c_{cool} & -U_{cool,air} & 0 \\
0 & 1 & -1/2 & -1/2 & 0 & 0 \\
0 & U_{cool,air} & 0 & 0 & -U_{cool,air} & -c_{air} \cdot (T_{air}^{rad,out} - T_{air}^{rad,in}) \\
0 & 0 & 0 & 0 & 1 & 0
\end{pmatrix}
\cdot
$$

$$
\cdot
\begin{pmatrix}
T_s^{core} \\
T_s^{core,out} \\
T_s^{core,in} \\
T_s^{h.e.} \\
T_s^{h.e.,in} \\
T_s^{h.e.,out} \\
T_{cool}^{h.e.} \\
T_{cool}^{h.e.,out} \\
T_{cool}^{h.e.,in} \\
T_{cool}^{rad} \\
T_{cool}^{rad,out} \\
T_{cool}^{rad,in} \\
T_{air}^{rad} \\
T_{air}^{rad,out}
\end{pmatrix}
=
\begin{pmatrix}
-\gamma_s & 0 & 0 \\
0 & 0 & 0 \\
0 & 0 & 0 \\
0 & 0 & 0 \\
0 & 0 & 0 \\
0 & 0 & 0 \\
0 & 0 & 0 \\
0 & 0 & 0 \\
0 & 0 & 0 \\
0 & 0 & 0 \\
0 & 0 & 0 \\
0 & 0 & 0 \\
0 & 0 & 0 \\
0 & 1/2 & 1/2
\end{pmatrix}
\cdot
\begin{pmatrix}
P \\
T_{air}^{rad,in} \\
T_{air}^{rad,out}
\end{pmatrix}
$$

	Nominal Value	Calculated Value	
		$U_{s,cool} \cdot A = 158900$	$U_{s,cool} \cdot A = 135000$
P	10 MW		-fixed-
T_s^{core}		637.0 °C	648.2 °C
$T_s^{core,out}$	662.8 °C	650.9 °C	662.1 °C
$T_s^{core,in}$	635.0 °C	623.2 °C	634.3 °C
$T_s^{h.e.}$		637.0 °C	648.2 °C
$T_s^{h.e.,in}$	662.8 °C	650.9 °C	662.1 °C
$T_s^{h.e.,out}$	635.0 °C	623.2 °C	634.3 °C
$T_{cool}^{h.e.}$		574.1 °C	574.1 °C
$T_{cool}^{h.e.,out}$	593.3	596.1 °C	596.1 °C
$T_{cool}^{h.e.,in}$	551.7 °C	552.1 °C	552.1 °C
T_{cool}^{rad}		574.1 °C	574.1 °C
$T_{cool}^{rad,out}$	551.7 °C	552.1 °C	552.1 °C
$T_{cool}^{rad,in}$	593.3 °C	596.1 °C	596.1 °C
T_{air}^{rad}		93.3 °C	93.3 °C
$T_{air}^{rad,out}$	148.9 °C	-fixed-	-fixed-
Γ_{air}	88 kg/s	88.67 kg/s	88.67 kg/s

Table 2.14: Case 1 - solution

Observing the table of results of Case 1 it is worth underlining the difference between fuel-salt temperatures when calculated with $U_{s,cool} \cdot A = 158900$ and their nominal values, which are very similar to the ones found with $U_{s,cool} \cdot A = 135000$, which is the modified value. It can be concluded that the value of the total heat exchange coefficient given in reports is overestimated. Coolant-salt temperatures are in both calculations very similar to their nominal values. Air mass flow is the same in both calculations and it is very close to the value given by reports when MSRE is working at its nominal power (10 MW).

Second Case - Temperature Imposed

In the second case air flow is fixed at 88 kg/s. Core outlet fuel-salt temperature is fixed and equal to 663 °C. Solution for vector of unknown variables is given in Table 2.15. The matrix product to be solved is the following one:

$$
\begin{pmatrix}
k_{eq} & -k_{eq} & \Gamma_s \cdot c_s & 0 & 0 & 0 & 0 & 0 & 0 \\
0 & 1 & -1/2 & 0 & 0 & 0 & 0 & 0 & 0 \\
0 & 0 & 0 & 0 & -1 & 0 & 0 & 0 & 0 \\
0 & 0 & 1 & 0 & 0 & -1 & 0 & 0 & 0 \\
0 & 0 & 0 & U_{s,cool} & -\Gamma_s \cdot c_s & \Gamma_s \cdot c_s & -U_{s,cool} & 0 & 0 \\
0 & 0 & 0 & 1 & -1/2 & -1/2 & 0 & 0 & 0 \\
0 & 0 & 0 & U_{s,cool} & 0 & 0 & -U_{s,cool} & -\Gamma_{cool} \cdot c_{cool} & \Gamma_{cool} \cdot c_{cool} \\
0 & 0 & 0 & 0 & 0 & 0 & 1 & -1/2 & -1/2 \\
0 & 0 & 0 & 0 & 0 & 0 & 0 & -1 & 0 \\
0 & 0 & 0 & 0 & 0 & 0 & 0 & 0 & 1 \\
0 & 0 & 0 & 0 & 0 & 0 & 0 & 0 & 0 \\
0 & 0 & 0 & 0 & 0 & 0 & 0 & 0 & 0 \\
0 & 0 & 0 & 0 & 0 & 0 & 0 & 0 & 0 \\
0 & 0 & 0 & 0 & 0 & 0 & 0 & 0 & 0
\end{pmatrix}
\cdots
$$

$$
\cdots
\begin{pmatrix}
0 & 0 & 0 & 0 & 0 & \gamma_s \\
0 & 0 & 0 & 0 & 0 & 0 \\
0 & 0 & 0 & 0 & 0 & 0 \\
0 & 0 & 0 & 0 & 0 & 0 \\
0 & 0 & 0 & 0 & 0 & 0 \\
0 & 0 & 0 & 0 & 0 & 0 \\
0 & 0 & 0 & 0 & 0 & 0 \\
0 & 0 & 0 & 0 & 0 & 0 \\
0 & 0 & 1 & 0 & 0 & 0 \\
0 & -1 & 0 & 0 & 0 & 0 \\
U_{cool,air} & \Gamma_{cool} \cdot c_{cool} & -\Gamma_{cool} \cdot c_{cool} & -U_{cool,air} & 0 & 0 \\
1 & -1/2 & -1/2 & 0 & 0 & 0 \\
U_{cool,air} & 0 & 0 & -U_{cool,air} & -\Gamma_{air} \cdot c_{air} & 0 \\
0 & 0 & 0 & 1 & -1/2 & 0
\end{pmatrix}
\cdot
$$

$$
\cdot
\begin{pmatrix}
T_s^{core} \\
T_s^{core,in} \\
T_s^{h.e.} \\
T_s^{h.e.,in} \\
T_s^{h.e.,out} \\
T_{cool}^{h.e.} \\
T_{cool}^{h.e.,out} \\
T_{cool}^{h.e.,in} \\
T_{cool}^{rad} \\
T_{cool}^{rad,out} \\
T_{cool}^{rad,in} \\
T_{air}^{rad} \\
T_{air}^{rad,out} \\
P
\end{pmatrix}
=
\begin{pmatrix}
\Gamma_s \cdot c_s & 0 & 0 \\
1/2 & 0 & 0 \\
-1 & 0 & 0 \\
0 & 0 & 0 \\
0 & 0 & 0 \\
0 & 0 & 0 \\
0 & 0 & 0 \\
0 & 0 & 0 \\
0 & 0 & 0 \\
0 & 0 & 0 \\
0 & 0 & 0 \\
0 & 0 & 0 \\
0 & -\Gamma_{air} \cdot c_{air} & 0 \\
0 & 1/2 & 0
\end{pmatrix}
\cdot
\begin{pmatrix}
T_s^{core,out} \\
T_{air}^{rad,in} \\
\Gamma_{air}
\end{pmatrix}
$$

	Nominal Value	Calculated Value	
		$U_{s,cool} \cdot A = 158900$	$U_{s,cool} \cdot A = 135000$
P	10 MW	10.19 MW	10.00 MW
T_s^{core}		648.6 °C	648.9 °C
$T_s^{core,out}$	662.8 °C	-fixed-	-fixed-
$T_s^{core,in}$	635.0 °C	634.5 °C	635.0 °C
$T_s^{h.e.}$		648.6 °C	648.9 °C
$T_s^{h.e.,in}$	662.8 °C	662.8 °C	662.8 °C
$T_s^{h.e.,out}$	635.0 °C	634.5 °C	635.0 °C
$T_{cool}^{h.e.}$		584.5 °C	574.8 °C
$T_{cool}^{h.e.,out}$	593.3 °C	607.0 °C	596.8 °C
$T_{cool}^{h.e.,in}$	551.7 °C	562.1 °C	552.7 °C
T_{cool}^{rad}		584.5 °C	574.8 °C
$T_{cool}^{rad,out}$	551.7 °C	562.1 °C	552.7 °C
$T_{cool}^{rad,in}$	593.3 °C	607.0 °C	596.8 °C
T_{air}^{rad}		94.8 °C	93.8 °C
$T_{air}^{rad,out}$	148.9 °C	151.8	149.8
Γ_{air}	88 kg/s	-fixed-	-fixed-

Table 2.15: Case 2 - solution

Air mass flow and fuel-salt core outlet temperature are fixed. Power is an unknown variable. Observing the table of results of Case 2, it is important to still underline the difference between nominal coolant-salt temperatures and their values when calculated with $U_{s,cool} \cdot A = 158900$. On the contrary, when coolant-salt temperatures are calculated with $U_{s,cool} \cdot A = 135000$, they result very similar to the nominal values.

Fuel-salt temperatures are in both calculations very similar or equal to their nominal values. Air temperature when leaving radiator is found to be almost the same as given in reports. Also, calculated power is very similar or equal to its nominal value of 10 MW.

2.5 ϵ-NTU method for heat exchanger and radiator performance analysis

The *ϵ-NTU method* is a particular approach to the analysis of heat exchangers. It is based on the definition of a new parameter, ϵ, which is the ratio of the actual heat transfer rate to the maximum possible heat transfer rate [16].

$$\epsilon = \frac{q}{q_{max}} \tag{2.21}$$

By definition the effectiveness, which is dimensionless, must be in the range $0 \leq \epsilon \leq 1$. For any heat exchanger it can be shown that [17]:

$$\epsilon = f\left(NTU, \frac{C_{min}}{C_{max}}\right) \tag{2.22}$$

where C_{min}/C_{max} is equal to C_c/C_h or C_h/C_c, depending on the relative magnitudes of the hot and cold fluid heat capacity rates. The *number of transfer units* (NTU) is a dimensionless parameter that is defined as:

$$NTU \equiv \frac{U \cdot A}{C_{min}} \tag{2.23}$$

The *effectiveness to NTU* relations have been developed for a variety of heat exchangers. For a *shell-and-tube heat exchanger* with only one shell pass the relation is given in Equation 2.24 [16]. The graphic showing the trend of this function, for different values of C_r is given in Figure 2.5.

$$\epsilon = 2 \cdot \left\{1 + C_r + \left(1 + C_r^2\right)^{1/2} \cdot \frac{1 + \exp\left[-\left(NTU\right) \cdot \left(1 + C_r^2\right)^{1/2}\right]}{1 - \exp\left[-\left(NTU\right) \cdot \left(1 + C_r^2\right)^{1/2}\right]}\right\}^{-1} \tag{2.24}$$

where C_r is the heat capacity ratio: $C_r \equiv C_{min}/C_{max}$.
The inverted relation, *NTU to effectiveness*, for the same type of heat exchanger is:

$$NTU = -\left(1 + C_r^2\right)^{-1/2} \cdot \ln\left(\frac{E-1}{E+1}\right) \tag{2.25}$$

with

$$E = \frac{2/\epsilon - (1 + C_r)}{\left(1 + C_r^2\right)^{1/2}} \tag{2.26}$$

When equation 2.25 is applied, the effectiveness ϵ is calculated as:

$$\epsilon = \frac{C_h \cdot (T_{h,i} - T_{h,o})}{C_{min} \cdot (T_{h,i} - T_{c,i})} \tag{2.27}$$

The $\epsilon - NTU$ method has been applied for the heat exchanger of the MSRE. Nominal fuel-salt and coolant-salt inlet and outlet temperatures and nominal salt flows have been used to evaluate $\epsilon - NTU$ method parameters. Results are given in Table 2.16.

The evaluation of the product $U \cdot A$ with the $\epsilon - NTU$ method gives the same result previously obtained when ΔT_{lm} has been used to calculate this value, so that all parameters concerning the heat exchanger(mass flows, inlet and outlet temperatures, power exchanged evaluated in different ways, etc.) result coherent with each other.

Moreover, it is possible to state that the nominal value of $U \cdot A$ should be *0.135 MW/°C* and the nominal value of *overall heat transfer coefficient* U, should be *5721 W/(m^2·°C)*.

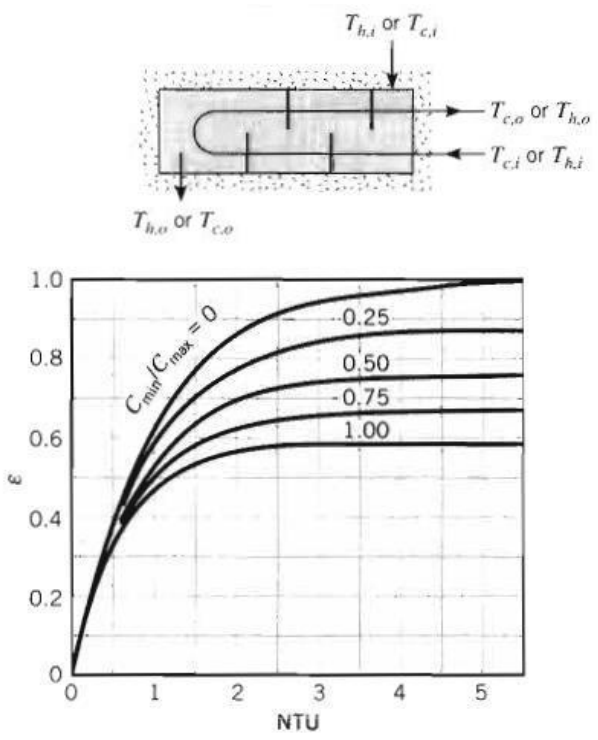

Figure 2.5: Effectiveness of a shell-and-tube heat exchanger with one shell and any multiple of two passes (two, four, etc. tube passes) (Equation 2.24 and 2.25)

Number of Shell Passes	1	
Number of Tubes	159	
Number of Tube Passes	318	
C_h	360.4×10^3	W/°C
C_c	246.0×10^3	W/°C
C_r	0.683	
ϵ	0.366	
E	3.12	
NTU	0.549	
$U_{s,cool} \cdot A^{h.e.}$	135.0×10^3	W/°C

Table 2.16: Evaluation of heat exchanger performance with $\epsilon - NTU$ method

The same method has been used to analyze the radiator, which is a cross-flow heat exchanger. Coolant-salt is the tube side fluid and air is the external fluid. Air flow is mixed. Coolant-salt flow is unmixed as it passes through the tubes. For a *Cross flow heat exchanger* with one fluid *mixed* and the other *unmixed*, the *effectiveness to NTU* and the *NTU to effectiveness* relations are given in Equations 2.28 and 2.30 [16].

$$C_{max} \textbf{ (mixed)}, C_{min} \textbf{ (unmixed)}$$

$$\epsilon = \frac{1}{C_r} \cdot \left(1 - \exp\left\{-C_r \left[1 - \exp\left(-NTU\right)\right]\right\}\right) \tag{2.28}$$

$$C_{min} \textbf{ (mixed)}, C_{max} \textbf{ (unmixed)}$$

$$\epsilon = 1 - \exp\left(-C_r^{-1} \left\{1 - \exp\left[-C_r \cdot (NTU)\right]\right\}\right) \tag{2.29}$$

$$C_{max} \textbf{ (mixed)}, C_{min} \textbf{ (unmixed)}$$

$$NTU = -\ln\left[1 + \frac{1}{C_r} \cdot \ln(1 - \epsilon \cdot C_r)\right] \tag{2.30}$$

$$C_{min} \textbf{ (mixed)}, C_{max} \textbf{ (unmixed)}$$

$$NTU = -\frac{1}{C_r} \cdot \ln\left[C_r \cdot \ln(1 - \epsilon) + 1\right] \tag{2.31}$$

The graphic showing the trend of these functions for different values of C_r is given in Figure 2.6. Effectiveness ϵ is calculated as it was in the previous case (Equation 2.27). Nominal coolant-salt, air inlet and air outlet temperatures, and nominal mass flows have been used to evaluate $\epsilon - NTU$ method parameters. Results are given in Table 2.17.

As it was mentioned at page 27, for what concern the radiator of MSRE, there is a good consistency between the values given by reports and the ones found through calculations.

Air Mass Flow		88	kg/s
C_h	UNMIXED	246.0 $\times 10^3$	W/°C
C_c	MIXED	89.3 $\times 10^3$	W/°C
C_{min}	MIXED	246.0 $\times 10^3$	W/°C
C_{max}	UNMIXED	89.3 $\times 10^3$	W/°C
C_r		0.363	
ϵ		0.2066	
NTU		0.2417	
$U_{cool,air} \cdot A^{rad}$		21.6 $\times 10^3$	W/°C

Table 2.17: Evaluation of radiator performance with $\epsilon - NTU$ method

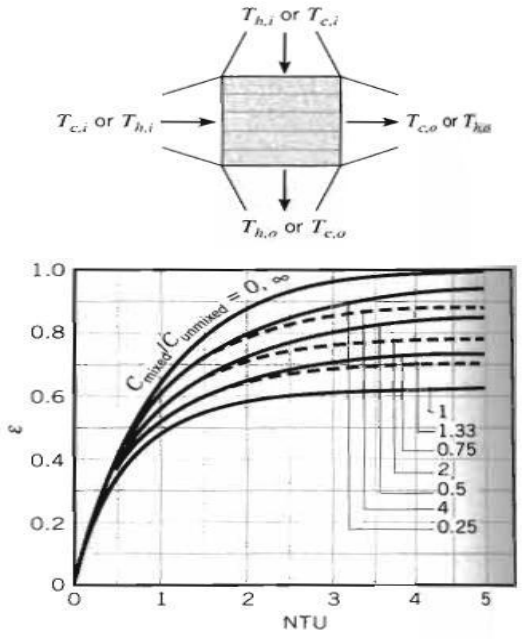

Figure 2.6: Effectiveness of a cross flow heat exchanger (Equations 2.28, 2.29, 2.30 and 2.31)

2.6 Brief description of control requirements and control strategy

In order to evaluate the actual data of the MSRE in steady-state condition it is necessary to have a knowledge of the control strategy adopted. Discussing the control of the MSRE, the most important feature of MSRE is that it is self-stabilizing and the system does not tend to run away following a power raise. This is due to the

negative temperature coefficients of both graphite and fuel salt, as it can be observed in Table 2.18. A power increase causes an increase of fuel and graphite temperatures. As temperatures increase, the feedback on reactivity is negative (see Chapter 4). In addition, the temperature gradients are no problem. As a result the control rods can be operated in the simplest manner possible, consistent with good reactivity control.

Thermal Feedback Coeffcients

	^{233}U fuel	^{235}U fuel	
Graphite temperature coefficient, α_g	-5.81	-6.66	pcm/°C
Fuel salt temperature coefficient, α_s	-11.03	-8.71	pcm/°C

Table 2.18: Values of thermal feedback coefficents for ^{233}U and ^{235}U fuel

In general, the two shim rods will be kept at equal distances of insertion, and the servo-operated regulating rod [4] will be inserted deeper to keep the tip out of the "shadow" of the shim rods. It's noteworthy that the capability of adding uranium at any time to compensate for burnup and stable poison buildup permits steady operation at full power with the rods almost completely withdrawn.

However the transient effects, such as those of ^{135}Xe and ^{149}Sm, will be compensated by control rod manipulation. The only requirement is that the rods be deep enough so that the insertion of negative reactivity is not delayed by travel time in regions of low effectiveness. The driven speed of all three rods is 1,27 cm/s in both directions [8].

One of the main requirements is that salts temperatures have to stay above 450 °C so that salt remains molten. This requirement is satisfied in the MSRE by helding constant the core outlet temperature of fuel salt as power is reduced. Its value is fixed at 663 °C. This implies that inlet fuel salt temperature, and coolant salt temperature also, increase as power level decreases [5]. It will be shown further that with this kind of operating strategy the minimum fuel salt and coolant salt temperatures are widely higher than their melting point. Also, the minimum temperaure is reached when the reactor is operating at full power. Indeed, the coolant salt at full power is about 540 °C (versus a melting temperature of 450 °C).

Fuel-salt and coolant-salt mass flows remain fixed at their nominal values even when the reactor is run at a power level lower than the full one. Nevertheless, since when the thermal power of the reactor is lower than full power, the heat removal request is lower, the air mass flow through radiator has to decrease as power decreases [6]. On the contrary, the air temperature leaving the radiator increases as the power level decreases (see Figure 2.7 and 2.8). At partial loadings of the reactor, the air flow will

[4] The two shim rods are for long-term control of reactivity (e.g. loss of reactivity because of poisons accumulation or fuel burnup), while the regulating rod is for subtle regulation of power level

[5] Actually, in the "starting mode" of operation at reactor power levels below 1 MW, the nuclear power is held constant. In the "run mode", at power levels above 1 MW, the fuel-salt temperature leaving the reactor is held constant (see report [6]).

be regulated by the by-pass damper, by changing the radiator door position, and by on-off control of the blowers.

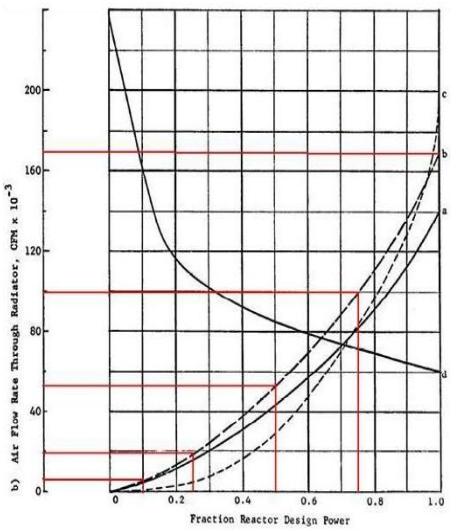

Figure 2.7: Air mass flow through radiator

2.7 Actual data - steady-state reactor power levels

In the following paragraphs, it will be faced the mismatch that was observed between ORNL prediction and experimental data found during operation of MSRE. First, a general description of this issue will be given. Further on, the causes of this disagreement will be discussed, and a new characterization of the reactor working in steady states will be developed. This steady-state characterization will be carried out at almost all power levels, going from full power to 10% of full design power [6].

During early power operation the heat transfer capability was found to be considerably lower than expected. At the time the design review was completed in 1966, it was concluded that the design methods were appropriate and the assumptions conservative [12]. The three remaining possible causes of low heat transfer were [12]:

1. That a build-up of scale was occurring on the tubes even though this was believed impossible.

2. That the tube surfaces were being blanketed with a gas film.

[6] At powers lower than 1 MW the neutron flux will be controlled directly, and the heat removal will be manually balanced against production (see report [8]). This is because heat losses of the system are not anymore negligible below this power level. Also, 1 MW of heat removed was used as the starting point of the automatic load system, altough this system was never used during operation of reactor (see report [9]).

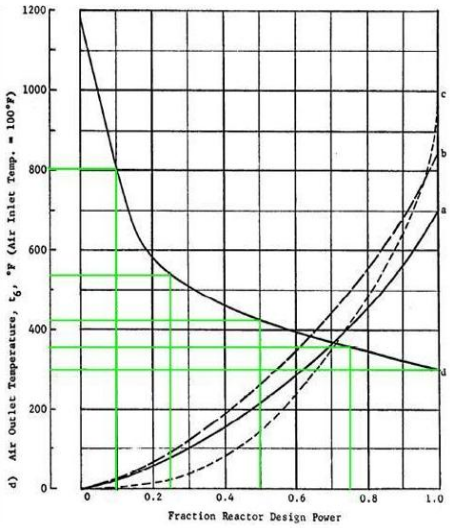

Figure 2.8: Air outlet temperature

3. That the physical properties of the fuel and coolant salts used in the design were not the correct valus.

Subsequent operation of the reactor shown that the heat transfer was constant with time, indicating no build-up of scale and that there was no evidence of gas filming. However, when the MSRE was first operated at significant power levels, the heat exchanger performance was observed to be below the design value. The conclusions reached were that the heat exchanger had been properly designed using the salt physical property data available at that time but that some of the physical properties, the thermal conductivity in particular, were in fact substantially different from the values used in the design. A reevaluation of the physical properties showed that the thermal conductivity of both the fuel and the coolant salt was sufficiently below the value used in design to account for the overestimate of the overall heat transfer coefficient [12].

Table 2.19 shows a comparison of the physical property data used in the original design to the actual data. The heat transfer coefficents re-calculated using these two sets of data are also shown [12]. For what concern the radiator, a little discrepancy between the re-calculated and observed performance was found. The cause for this discrepancy has not been definitely established.

The initial overestimate of the heat exchanger performance was completely resolved by the revised physical property data for the fuel and coolant salts. During subsequent operation of the reactor no loss of heat transfer capacity was found and no other difficulties occurred [9].

Fuel-salt and coolant-salt temperatures have been re-calculated with new values of overall heat transfer coefficient but keeping the nominal thermal power the same

		Original		Current	
		Fuel	Coolant	Fuel	Coolant
Thermal conductivity	W/(m·°C)	4.76	6.06	1.44	1.14
Viscosity	Pa·s	0.0074	0.0083	0.0077	0.0098
Density	kg/m^3	2472	1922	2262	1972
Specific Heat	J/(kg ·°C)	1926	2386	1982	2416
Film coefficient	W/(m^2·°C)	20000	32040	8500	11300
Overall coefficient	W/(m^2· °C)	6734		3509	
$U_{s,cool}$· A	W/°C	135 $\times 10^3$		82.8 $\times 10^3$	

Table 2.19: Physical properties of fuel and coolant salts used in MSRE heat exchanger design and evaluation

as it was in the first analysis (see page 32). It is evident that obtained results would not have been acceptable, since, within the core, fuel-salt temperatures would be way higher than their nominal values, see Table 2.20.

It was immediately evident that so high temperatures in the core (up to 740 °C) were not tolerable. The nominal power had to be lowered so that fuel-salt maximum temperature was respected and close to its nominal value of 663 °C. The new nominal full power was established to be 8 MW [9].

In order to find the values of temperatures and mass flows when the reactor is operating at partial loadings, it is necessary to know which parameters remain fixed and which others change in order to obtain the desired power level. As it was described in section 2.6, fuel salt and coolant salt mass flows do not vary as power level is changed. Indeed, the control of the power level of MSRE is achieved through the variation of the radiator heat removal capability. As the goal is to decrease (increase) power level, the radiator heat removal capability is decreased (increased). Consequently, coolant salt temperature and, with the loop-typical transport delays, fuel salt temperature increase (decrease). Therefore, because the temperature coefficients of rectivity of both fuel salt and grafite are negative, the thermal feedbacks lead to the desired effect, lowering (raising) the thermal power. Clearly, this effect is primarily due to the fuel salt reactivity coefficient, since it takes longer for the graphite to feel the temperature alteration because of salt and graphite heat capacities. Thereof, it is evident that the reactor is operated with a "reactor follows" control strategy.

2.7.1 Extrapolated functions of temperatures and heat transfer coefficients

In the following pages, all fundamentals parameters, such as salt and air temperatures, air flow and log mean ΔTs, are plotted as a function of power where power is the indipendent variable. A new characterization of steady-states at different power levels is obtained, coherently with the actual data (new values of physical properties) found

		Hypotetical temperature values for $U_{s,cool} \cdot A = 82.8 \times 10^3$
P	10 MW	-fixed-
T_s^{core}		721.2 °C
$T_s^{core,out}$	662.8 °C	735.9 °C
$T_s^{core,in}$	635.0 °C	706.5 °C
$T_s^{h.e.}$		721.2 °C
$T_s^{h.e.,in}$	662.8 °C	735.9 °C
$T_s^{h.e.,out}$	635.0 °C	706.5 °C
$T_{cool}^{h.e.}$		600.4 °C
$T_{cool}^{h.e.,out}$	593.3 °C	620.0 °C
$T_{cool}^{h.e.,in}$	551.7 °C	580.9 °C
T_{cool}^{rad}		600.4 °C
$T_{cool}^{rad,out}$	551.7 °C	620.0 °C
$T_{cool}^{rad,in}$	593.3 °C	580.9 °C
T_{air}^{rad}		93.3 °C
$T_{air}^{rad,out}$	148.9 °C	-fixed-
Γ_{air}		88.67 kg/s

Table 2.20: Hypotetical value of fuel and coolant salt temperatures with power and $T_{air}^{rad,out}$ fixed

through the years the reactor has been operated.

These functions will be scaled to the actual data which were found during MSRE operation and compared with their trand as they were taken from the nominal-design values given before the heat transfer capability of heat exchanger was found to be less than designed (see page 41). Moreover, these functions will be used to find the actual values of temperatures and other parameters.

As it was previously discussed (see footnote, page 40), the range of validity of this equation goes from full power, (design power or actual-experimental), to 10% of full power, since at lower power the control strategy is different (nuclear power is held constant instead of fuel outlet temperature). The functions reproducing experimental data are scaled from the original-design ones, equalizing, for diffent values of power, the mean logarithmic ΔTs resulting from the following two different formulations:

$$\Delta T_{lm} = \frac{P}{U_{s,cool} \cdot A} \tag{2.32}$$

$$\Delta T_{lm} = \frac{(T_h - T_c)_2 - (T_h - T_c)_1}{ln\frac{(T_h - T_c)_2}{(T_h - T_c)_1}} \tag{2.33}$$

Interpolating the points found at these differnt power levels, the analitical functions describing air mass flow, heat transfer coefficient, air outlet temperature have been found. The extrapolated functions are presented in the following list, and their trends are graphed and compared to the orignal ones in Figures 2.9, 2.10, 2.11, 2.12 and 2.13.

- Air mass flow [m^3/s] as a function of thermal power [MW]:

$$\Gamma_{air}(P) = 0.7202\,P^2 + 1.9036\,P - 0.0949 \tag{2.34}$$

- Overall heat transfer coefficient times heat transfer area [W/°C] as a function of thermal power [MW]:

$$U_{cool,rad} \cdot A(P) = 2202\,P + 233.18 \tag{2.35}$$

- Air outlet temperature [°C] as a function of thermal power [MW]:

$$T_{air}^{rad,out}(P) = 0.2329\,P^4 - 5.6096\,P^3 + 50.103\,P^2 - 214.99\,P + 866.79 \tag{2.36}$$

- Air outlet temperature [°C] as a function of air mass flow [m^3/s]:

$$T_{air}^{rad,out}(\Gamma_{air}) = 543.77\,\Gamma_{air}^{-0.288} \tag{2.37}$$

- Overall heat transfer coefficient times heat transfer area [W/°C] as a function of air mass flow [m^3/s]:

$$U_{cool,rad} \cdot A(\Gamma_{air}) = -2.1948\Gamma_{air}^2 + 395.96\Gamma_{air} + 1853 \tag{2.38}$$

Air outlet temperature has a certain variation with power (see Figure 2.13) so that, being air inlet temperature and core outlet temperature of fuel salt held constant (as it happens when the reactor is operated), it can be observed that the ΔT_{lm} on radiator remains roughly constant as power varies. This condition implies that, being $P = U_{cool,air} \cdot A \cdot (\Delta T_{lm})$, the product $U_{cool,air} \cdot A$ varies linearly with power (see Figure 2.11). Moreover, since Γ_{air} varies nonlinearly with power (see Figure 2.9), it follows that $U_{cool,air} \cdot A$ varies nonlinearly with Γ_{air} (see Figure 2.10).

Air mass flow Γ_{air}, as it was said before, can be regulated in three ways: by means of a by-pass damper, which regulates the air flow, by on-off control of the blowers (below 5 MW one blower only is exerted), and by adjusting the radiator door position. Since air flow diminishes more than linearly with power, $U_{cool,air} \cdot A$ diminishes less than linearly with air flow. In more detail, it should be analysed how the two factors of this product vary, since actually the control of air flow rate is done by decreasing the ingoing section into radiator. Therefore, less exchanging surface of tubes is cooled down by the air flow and a decrease of actusl heat transfer area is obtained. Nevertheless, in this work the whole product $U_{cool,air} \cdot A$ will always be considered, since it doesn't worth going into more details to achieve the prefixed goal, which is to study the dynamical behaviour of the whole power plant.

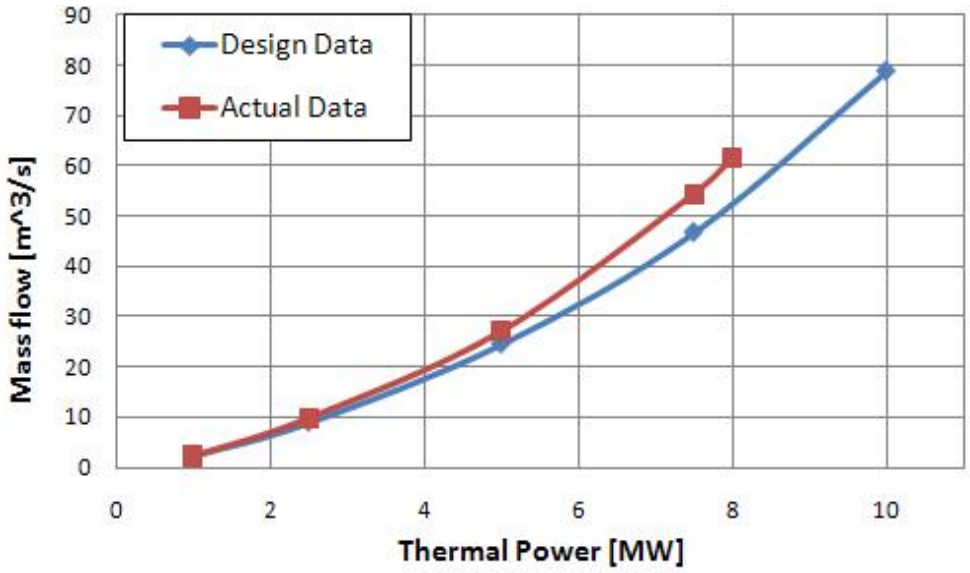

Figure 2.9: Air flow as a function of power

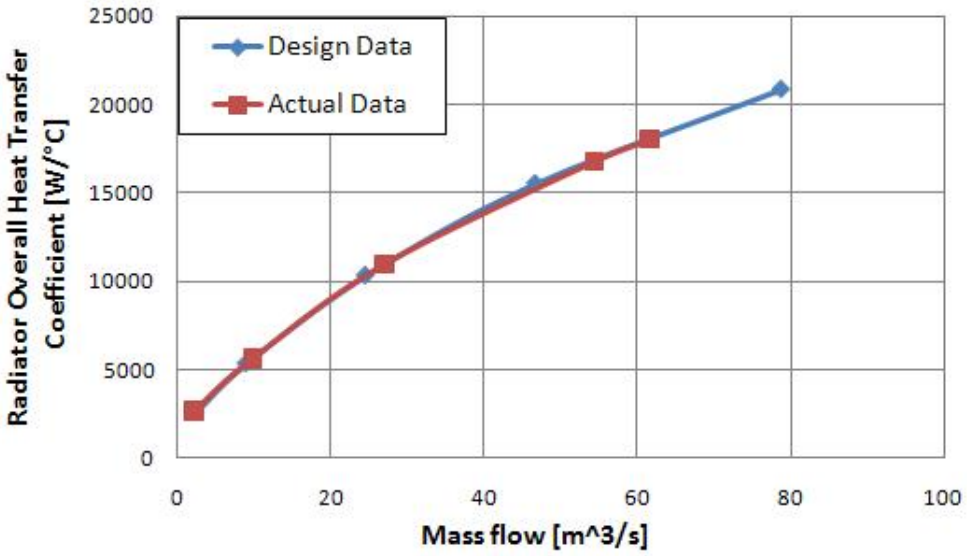

Figure 2.10: $U_{cool,air} \cdot A$ as a function of air mass flow

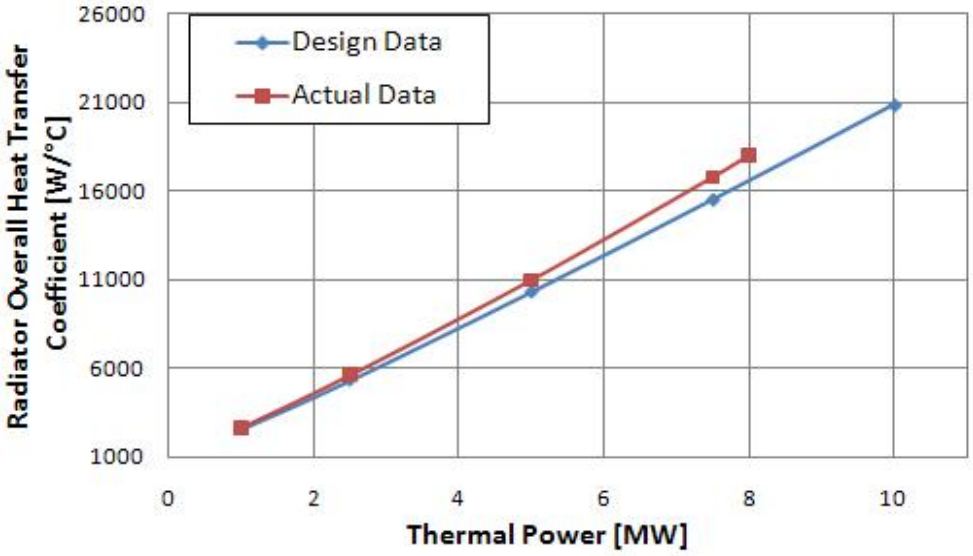

Figure 2.11: $U_{cool,air} \cdot A$ as a function of power

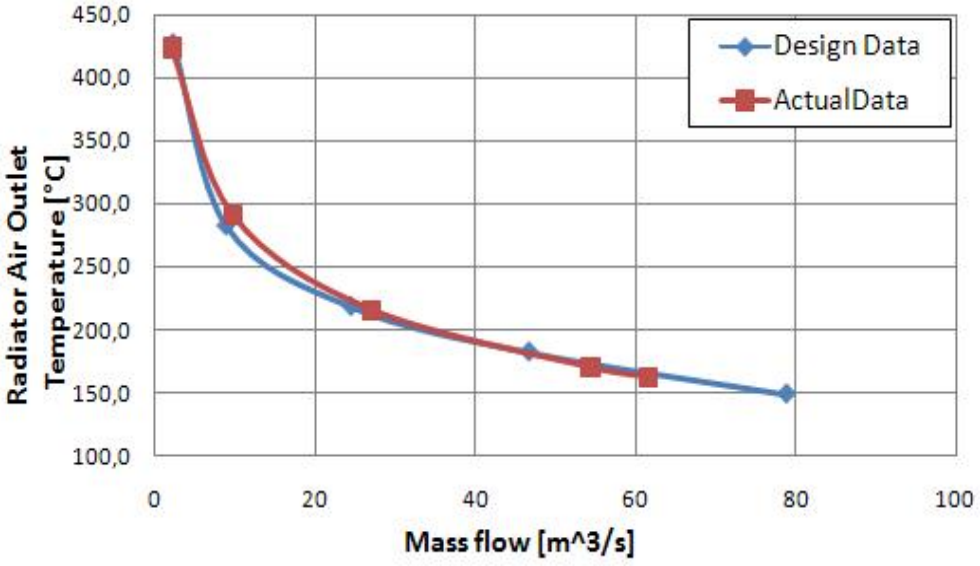

Figure 2.12: Air outlet temperature as a function of air mass flow

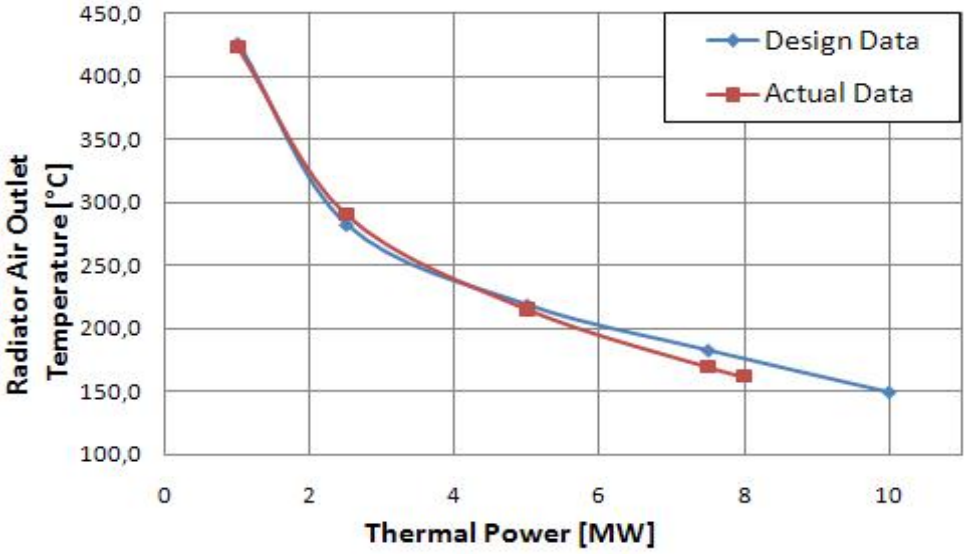

Figure 2.13: Air outlet temperature as a function of power

Chapter 3

The MSRE dynamics

The objective of this chapter is to create a model of the MSRE plant. The model will have to include the core, taking into account the power generation in the fuel salt and in the graphite core structure, the circulation of fuel salt, the heat exchanging between fuel salt and coolant salt, circulation of coolant salt and heat dissipation of coolant while going through the radiator. The purpose of this work is a model suitable for a preliminary analysis of MSRE plant dynamics, capable of reproducing the behaviour of the whole plant during transients. The model will have to be appliable for studying both operating and accidental conditions (starting from a stationary state at any power level).

In the light of the prefixed goal, it can be stated that the main interest is the evaluation and the observation of the integral quantities, such as thermal power, and of some significant local quantities, such as fuel salt temperature in the core region. For simplicity zero-dimensional neutron kinetics is adopted in all this work. Consequently, thermal feedback (due to temperature coefficient of reactivity) are assumed to be dependant upon average temperatures, which are representative of the overall situation of the core graphite and of the fuel salt within the core. Therefore, single channel analysis is not necessary for the purpose of computing thermal feedbacks.

Also, as models will be either zero or one-dimensional, radial profile of the core temperature is not simulated, while the axial tmeperature profile is reproduced when the one-dimensional models are considered. For the sake of reproducing the plant dynamic behaviour temperatures regarded as the most significant ones are average, inlet and outlet temperatures of the fuel salt in each component that will be modelled. The features and limits of any implemented model will be discussed. The main simplifications and approximations adopted are listed and discussed here below and the most important issues will be recovered as they will emerge again during the adjustment of the model.

First of all, it is noteworthy that neutron slowing down and diffusion are not reproduced in any of the model. Neutrons are assumed to originate as already thermalized

("one energy-group approximation" is always employed) and neutron kinetics is taken as zero-dimensional in all models. Nevertheless, the axial profile of power generation is reproduced in one-dimensional models since power generation, calculated as directly proportional to neutron population, is properly distributed over the core height.

A repartition coefficient is used in order to consider that a fraction of power is generated in graphite and the complementary fraction is generated in the fuel salt. Power generation has been considered to occur entirely within the core height, indeed decaying of precursors in the out-of-core primary loop is neglected.

Modelling of precursors (fission fragments which are going to decay to fission products emitting one or more neutrons) consists of a six groups approximation, each of these with its characteristic mean life. A distinctive feature of molten salt reactors is that fuel is circulating. Thereof, a fraction of precursors leaves the core (*precursor drift*) and decays in the primary loop before reentering the core, therefore leading to a net loss of reactivity. This loss of reactivity has to be compensated, otherwise the reactivity would be negative and the reactor would shut down, not being able to remain critical.

As mentioned, the objective of this work is to obtain a plant model suitable for studying the transient response of the reactor. It can be stated that the dynamic behaviour of the reactor is an outcome which depends primarily of three factors: energy generation (which depends on neutronics), heat transfer (between the graphite and the fuel salt, and from the fuel salt to the coolant salt) and heat removal from the plant.

The energy generation is regulated by the reactivity insertion/withdraw through the control rods and by the influence of graphite and fuel salt temperatures on the value of reactivity. Modelling of neutron popultation, including thermal feedbacks, and precursor drift achieve this goal. For what concern heat transfer and removal, the matter is obtainining a reliable reproduction of temperatures and temperature differences in the power plant components. In order to accomplish this goal, the energy conservation law constitutes the basis of the implemented models, while mass and momentum conservation laws have not been used in the construction of the model. It follows that no pressure drops during fuel salt and coolant salt circulation have been modelled.

Also, it is assumed that the fuel salt pump always ensures the nominal salt flow rate, except in flow rate transients, such as in case of a pump break (see page 110), or in case of flow rate transients. Transit times (from a component to the next one) are managed as assigned constant values except in the mentioned cases.

The mass flux (the mass flow over the cross section, measured in kg/m^2s) is constant because of mass conservation law. However, a constant mass flux can not be rendered in considering salt speed to be constant and always equal to a certain value. Indeed, fuel velocity is constant in the axial direction when salt is going through the core or the heat exchanger, because of effects of temperatures change. When the salt warms up, its

density reduces and, if salt mass flow remains the same, its speed increases. Viceversa, when the salt cools down, the opposite effect is observed: its velocity decreases as its density increases. The most important consequence of the density variation is its feedback on reactivity: as the fuel salt density decreases, less fuel is contained in the core height. Therefore, as density increases the feedback on reactivity is positive and viceversa. However, since the fluids are modelled as incompressible in the model equations (mass and momentum conservation are not modelled), this density effect it is directly included in the thermal feedback coefficients α_g and α_s. They are also comprehensive of the Doppler effect, which contributes to the negative feedback on reactivity, too.

Moreover, heat losses occurring during fuel salt circulation and coolant salt circulation are neglected (and negligible in a certain range of thermal power, from over 100% to ≈10% of full power, which is also the range of validity of the developed models, see page 40), therefore all thermal power generated in the fuel salt is transferred to the coolant and then dumped to the air radiator. Finally, no external forces are applied to the fluid in the components which are considered in the developed models.

Thereof, the law of energy conservation simplifies (kinetic energy terms are negligible if compared to others):

$$\rho\, V\, \frac{d\, u}{dt} \;=\; \dot{m}\, h_{in} - \dot{m}\, h_{out} + q + \rho\, V\, Q_g \tag{3.1}$$

where:
ρ = specific mass [kg/m^3]
h = specific enthalpy [J/kg]
u = internal energy [J/kg]
V = control volume [m^3]
q = inward heat flow [W]
Q_g = power generation density [W/kg]

Now, definition of enthalpy is introduced:

$$h \;=\; u + p\, v\ , \tag{3.2}$$

where:
p = pressure [Pa];
v = specific volume [m^3/kg].

Neglecting the term p v, and knowing that the internal energy is defined as:

$$u \;=\; c\, T \tag{3.3}$$

where $c = c_p = c_v$ since the fluid is assumed to be incompressible, and also knowing that all physical properties (such as specific heat capacities, thermal conductivities,

etc.) are assumed not to vary with temperature, time and space[1], it results:

$$M\ c\ \frac{dT}{dt}\ =\ \dot{m}\ c\ (T_{in} - T_{out}) + A\ q'' + P_g \tag{3.4}$$

where:
A = area bounding the control volume [m^2]
q" = inward heat flux [W/m^2]
c = specific heat capacity [J/(kg K)]
M = mass contained in the control volume [kg]
P_g = power generated in the control volume [W]

Finally, the Newton's law for heat flux was introduced in order to model the heat exhange between fuel salt and graphite:

$$q''\ =\ \hat{h}\ (T_{g,surf} - T_{s,bulk}) \tag{3.5}$$

where:
$\hat{h}$ = heat transfer coefficient [$W/(m^2\ K)$]
$T_{g,surf}$ = surface temperature of the graphite [K]
$T_{s,bulk}$ = bulk temperature of the salt [K]

However, knowing that all the models developed in this work will be at most one-dimensional, radial diffusion will not be solved in order to obtain a radial temperature profile in the channel or in the graphite block containing it. Thereof, the third type boundary condition becomes a continuity condition between the fuel bulk temperature and the graphite average temperature: an equivalent overall heat transfer coefficient k_{eq} in $W/(m^2\ K)$ regulates this difference (see footnote at page 25). This global coefficient is representative of convection in the fuel salt, also including power generation and the Poppendiek effect (see page 24), and conduction in the graphite blocks. Introducing power generation in the fuel salt which is cooling down the wall of graphite, the law of energy conservation becomes:

$$M\ c\ \frac{dT_{s,bulk}}{dt}\ =\ \dot{m}\ c\ (T_{s,in} - T_{s,out}) + A\ k_{eq}\ (T_{g,ave} - T_{s,bulk}) + P_g \tag{3.6}$$

Finally, in the models developed in the following sections the poisoning effect due to the build-up of stable neutron absorbers, such as the xenon, and the fuel burnup effect have been neglected. The model is not appropriate for long term simulation. However, it is not the objective of this work.

All models showed in this chapter, and developed and described in the following sections, refer to Figure 3.1. All models have been run with Simulink, a tool of

[1]This approximation is not acceptable for the thermal conductivity of the graphite, since its value is very different whether considering the longitudinal or axial direction (see Table 2.5). However, as it will be seen further on, conduction in the axial direction will be neglected in developed models.

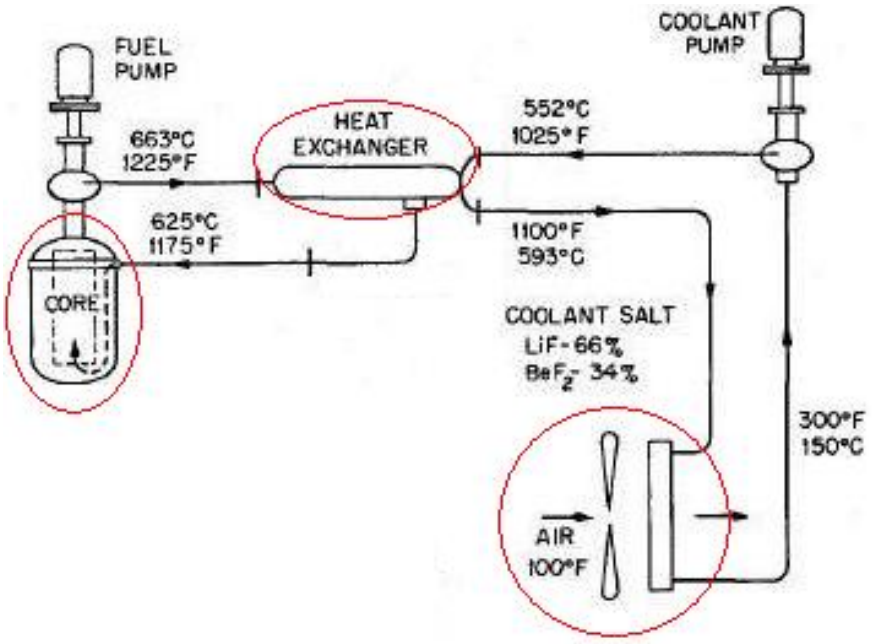

Figure 3.1: Simplified layout of MSRE: main components are red-rimmed

MATLAB® . A certain number of equations describes the neutronics, and so on for the core, the heat exchanger and the radiator. Some informations are conveyed from a group of equations to another one so that the equation system results solvable by the software. (To have a deeper look into the model architecture see page 74). As it will be further explained in section 3.5 all models are realized with Simulink, which is a tool capable of managing ordinary differential equations (ODE). The Simulink models are organized as a series of blocks, where the outputs of one are inputs for another one and so on. Starting from equations of neutronics, all differential equations inserted in Simulink are reported.

3.1 Zero-dimensional model

At first, the simplest approach was adopted for creating a preliminary model. It constists of a zero-dimensional model, where each of main components is represented with a very simple scheme.

First of all, a zero-dimensional neutron kinetics has been assumed, neglecting neutron slowdown, diffusion and transport. The differential equations describing core neutronics are: one equation for the neutron population in the core, and six equation for precursor population in the core (one for each group).

$$\frac{dn(t)}{dt} = \underbrace{\frac{\rho(t)-\beta}{\Lambda}\, n(t)}_{prompt\,neutrons} + \underbrace{\sum_{i=1}^{6} \lambda_i\, c_i(t)}_{delayed\,neutrons} \tag{3.7}$$

$$\frac{dc_i(t)}{dt} = \underbrace{-\lambda_i\, c_i(t)}_{decay\,in\,the\,core} + \underbrace{\frac{\beta_i}{\Lambda}\, n(t)}_{formation\,in\,the\,core} - \underbrace{\frac{c_i(t)}{\tau_c}}_{leaving\,the\,core} + \underbrace{\frac{c_i(t-\tau_l)\, e^{-\lambda_i\,\tau_l}}{\tau_c}}_{reentering\,the\,core}, \text{ for i=1:6} \tag{3.8}$$

where:
n = neutron population [neutrons]
t = time [s]
ρ = reactivity [2]
β = total delayed-neutron fraction
β_i = delayed-neutron fraction for i-th precursor group ($\sum_i \beta_i = \beta$)
Λ = prompt neutron lifetime [s]
λ_i = decay constant of i-th precursor group [s^{-1}]
c_i = i-th precursor population [i-th precursors]
τ_c = core transit time [s]
τ_l = primary loop transit time (except the core) [s]

Solving equations 3.7 and 3.8 for a stationary state (time derivatives equal to zero), it can be found the value of reactivity in order to keep the reactor critical. Solution for a stationary state is shown:

$$0 = \frac{\rho-\beta}{\Lambda}\, n_0 + \sum_{i=1}^{6} \lambda_i \cdot c_{i,0}$$

$$0 = -\lambda_i\, c_{i,0} + \frac{\beta_i}{\Lambda}\, n_0 - \frac{c_{i,0}}{\tau_c} + \frac{c_{i,0}\, e^{-\lambda_i\,\tau_l}}{\tau_c}, \text{ for i=1:6;}$$

[2] Usually, the neutron moltiplication factor k is also used. The relation between ρ and k is: $\rho = (k-1)/k$. However, in this work the reactivity will be always used.

Hence:

$$c_{i,0} = \frac{\beta_i \, n_0}{\Lambda \left[\lambda_i + \frac{1}{\tau_c}\left(1 - e^{-\lambda_i \, \tau_l}\right)\right]}, \text{ for i=1:6}$$

$$\rho_0 = \beta - \sum_{i=1}^{6} \frac{\beta_i \, \lambda_i}{\lambda_i + \frac{1}{\tau_c}\left(1 - e^{-\lambda_i \, \tau_l}\right)} \tag{3.9}$$

where:
τ_c = core transit time [s]
τ_l = external loop transit time [s]

Nominal values of core and external loop transport times are given in Table 3.2. The equation that expresses $\rho(t)$ as a function of the other variables of the system is:

$$\rho(t) = \rho_0 + \alpha_h \, \Delta h + \alpha_g \, (T_g(t) - T_{g,0}) + \alpha_s \, (T_s(t) - T_{s,0}) \tag{3.10}$$

where the reactivity feedback coefficients α_g and α_s have been given in Tables 2.9 and 2.10 for both fuels employed in simulations, and are assumed to be constant at the tempearture range of interest.
In Eqn. 3.10 the value of ρ_0, which is the value of reactivity to compensate for precursor drift, is known from Eqn. 3.9 and $\Delta\rho_h$, which is the reactivity inserted (withdrawn) starting from the steady state value ρ_0, can be imposed.

Looking at equation 3.9 it is immediately evident how the fuel circulation induces a net loss of precursors (the ones decaying outside the core) and therefore a net loss of reactivity. Thus, it is necessary to compensate for this loss of reactivity, in order to ensure the reactor criticality. Moreover, it is observable that, in this calculation, the value of "compensation" reactivity ρ_0 required to compensate for precursor drift, ends up being independent of the neutron density, and therefore independent of the thermal power level. On the contrary it is evident the reliance on transit times. The value of "compensation" reactivity is shown in Table 3.1, together with all other values of variables[3] in steady state at nominal power [19]. Values of decay constants (λ_i) and delayed neutrons fractions (β_i) have been given in Tables 2.9 for fuel type C (U-235) and 2.10 for fuel type A (U-233).

The link between the neutronics and thermo-hydrodynamics equations is constitued by the thermal power signal; the core thermal power is calculated as a function of the neutronic population in the core. A direct proportionality dependency between thermal power and neutron density is adopted. Being P_0 the thermal power associated to the neutron population n_0, it is obtained:

$$P = P_0 \cdot \frac{n}{n_0} \tag{3.11}$$

[3]The value of the neutron population n_0 is taken as a reference, although it can not be considered more than a rapresentative estimate. However, changing this value would not compromise at all the model, but it would just affect the absolute value of neutron and precursor populations because it ends up being just a scaling factor in Eqn. 3.11. This value was calculated through a 2-D model developed with a multi-physics tool in a preceeding work [18].

Neutron and Precursor Population at 8 MW		
Neutron population	n_0	$2.7 \cdot 10^9$
Loss of reactivity [pcm]	ρ_0	245.9
i-th group	Precursor population	
$c_{1,0}$	$6.8778 \cdot 10^{10}$	
$c_{2,0}$	$1.9929 \cdot 10^{11}$	
$c_{3,0}$	$6.5598 \cdot 10^{10}$	
$c_{4,0}$	$6.6251 \cdot 10^{10}$	
$c_{5,0}$	$6.4210 \cdot 10^{9}$	
$c_{6,0}$	$9.4403 \cdot 10^{8}$	

Table 3.1: Initial steady-state values for neutronics equations at full power (8 MW)

The basic idea of the thermo-hydrodynamics model described in the present section is that the representative temperature of a fluid going through any component can be calculated as the average between its inlet and outlet temperature. This averaged temperature is the only state variable describing a fluid in a component. State variables representing fluids are here reported:

$$T_s^{core} = \frac{T_s^{core,out} + T_s^{core,in}}{2} \tag{3.12}$$

$$T_s^{h.e.} = \frac{T_s^{h.e.,out} + T_s^{h.e.,in}}{2} \tag{3.13}$$

$$T_{cool}^{h.e.} = \frac{T_{cool}^{h.e.,out} + T_{cool}^{h.e.,in}}{2} \tag{3.14}$$

$$T_{cool}^{rad} = \frac{T_{cool}^{rad,out} + T_{cool}^{rad,in}}{2} \tag{3.15}$$

$$T_{air}^{rad} = \frac{T_{air}^{rad,out} + T_{air}^{rad,in}}{2} \tag{3.16}$$

In the zero-dimensional model, the differential equations describing thermo- hydrodynamics in the core are: one for the representative temperature of the graphite, and one for the average temperature of the fuel salt within the core. They are directly inferred from the law of energy conservation (see Eqn. 3.6). Explanation of symbols, for these equations and all following ones, is given at page 29. Figure 3.2 shows the basic scheme underlying to the system composed by equations from 3.11 to 3.26. Now, considering the law of energy conservation as obtained in Eqn. 3.6, it can be written:

$$M_g \, c_g \, \frac{dT_g}{dt} = \gamma_g \, P - k_{eq} \, (T_g - T_s) \tag{3.17}$$

$$M_s^{core} \, c_s \, \frac{dT_s}{dt} = \gamma_s \, P + k_{eq} \, (T_g - T_s) - \Gamma_s \, c_s \, (T_s^{core,out} - T_s^{core,in}) \tag{3.18}$$

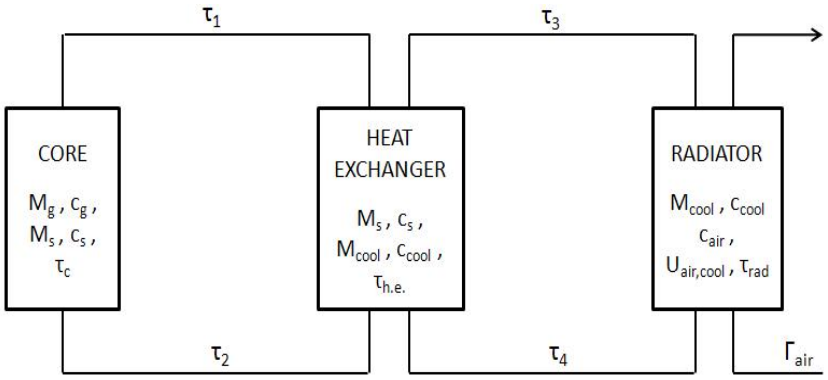

Figure 3.2: Basic scheme and significant quantities of the plant model

As concerns the whole primary loop, new state variables are introduced in order to model the heat exchanger. The salt core outlet temperature is conveyed to the heat exchanger with an appropriate transport delay, just like the salt heat exchanger outlet temperature is conveyed to the core with a (different) transport delay. The same kind of connections exists between the heat exchanger and the radiator. The four equations linking outlet temperatures to inlet temperatures of the following component are:

$$T_s^{h.e.,in}(t) = T_s^{core,out}(t-\tau_1) \quad (3.19)$$
$$T_s^{core,in}(t) = T_s^{h.e.,out}(t-\tau_2) \quad (3.20)$$
$$T_{cool}^{rad,in}(t) = T_{cool}^{h.e.,out}(t-\tau_3) \quad (3.21)$$
$$T_{cool}^{h.e.,in}(t) = T_{cool}^{rad,out}(t-\tau_4) \quad (3.22)$$

The values of the characteristic transport times are given in Table 3.2. The differential

Nominal Transit Times			
τ_c	Core transit time	8.46	s
τ_l	Primary loop external transit time	16.44	s
τ_p	Primary loop total transit time	24.90	s
τ_1	Hot leg primary loop transit time	5.77	s
τ_2	Cold leg primary loop transit time	8.67	s
τ_3	Hot leg secondary loop transit time	4.71	s
τ_4	Cold leg secondary loop transit time	8.24	s

Table 3.2: Values of nominal transport times

equations used to create a model of the heat exchanger are: one for the average temperature of the fuel salt within the heat exchanger, and one for the average temperature

of coolant salt in the heat exchanger. They both derive from the law of energy conservation (as appears in Eqn. 3.6), where the average temperatures are always defined as the sum of inlet and outlet divided by two.

$$M_s^{h.e.} c_s \frac{dT_s^{h.e.}}{dt} = -U_{s,cool}(T_s^{h.e.} - T_{cool}^{h.e.}) - \Gamma_s c_s (T_s^{h.e.,out} - T_s^{h.e.,in}) \tag{3.23}$$

$$M_{cool}^{h.e.} c_{cool} \frac{dT_{cool}^{h.e.}}{dt} = U_{s,cool}(T_s^{h.e.} - T_{cool}^{h.e.}) - \Gamma_{cool} c_{cool} (T_{cool}^{h.e.,out} - T_{cool}^{h.e.,in}) \tag{3.24}$$

Likewise, the differential equations used to create a model of the radiator are: one for the average temperature of the coolant salt within the radiator, and one for the average temperature of air which cools down the pipes.

$$M_{cool}^{rad} c_{cool} \frac{dT_{cool}^{rad}}{dt} = -U_{cool,air}(T_{cool}^{rad} - T_{air}) - \Gamma_{cool} c_{cool} (T_{cool}^{rad,out} - T_{cool}^{rad,in}) \tag{3.25}$$

$$M_{air}^{rad} c_{air} \frac{dT_{air}^{rad}}{dt} = U_{cool,air}(T_{cool}^{rad} - T_{air}^{rad}) - \Gamma_{air} c_{air} (T_{air}^{rad,out} - T_{air}^{rad,in}) \tag{3.26}$$

Hence, it has been obtained a system of 24 equations with 26 variables. Therefore two of this variables have either to be fixed or to be already known. It is assumed that the air inlet temperature ($T_{air}^{rad,in}$) is known, constant and equal to ≈37.8 °C (100 °F), see [9].

The other unknown variable is the reactivity managed by the control rods, $\Delta\rho_h$, which is a controlled variable, and will be set according to the type of analysis, depending on the various scenarios that it is meant to simulate. The only free input of the system is therefore the reactivity inserted or withdrawn through control rods movement, starting from the steady-state position.

In order to be initialized, the system needs an information on the thermal power level of the stationary state which is working at. This information is used both in calculating the initial neutron population (through Eqn. 3.11) and in regulating the radiator heat removal load. Indeed, the power signal is processed and converted into a signal of air mass flow and global heat transfer coefficient, according to the functions extrapolated from data taken by the analysis of stationary working levels (see 44).

So far, it has been implemented a model whose state variables are the average temperatures of the fluid in each component, computed as half the sum of inlet and outlet temperature. However, an undesired consequence of this modelling approach is that a sudden increase on inlet temperature causes an istantaneous decrease on outlet temperature, which is clearly unphysical. This happens because the average temperature, calculated as one half the sum of inlet and outlet, is the only state variable and it can not undergo to step variations: it follows that a step on inlet temperature causes a step of the outlet temperature in the opposite direction. Therefore, although the variation of the state variable (average temperature) is correct, it is evident that the decrease of outlet temperature is unacceptable as this variation is felt by next component in the circulation loop.

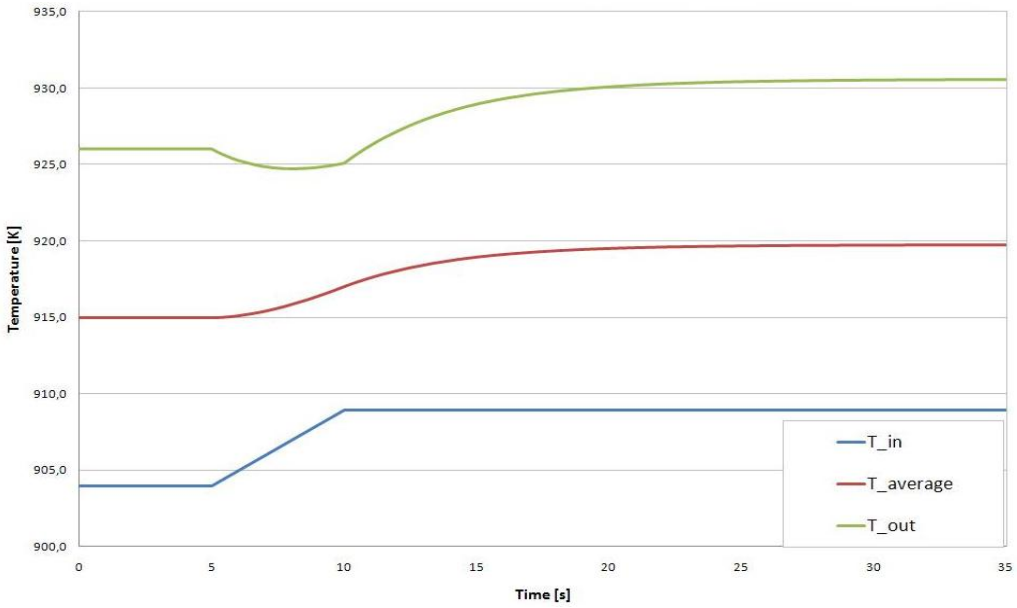

Figure 3.3: Variation of average and outlet temperature, following a 5 seconds ramp increase of inlet temperaure

In Fig. 3.3 it can actually be observed that a ramp increase on inlet temperature, causes an initial decrease on outlet temperature, while the average temperature starts increasing smoothly at the same time the ramp starts, just like expected.

It is evident how with this modelling approach the problem rises as the outlet temperature is conveyed, with the appropriate transport delay, to the subsequent component. In order to circumvent this undesired behaviour, in the following section the partial differential equation describing a one-dimensional energy transfer has been considered.

3.2 One-dimensional continuous model of the core

Starting from equation 3.27, which describes the situation represented in Fig. 3.4, it has been elaborated a model which reproduces this partial differential equation. The model is very simplified and it barely represents the thermo-hydrodynamics of the core. Indeed, neutronics is not taken into account, just like the secondary circuit of the plant is not modelled. Moreover, in this equation it is assumed that the thermal power is entirely generated in the fuel salt, while the contribute of graphite is neglected.

$$\begin{aligned} -\Gamma_s c_s (T + \frac{\partial T}{\partial x} dx - T) &= W dx - c_s \frac{\partial T}{\partial t} dm \\ -\Gamma_s c_s \frac{\partial T}{\partial x} &= W - \frac{\Gamma_s}{v} c_s \frac{\partial T}{\partial t} \end{aligned} \tag{3.27}$$

where:

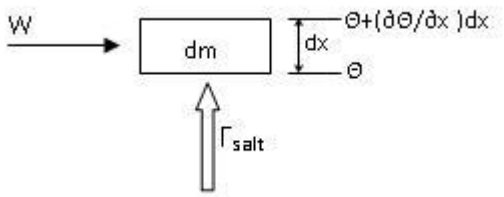

Figure 3.4: Continuous modelling scheme of a channel slice

W : linear power generated in the infinitesimal space dx [W/m];
$-\Gamma_s\, c_s(\partial T/\partial x)dx$: power removed by salt mass flow;
$c_s(\partial T/\partial t)dm$: power accumulated within the infinitesimal mass dm;
$dm(=\Gamma_s\, dx/v)$: infinitesimal mass contained in dx [kg];
$v(=L\,/\tau_0)$: fuel salt velocity, where L and τ_0 are the total core lenght and the core transit time [m/s];
$M_s^{core}(=\Gamma_s\,\tau_0)$: fuel salt mass in the core [kg];

The Simulink layout of this model is shown in Figure 3.5. It can be observed that its inputs are the total thermal power and the fuel salt inlet temperature. The block ends up being a trasformation from inlet to outlet temperature, with thermal power as the only parameter which can undergo a variation. Using Laplace transform partial derivative equations can be reduced to ordinary derivative equations. This operation is necessary since Simulink doesn't allow the use of PDE. The transformation is shown:

$$\begin{aligned} \frac{1}{v}\frac{\partial T(x,t)}{\partial t} - \frac{\partial T(x,t)}{\partial x} &= \frac{q'(x,t)}{\Gamma_s c_s} \\ \int_{-\infty}^{+\infty} \left[\frac{1}{v}\frac{\partial T(x,t)}{\partial t} - \frac{\partial T(x,t)}{\partial x}\right] e^{-s\,t}\, dt &= \int_{-\infty}^{+\infty} \left[\frac{q'(x,t)}{\Gamma_s c_s}\right] e^{-s\,t}\, dt \end{aligned}$$

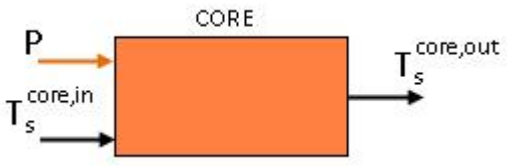

Figure 3.5: Simulink model layout of CONTINUOUS one-dimensional core

$$\begin{aligned} \frac{s}{v}\widetilde{T}(x,s) - \frac{T_0(x)}{v} + \frac{d\widetilde{T}(x,s)}{dx} &= \frac{\widetilde{q'}(x,s)}{\Gamma_s\, c_s} \\ \frac{d\widetilde{T}(x,s)}{dx} + \left(\frac{s}{v}\right)\widetilde{T}(x,s) &= \left[\frac{\widetilde{q'}(x,s)}{\Gamma_s\, c_s} + \frac{T_0(x)}{v}\right] \end{aligned} \tag{3.28}$$

The transformed equation is an ordinary differential equation in the x variable, and it can be easily integrated. Therefore, integrating in dx and giving the appropriate initial conditions, it can be obtained the expression that, applied to the inlet temperature, transforms it into the outlet temparture, knowing the amount of power generated within the core. Also, power is assumed to be uniformely distributed (q' is a constant), because the interest is only on salt outlet temperature variations. The following expression is obtained:

$$\widetilde{T}(x,s) = q'(s)\, L\left[\frac{1}{\Gamma_s c_s \tau_c}\,\frac{1-e^{-s\frac{x}{v}}}{s}\right] + \frac{T_{s,0}}{s}\left(1-e^{-s\frac{x}{v}}\right) + T_s^{core,in}(s)\left(e^{-s\frac{x}{v}}\right) \tag{3.29}$$

If the value x is fixed equal to the core height (x=L), the expression of $T_s^{core,out}$ is obtained:

$$\widetilde{T}_s^{core,out} = P(s)\left[\frac{1}{\Gamma_s c_s \tau_c}\,\frac{1-e^{-s\tau_c}}{s}\right] + \frac{T_{s,0}}{s}\left(1-e^{-s\tau_c}\right) + T_s^{core,in}(s)\left(e^{-s\tau_c}\right) \tag{3.30}$$

Transfer functions can be implemented in Simulink as far as the values of poles and zeros are known. Indeed, it is necessary to use a *zero-pole* block, which requires to fix its parameters: zeros, poles, and gain of the transfer function. In order to introduce this specific transfer function in Simulink, the term $\exp(-s\,\tau_c)$ has to be approximated in a polinomial form. The Padè approximation is applied as it transforms an exponential function into a polynomial whose denominator has the same order of the numerator [20]. It follows that a proper transfer function is obtained (as required by the Simulink *zero-pole* block). The order of Padè approximation can be chosen by the user.

In response to a ramp of 10 °C on inlet temperature (increase with a coefficient of 1 °C per second), both average temperature and outlet temperature of fuel salt start increasing, contrarily to what happened with the zero-dimensional model.

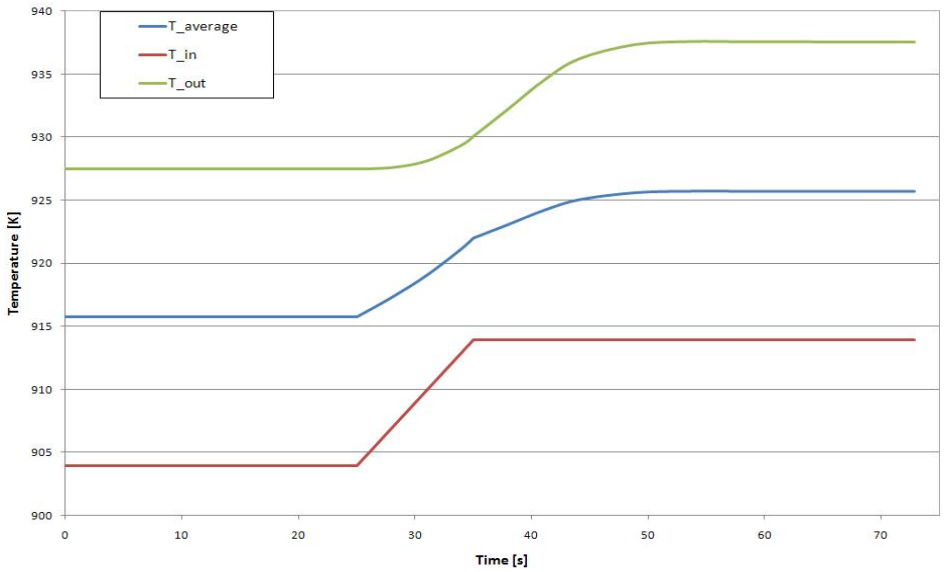

Figure 3.6: Response of the continuous model to a inlet temperature ramp of 10 °C

The model response is graphed in Figure 3.6 (in this example the order of Padè approximation is 6). Still, looking at Eqn. 3.29 it is evident that a step variation of thermal power (P(s)=P_1/s) turns out in a ramp variation of salt outlet temperature ($T_s^{core,out} = P_1/s^2 + \ldots$).

Using Laplace transform for all equations of the system would enormously complicate the model. Transport delays in time domain would all become exponential functions in frequency domain, and should therefore be approximated with Padè in order to appear as proper transfer function. Thus, it was figured out that the simplest way of approaching this system of partial differential equations was to apply a numerical method of discretization, so to obtain ordinary differential equations. Obviously it will be obtained a system composed of a higher number of ODEs if compared with the number of PDEs that were initially present. In the following section a discretization method will be implemented and, as mentioned, the problem will be then solvable entirely in the time domain, not being necessary to apply the Laplace transform.

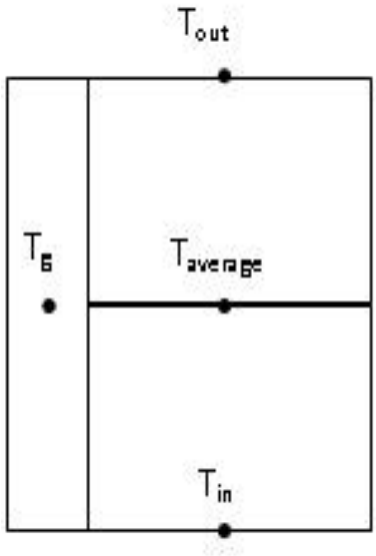

Figure 3.7: Discretization grid for *upwind* method

3.3 One-dimensional "discrete" model - UPWIND method

A finite difference discretization method is applied to Eqn. 3.27, which is reported here. It is a partial differential equation, which describes power generation within the fuel salt and one-dimensional energy transport. The discretization of this equation will be taken as a reference model for all other equations which constitute the system representing the plant.

$$-\Gamma_s c_s \frac{\partial T}{\partial x} = W - \frac{\Gamma_s}{v} c_s \frac{\partial T}{\partial t}$$

Applying a one-side discretization of the first derivative to the spatial term, the *upwind* discretization method (see [21]), and assuming that the fuel salt in the core region can be modelled as a grid of 3 nodes (see Fig. 3.7), it was obtained:

$$\Gamma_s c_s \frac{dT_{out}}{dt} + v \Gamma_s c_s \frac{T_{out} - T_{av}}{L/2} = W \cdot v$$

$$\Gamma_s c_s \frac{dT_{av}}{dt} + v \Gamma_s c_s \frac{T_{av} - T_{in}}{L/2} = W \cdot v$$

Hence:

$$\frac{M_s^{core}}{2} c_s \frac{dT_{out}}{dt} + \Gamma_s c_s (T_{out} - T_{av}) = \frac{P}{2} \tag{3.31}$$

$$\frac{M_s^{core}}{2} c_s \frac{dT_{av}}{dt} + \Gamma_s c_s (T_{av} - T_{in}) = \frac{P}{2} \tag{3.32}$$

where partial derivatives have become total derivatives since now the temperatures are only functions of time (spatial variable has been removed by the discretization).

Then, the graphite was included, adding another node to the system and therefore another equation. Consequently, it was added to both equations of fuel salt and graphite a term which takes into account the heat exchange between graphite and fuel salt (considering the exchange to happen between the average temperatures of each of them).

The heat exchange was considered just like a power source and, for what concerns fuel salt equations, it was divided in two equal contributions in the two energy conservation equations of fuel salt (Eq. 3.31 and 3.32). Also, knowing that part of the thermal power is generated in the graphite structure, the coefficients of power fractions γ_g and γ_s were opportunely introduced. The equations representing the core subsystem become:

$$M_g\, c_g \frac{dT_g}{dt} = \gamma_g\, P - k_{eq}\, (T_g - T_{av}) \tag{3.33}$$

$$\frac{M_s^{core}}{2} c_s \frac{dT_s^{core,out}}{dt} + \Gamma_s\, c_s (T_s^{core,out} - T_s^{core}) = \frac{\gamma_s\, P}{2} + \frac{k_{eq}}{2}(T_g - T_s^{core}) \tag{3.34}$$

$$\frac{M_s^{core}}{2} c_s \frac{dT_s^{core}}{dt} + \Gamma_s\, c_s (T_s^{core} - T_s^{core,in}) = \frac{\gamma_s\, P}{2} + \frac{k_{eq}}{2}(T_g - T_s^{core}) \tag{3.35}$$

Using this method the problem of unphysical variation of outlet temperature is solved again (see Fig. 3.8, compared to Fig. 3.3). As the ramp on inlet temperature starts,

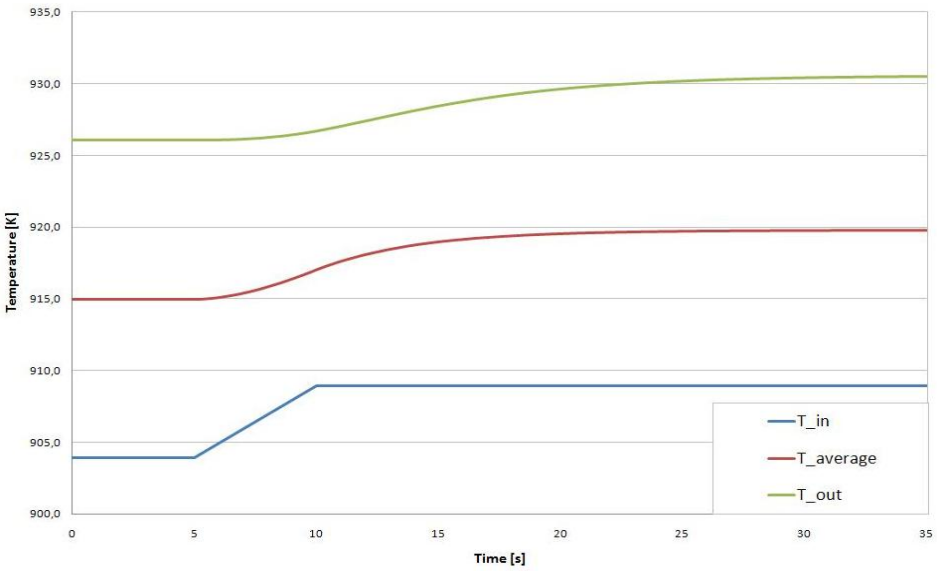

Figure 3.8: Variation of average and outlet temperature, following a 5 seconds ramp increase of inlet temperaure

average and outlet temperatures start rising. Looking at the figure, it is clearly observable that outlet temperature increases more slowly than average temperature, as it is physically expected.

The same discretization method was applied for fuel salt and coolant salt equations in the heat exchanger. In this modelling approach, the heat exchange between the the fuel salt and the coolant salt depends on their average temperatures. Equations describing the heat exchanger subsystem become:

$$\frac{M_s^{h.e.}\, c_s}{2}\frac{dT_s^{h.e.,out}}{dt} = -\Gamma_s\, c_s(T_s^{h.e.,out} - T_s^{h.e.}) - \frac{U_{s,cool}}{2}(T_s^{h.e.} - T_{cool}^{h.e.}) \quad (3.36)$$

$$\frac{M_s^{h.e.}\, c_s}{2}\frac{dT_s^{h.e.}}{dt} = -\Gamma_s\, c_s(T_s^{h.e.} - T_s^{h.e.,in}) - \frac{U_{s,cool}}{2}(T_s^{h.e.} - T_{cool}^{h.e.}) \quad (3.37)$$

$$\frac{M_{cool}^{h.e.}\, c_{cool}}{2}\frac{dT_{cool}^{h.e.,out}}{dt} = -\Gamma_{cool}\, c_{cool}(T_{cool}^{h.e.,out} - T_{cool}^{h.e.}) + \frac{U_{s,cool}}{2}(T_s^{h.e.} - T_{cool}^{h.e.}) \quad (3.38)$$

$$\frac{M_{cool}^{h.e.}\, c_{cool}}{2}\frac{dT_{cool}^{h.e.}}{dt} = -\Gamma_{cool}\, c_{cool}(T_{cool}^{h.e.} - T_{cool}^{h.e.,in}) + \frac{U_{s,cool}}{2}(T_s^{h.e.} - T_{cool}^{h.e.}) \quad (3.39)$$

Finally, appling again the upwind method, the equations describing the radiator subsystem become:

$$\frac{M_{cool}^{rad}\, c_{cool}}{2}\frac{dT_{cool}^{rad,out}}{dt} = -\Gamma_{cool}\, c_{cool}(T_{cool}^{rad,out} - T_{cool}^{rad}) - \frac{U_{cool,air}}{2}(T_{cool}^{rad} - T_{air}^{rad}) \quad (3.40)$$

$$\frac{M_{cool}^{rad}\, c_{cool}}{2}\frac{dT_{cool}^{rad}}{dt} = -\Gamma_{cool}\, c_{cool}(T_{cool}^{rad} - T_{cool}^{rad,in}) - \frac{U_{cool,air}}{2}(T_{cool}^{rad} - T_{air}^{rad}) \quad (3.41)$$

$$\frac{M_{air}^{rad}\, c_{air}}{2}\frac{dT_{air}^{rad,out}}{dt} = -\Gamma_{air}\, c_{air}(T_{air}^{rad,out} - T_{air}^{rad}) + \frac{U_{cool,air}}{2}(T_{cool}^{rad} - T_{air}^{rad}) \quad (3.42)$$

$$\frac{M_{air}^{rad}\, c_{air}}{2}\frac{dT_{air}^{rad}}{dt} = -\Gamma_{air}\, c_{air}(T_{air}^{rad} - T_{air}^{rad,in}) + \frac{U_{cool,air}}{2}(T_{cool}^{rad} - T_{air}^{rad}) \quad (3.43)$$

Reactor neutronics is modelled with a point-kinetic, as it was in the zero-dimesional model (see section 3.1). Therefore the equations are the same, see Eqn. 3.7, and 3.8. The thermal feedback is calculated through the average temperatures of graphite and fuel salt.

Giving an overview to the model just realized, it can be noticed that there are 5 ordinary differential equations and 5 state variable more than in the zero-dimensional model, a very small effort in the light of the effect that has been achieved. However, the model can still be improved: in particular, for what concerns the model of the core, it would be worth knowing and taking into account the (axial) power distribution, the temperature profile and the precursor density along the core height. It can be stated that, increasing the number of nodes composing the core, these goals would be reached, and it can be hypothesized that, implementing different discretizing methods, the model would be more general. In the following section, these two improvements are developed.

3.4 One-dimensional discrete model - *θ-method*

The goal of this section is to increase both the accuracy of the model and the choice options for the user. First of all, a more general discretization method was applied to the energy equation of the core block. Indeed, the *θ-method* was chosen as it allows the user to choose the kind of discretization by changing just a parameter (see [21]). The purpose of this kind of discretization is to have the chance to set the weight given to each derivative, thus obtaining, for example, the *upwind* method for $\theta = 1$ or the *Crank-Nicolson* scheme for $\theta = 1/2$.
The method is applied to the spatial derivative, instead of being applied to the time derivative like in [21]. No difference can be noticed from the computational point of view, since in the equation the spatial and temporal partial derivatives appear symmetrically: indeed both derivatives appear as a first derivative (diffusion is not considered) and in a linear dependency relation. Referring to equation 3.27:

$$-\Gamma_s c_s \frac{\partial T}{\partial x} = W - \frac{\Gamma_s}{v} c_s \frac{\partial T}{\partial t},$$

the equations representing the core subsystem were obtained as follows (supposing to have a three nodes grid for the fuel salt, two equations were obtained):

$$v\frac{T_s^{core,out} - T_s^{core}}{L/2} = \theta(-\frac{dT_s^{core,out}}{dt}) + (1-\theta)(-\frac{dT_s^{core}}{dt}) + \frac{W\,L}{\Gamma_s\,c_s\,\tau_0}$$
$$v\frac{T_s^{core} - T_s^{core,in}}{L/2} = \theta(-\frac{dT_s^{core}}{dt}) + (1-\theta)(-\frac{dT_s^{core,in}}{dt}) + \frac{W\,L}{\Gamma_s\,c_s\,\tau_0}$$

Simplifying, reordering and adding the terms that keep into account the heat exchange with the graphite and the power generation within the fuel salt, the equations become:

$$\theta(\frac{dT_s^{core,out}}{dt}) + (1-\theta)(\frac{dT_s^{core}}{dt}) =$$
$$= \frac{-2}{\tau_0}(T_s^{core,out} - T_s^{core}) + \frac{\gamma_s\,P}{\Gamma_s\,c_s\,\tau_0} + \frac{k_{eq}}{\Gamma_s\,c_s\,\tau_0}(T_g - T_s^{core}) \tag{3.44}$$
$$\theta(\frac{dT_s^{core}}{dt}) + (1-\theta)(\frac{dT_s^{core,in}}{dt}) =$$
$$= \frac{-2}{\tau_0}(T_s^{core} - T_s^{core,in}) + \frac{\gamma_s\,P}{\Gamma_s\,c_s\,\tau_0} + \frac{k_{eq}}{\Gamma_s\,c_s\,\tau_0}(T_g - T_s^{core}) \tag{3.45}$$

Finally, the graphite equation is introduced:

$$\frac{dT_g}{dt} = \frac{\gamma_g\,P}{M_g\,c_g} - \frac{k_{eq}}{M_g\,c_g}(T_g - T_s^{core}) \tag{3.46}$$

As general rule, the value of the parameter θ can be fixed in the range $0 \leq \theta \leq 1$. Nevertheless, it can be affermed that *the θ-scheme is unconditionally stable for all the values* $1/2 \leq \theta \leq 1$, *and conditionally stable if* $0 \leq \theta < 1/2$ (see [21]).

Since it is not of interest for this work to investigate either which is the stability limit for this discretization scheme, or to force the user to pay attention to an eventual stability limit depending of the number of regions he chooses, a stability analysis is not made, and, in this work, the value of the parameter θ can be fixed in the range $1/2 \leq \theta \leq 1$. The equations constituting the model of the heat exchanger and the radiator remain the same ones as in the model seen in section 3.3.

A second upgrade of the model was realized increasing the number of nodes which are used to model the core region and giving the user the chance to fix the number of core sub-regions as a parameter. Each core region is formed by 3 nodes, respectively representing the average temperature and the outlet temperature of the fuel salt, and the temperature of the graphite in the corresponding region (see figure 3.9). Increasing

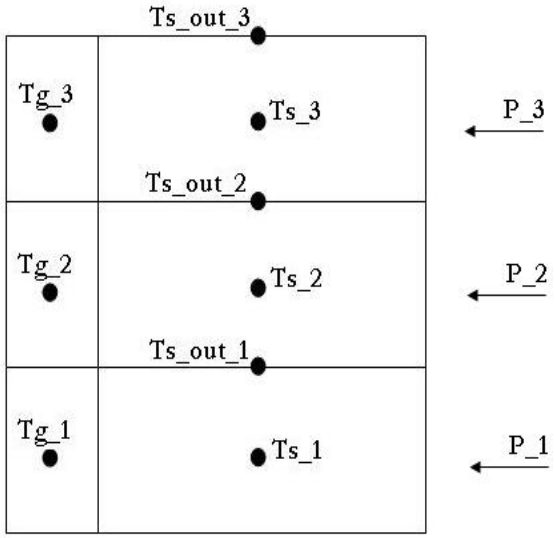

Figure 3.9: Example of discretization with three regions

the number of regions and therefore the number of nodes that constitute the grid, a better model of the core is achievable. Using a higher number of regions the model gets closer and closer to the one dimensional continuous model (see section 3.2).

The system of equations for the i-th core region is:

$$\frac{dT_{g,i}}{dt} = \frac{\gamma_g P_i}{M_{g,i}\, c_g} - \frac{k_{eq}}{M_{g,i}\, c_g}(T_{g,i} - T_{s,i}) \tag{3.47}$$

$$\theta(\frac{dT^{out}_{s,i}}{dt}) + (1-\theta)(\frac{dT_{s,i}}{dt}) = \frac{-2}{\tau_{0,i}}(T^{out}_{s,i} - T_{s,i}) + \frac{\gamma_s P_i}{\Gamma_s\, c_s\, \tau_{0,i}} + \frac{k_{eq,i}}{\Gamma_s\, c_s\, \tau_{0,i}}(T_{g,i} - T_{s,i}) \tag{3.48}$$

$$\theta(\frac{dT_{s,i}}{dt}) + (1-\theta)(\frac{dT^{in}_{s,i}}{dt}) = \frac{-2}{\tau_{0,i}}(T_{s,i} - T^{in}_{s,i}) + \frac{\gamma_s P_i}{\Gamma_s\, c_s\, \tau_{0,i}} + \frac{k_{eq,i}}{\Gamma_s\, c_s\, \tau_{0,i}}(T_{g,i} - T_{s,i}) \tag{3.49}$$

It is evident that the axial conduction in graphite is neglected. This is reasonable because of the problem geometry: the height of each graphite block is much bigger than its width and depth (the fuel salt channel has the same shape).

Looking at the system of equations which describes each region (equations 3.47, 3.48 and 3.49), it can be observed that it needs three inputs: the inlet temperature, the time-derivative of the inlet temperature and the power. Nevertheless, inlet temperature and its derivative depend on the previous region equations, so for *i-th* region they are expressed through the equations of *(i-1)-th* region and so on to the first (fuel incoming) region. Only for the first region inlet temperature and its derivative are effectively two inputs. The fraction of power assigned to each region is always given as input. The system of equations is inserted in the Simulink as a matrix equation:

$$\begin{aligned} \dot{\underline{x}} &= \underline{\underline{A}} \cdot \underline{x} + \underline{\underline{B}} \cdot \underline{u} \\ \underline{y} &= \underline{\underline{C}} \cdot \underline{x} + \underline{\underline{D}} \cdot \underline{u} \end{aligned} \tag{3.50}$$

where
$\underline{x}$: is a vector of temperatures of lenght 3·N (with N equal to the number of regions);
$\underline{u}$: is a vector of inputs of lenght N+2 (N thermal powers of N regions, inlet temperature and its derivative);
$\underline{y}$: is a vector of outputs of lenght 3 ·N (3N temperatures which are sent to the NEUTRONICS block to calculate feedbacks on reactivity).

Also, the neutronics equations have been changed in order to considerate the transport of precursors from a region to the next one. Since there are 6 groups of precursors, there will be 6 equations of precursor population for each region. On the contrary, the equation describing neutron population in the N regions is only one: it can be supposed that neutron diffusion [4] happens at a speed high enough (if compared with fuel salt velocity) so that it can be stated that one reactivity value is representative of the core situation and a zero-dimensional kinetics can be adopted for modelling of neutronics.

The equations are (superscript j identifies the group of precursors and goes from 1 to 6, and x is the spatial coordinate):

$$\frac{\partial n(t)}{\partial t} = \frac{\rho(t) - \beta}{\Lambda}\, n + \sum_{j=1}^{6} \int_{-\frac{L}{2}}^{+\frac{L}{2}} \lambda^j\, \hat{c}^j(x,t) dx \tag{3.51}$$

$$\frac{\partial \hat{c}^j(x,t)}{\partial t} + \underbrace{v\, \frac{\partial \hat{c}^j(x,t)}{\partial x}}_{Precursor\ transport} = \frac{\beta^j}{\Lambda} \hat{n}(x,t) - \lambda^j \hat{c}^j(x,t) \tag{3.52}$$

[4] Neutron transport is not considered, since it would be negligible if compared to diffusion (for assuming this, the main hypothesis is that the macroscopic absorption cross section is much less than the macroscopic scattering cross section, $\Sigma_a \ll \Sigma_s$) [22].

where:
$n(t)$ = total number of neutrons
$\hat{n}(x,t)$ = neutron density [neutrons/m]
$c^j(t)$ = total number of precursors of *j-th* group
$\hat{c}^j(x,t)$ = *j-th* group precursor density [precursors/m]

Equations 3.51 and 3.52 were discretized using an *upwind* scheme on the spatial coordinate (see Fig. 3.12 for a graphical representation):

$$\frac{d\,n(t)}{dt} = \frac{\rho(t)-\beta}{\Lambda}\,n + \frac{L}{N}\sum_{i=1}^{N}\left[\sum_{j=1}^{6}\lambda^j\hat{c}_i^j(t)\right] \tag{3.53}$$

$$\frac{d\,\hat{c}_i^j(t)}{dt} + v\,\frac{\hat{c}_i^j(t)-\hat{c}_{i-1}^j(t)}{L/N} = \frac{\beta^j}{\Lambda}\hat{n}_i - \lambda^j\hat{c}_i^j(t) \tag{3.54}$$

where subscript i denotes the region and ranges from 1 to N, L is the core height and N the number of regions. Finally, knowing that the core height is equal to the product of the core holdup time τ_c times the fluid velocity, assuming reactivity is expressed as a stationary value ρ_0 (necessary to compensate the loss of reactivity caused by precursor drift) plus a variation from this stationary value $\delta\rho$, and introducing the expressions of total number of neutrons and precursors in each node as functions of their density [5]:

$$\begin{aligned} n_i &= \frac{L}{N}\,\hat{n}_i \\ c_i^j &= \frac{L}{N}\,\hat{c}_i^j\ ; \end{aligned}$$

after some simplifications it is obtained:

$$\frac{d\,n(t)}{dt} = \frac{\rho_0+\delta\rho(t)-\beta}{\Lambda}\,n + \sum_{i=1}^{N}\left[\sum_{j=1}^{6}\lambda^j c_i^j(t)\right] \tag{3.55}$$

$$\frac{d\,c_i^j(t)}{dt} + \frac{c_i^j(t)-c_{i-1}^j(t)}{(\tau_c/N)} = \frac{\beta^j}{\Lambda}n_i - \lambda^j c_i^j(t) \tag{3.56}$$

It is worth noticing that precursor equation 3.56 assumes a particular significance for the first region (i=1), since $c_{i-1}^j(t)$ are not precursors of region (i-1 = 0) but the circulating precursors that are re-entering in the core. Looking at equations of precursors (type 3.56), it is evident that the knowledge of the total neutron population in the core region is not sufficient for solving the neutronics subsystem. Indeed, it is necessary to know the axial profile of neutron population in order to assign to each

[5] It is done in order to obtain a dimensional homogenity between neutron and presursor equations. Also, it results easier to calculate the loss of reactivity when considering the total number of reentering precursors instead of their density (see Eqn. 3.63).

i-th region the correct term of precursor formation. Being the average life Λ of a neutron on the order of 10^{-4} s, the salt speed v in the core region about 0.2 m/s, and the thermal diffusion lenght L_T in graphite about 60 cm (see [22]), the transport of neutrons due to the salt convection can be neglected. Indeed, the ratio between the average distance covered by a neutron because of salt motion and the diffusion lenght results:

$$\frac{\delta_{CONV}}{\delta_{DIFF}} \sim \frac{v\,\Lambda}{L_T} \ll 10^{-3}$$

This allows to write the equation of neutron diffusion neglecting the term which should account for neutron convection due to salt motion (it is reasonable because the diffusive neutron current is much bigger than the "convective" neutron current):

$$D\,\nabla^2\phi - \Sigma_a\,\phi + \nu\Sigma_f\,\phi \;=\; \frac{1}{v}\frac{\partial\phi}{\partial t} \tag{3.57}$$

and solving it through the separation of variables (using Fourier series for expressing spatial terms, see [22] page 132 and following), the steady-state flux profile for a finite cylinder (which is the shape of the core) results:

$$\phi(x,r) \;\propto\; J_0\left(\frac{2.405}{R}r\right)\; cos\left(\frac{\pi}{H}x\right) \tag{3.58}$$

where:
D = diffusion coefficient [cm]
ϕ = neutron flux (scalar) [n/(cm^2 s)]
Σ_a = macroscopic absorption cross section [cm^{-1}]
Σ_f = macroscopic fission cross section [cm^{-1}]
ν = number of neutrons emitted per fission event
v = average speed modulus of thermal neutrons [cm/s]
J_0 = zero-order Bessel function of first kind
R = core radius of extrapolation [cm]
r = radius [cm]
H = core height of extrapolation [cm]
x = height [cm]

It can be observed that only the first harmonic of the series survives, both for radial and axial solution. The other eigenfunctions composing the series are damped by the time dependent term (which consists of a negative exponential) [22]. It is worth noticing that the distribution of linear power, q'(x), has the same shape of the neutron axial profile. Therefore, it was implemented a simple system that associates a certain neutron population and a certain power fraction to each core region, according to its position.

Knowing that the cited solution was found for a reactor with not circulating fuel (see [23]), it is accetable to assume the same distribution (axially shaped like a cosine) for the linear power of this molten salt rector because neutron transport due to the salt

motion (neutron convection) from a core region to the next one is negligible. Moreover, it should be noted that power fraction due to delayed neutrons can be considered negligible (total delayed neutron fraction β is 0.00666 for U-235 fuel or 0.00264 for U-233 fuel, hence less than 1%). Otherwise, a contribute from decay of precursors should have been kept into account with a different distribution than a cosine, and shoud have been summed to the cosine distribution of prompt neutrons, but for simplicity this has not been done.

Nevertheless, it is reasonable not to keep this different distribution into account, approximating the linear power in this model with a cosine, whose maximum stays at half the core height, in this case at $x = 0$ (the core extends from $x = -L/2$ to $x = L/2$, see Figure 3.10). If L is the total core height, the linear power distribution

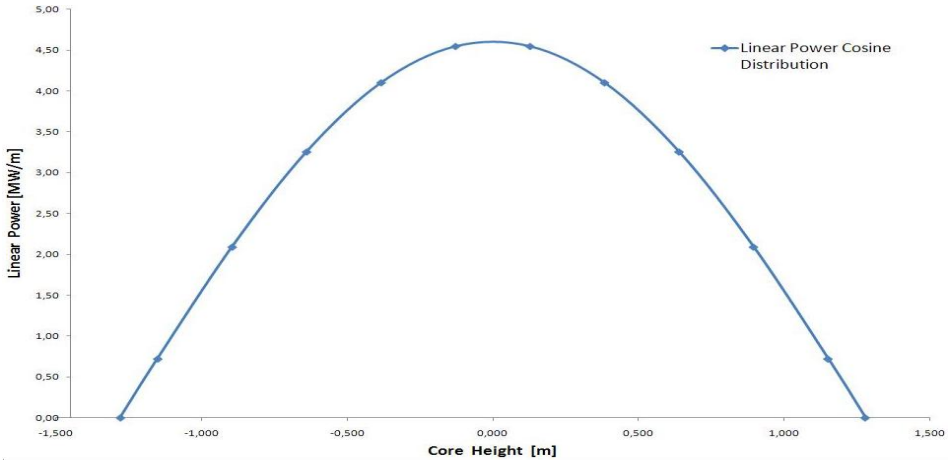

Figure 3.10: Linear power distribution as a function of the core height

is given by:

$$q' = A cos\left(\frac{\pi}{L}x\right) \tag{3.59}$$

where the amplitude A can be calculated knowing that the integral of linear power on the total core height has to give the total thermal power:

$$P = \int_{-L/2}^{L/2} A\, cos(\frac{\pi}{L}x)dx = \left[A\frac{L}{\pi}cos(\frac{\pi}{L}x)\right]_{-L/2}^{L/2} = 2\,A\frac{L}{\pi}$$

$$A = P\frac{\pi}{2\,L}$$

In order to reproduce this distribution, knowing the number of region and therefore the height Δx of each region (whose sum gives the core total height), the integral of linear power in the appropriate interval is taken (see equation 3.60), and this $i - th$

power value is associated to the corresponding $i-th$ region (see Figure 3.11).

$$\int_{\frac{L}{N}(i-1)-\frac{L}{2}}^{\frac{L}{N}(i)-\frac{L}{2}} \left[P\frac{\pi}{2\,L}cos(\frac{\pi}{L}x)\right]dx = \frac{P}{2}\left[sin\left(\frac{\pi}{N}(i)-\frac{\pi}{2}\right)-sin\left(\frac{\pi}{N}(i-1)-\frac{\pi}{2}\right)\right] =$$

$$= \frac{P}{2}\left[cos\left(\frac{\pi}{N}(i)\right)-cos\left(\frac{\pi}{N}(i-1)\right)\right] \tag{3.60}$$

The same considerations remain valid for the neutron population distribution, where

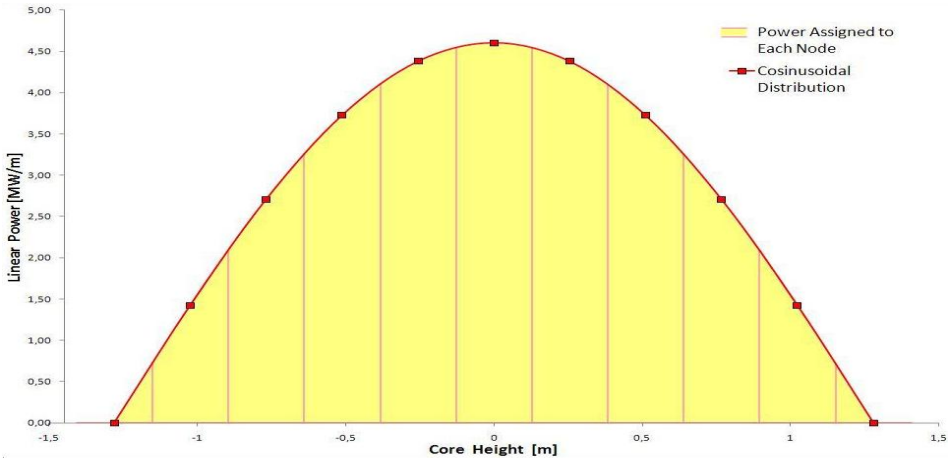

Figure 3.11: Fraction of power associated to the corresponding region

the value of the i-th region neutron population is calculated with the same method. The neutronics model ends up being formed by one equation for the neutron population (3.55), 6·N equations of precursors of type 3.56 and a matrix which transforms the temperature variations into reactivity variations.

In Simulink, the neutronics subsystem receives the vector of core temperatures as input, calculates the average temperature of fuel salt and graphite and the variation of reactivity ($\delta\rho$) due to temperature feedback on reactivity. Then it adds to $\delta\rho$ the eventual reactivity insertion due to control rods movement. The control rods rectivity insertion is clearly an external input to the whole system. The value of reactivity variation is sent to the state-space system (which is a system composed of equation of type 3.50), together with the precursor population which is re-entering in the core after having gone through the primary loop.

If the out-of-core primary loop transport time τ_l is known, the re-entering population can be calculated. Indeed, it can be expressed as the precursor population present in region N at time $t-\tau_l$ minus the precursors that decay during the transport time:

$$c_0^j(t) = c_N^j(t-\tau_l)\cdot e^{-\lambda^j\,\tau_l} \tag{3.61}$$

with j going from 1 to 6.

In figure 3.12 the discretization scheme used for MSRE neutronics in the current model is shown.

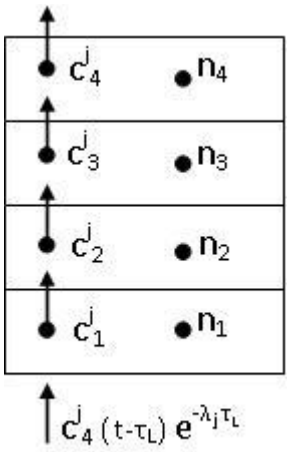

Figure 3.12: Example of a 4 regions discretization of MSRE neutronics

Stationary values are necessary for running the Simulink model, since it needs to be initialized. The stationary values of: population of the j-th precursor group in the i-th region, re-entering precursors and reactivity compensation, can be calculated setting, in equations 3.55 and 3.56, reactivity variation $\Delta\rho$ and all derivatives equal zero, and knowing the relation between precursors leaving the core and re-entering it (see Eqn. 3.61.

In solving equation 3.61, it is worth to notice that the value of precursors in core region N at time $t - \tau_l$ is the same at time t since the system is in a steady-state. The values of i-th neutronic populations are known from the stationary power which the reactor is working at, since the axial distribution of neutron population is known. Solving first for values of precursors (from equations of type 3.56), it is found that the j-th system is composed of N equation (as mentioned, subscript i is for the region and superscript j for the group of precursors, while subscript *0* denotes the stationary value of a variable), where, as seen above, only the equation of the first region is different from the others:

$$\begin{aligned} c_{0,1}^j &= \frac{\frac{N}{\tau_c}\, c_{0,N}^j e^{-\lambda^j \tau_l} + \frac{\beta^j}{\Lambda}\, n_{0,1}}{\frac{N}{\tau_c} + \lambda^j} \\ c_{0,i}^j &= \frac{\frac{N}{\tau_c}\, c_{0,i-1}^j + \frac{\beta^j}{\Lambda}\, n_{0,i}}{\frac{N}{\tau_c} + \lambda^j} \end{aligned} \tag{3.62}$$

The stationary value of "compensation" reactivity can now be easily obtained (from

equation 3.55):

$$\rho_0 \;=\; \beta - \frac{\Lambda}{n_0}\sum_{i=1}^{N}\left[\sum_{j=1}^{6}\lambda^j\, c_{0,i}^j\right] \;=\; \beta - \frac{\Lambda}{n_0}\sum_{j=1}^{6}\lambda^j\, c_0^j \tag{3.63}$$

In the Simulink model, the neutronics subsystem is constituted of a block whose output is a vector of lenght N composed of the thermal power of each i-th region. The i-th region power P_i is obtained from the i-th region neutron population n_i, since power and neutron population are in a relation of direct proportionality (assuming Σ_f to be constant all over the core height). The layout of the Simulink block containing neutronics equations is shown in figure 3.13.

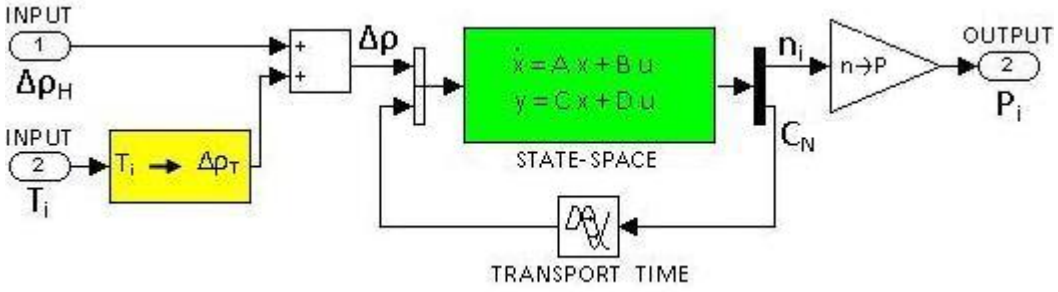

Figure 3.13: Layout of the NEUTRONICS block in the Simulink model

A complete Matlab code used to implement this model for a simulation with N core regions is given in Appendix 4.4.5.

3.5 General Simulink scheme of MSRE models

As any of the model was implemented in Simulink, a general layout has been adopted. The Simulink diagram was organized as follows: ordinary differential equations (or state-space systems where a N regions model was created) have been subdivided in four blocks. One block is for NEUTRONICS and its inputs are: a representative tem-

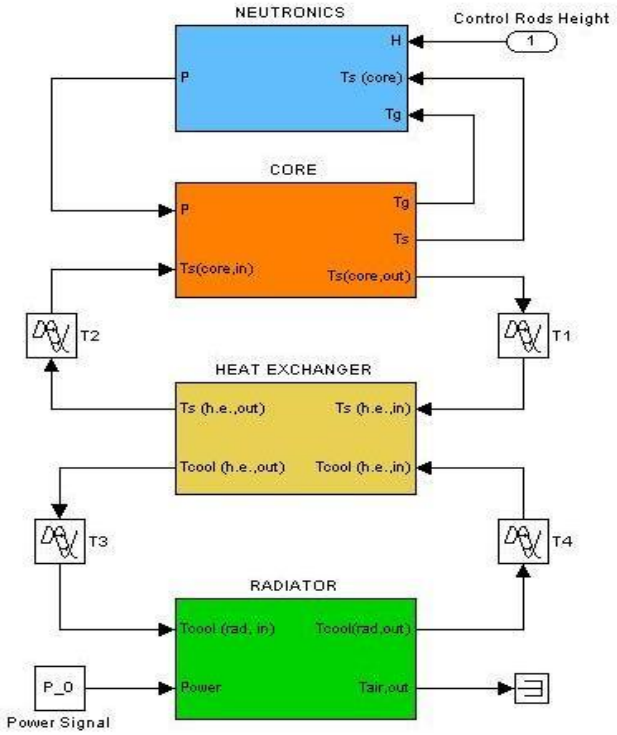

Figure 3.14: General model layout

perature (or a vector of temperatures) for the graphite, a representative temperature (or a vector of temperatures) for the fuel salt within the core, and a control rods height (or directly a reactivity value). Its output is the thermal power (or a vector of i-th powers).

A second block, called CORE, receives the thermal power and the fuel salt inlet temperature as inputs. Its outputs are the representative temperatures for the graphite and the fuel salt, and the fuel salt outgoing temperature. As mentioned, these inputs and outputs are vectorial quantities as a N nodes discretization is adopted.

A third block, called HEAT EXCHANGER, has fuel salt and coolant salt incoming temperature as inputs and their outgoing temperatures as outputs. Finally, a fourth block, called RADIATOR, receives the coolant salt incoming temperature and the

power signal as inputs. This signal is used to regulate the air flow and the radiator exchanging surface as required at that desired steady-state power level. As the control strategy of MSRE was of "reactor follows" type, this signal will also be used to produce power transients (as it was really used to regulate the power level). The RADIATOR block outputs are the coolant salt outgoing temperature and, if desired, the air outlet temperature.

Each one of the last three blocks contains two or four ordinary differential equations, according to the model complexity. The NEUTRONICS block contains always one ordinary differential equations for neutrons population (see Eqn. 3.7 or 3.55) but, while the zero-dimensional model has only 6 equations for precursors, one for each group, all one-dimensional discretized models have $6\times$N equations for precursors (see Eqn. 3.8 and 3.56).

Any block representing a physical component (core, heat exchanger and radiator) is connected to the preceeding one and to the following one by means of transport delay blocks. It is assumed that the precursor transport around the loop is a pure delay. The time delay is the nominal time that takes the fuel salt and coolant salt to go through the hot leg and the cold leg, respectively of the primary and secondary loop. Transport times are assumed to be constant and equal to their nominal value, except in analysis of mass flow transients (operating and accidental conditions, see chapter 4). The model layout is shown in Fig. 3.14.

Finally, a comparison between the plant model adopted by ORNL and the best available model developed in this chapter is considered. Looking at Figures 3.15 and 3.16, it is clearly observable that the ORNL model core region is constituted of several core-subregions, which are distributed both in series and in parallel, while in this work the best available model can be constituted of N "in series" core subregions. It follows that the ORNL model somehow takes into account the radial distribution of power (and neutron density, also) and the different mass flow which goes through the various parallel subregions. Also, the ORNL model correctly interposes the metal material between the two exchanging fluids both in the primary heat exchanger and in the radiator, while in this work it was neglected.

However, in the best available model of this thesis work the axial distributions of precursors is modelled, while it wasn't in the ORNL model.

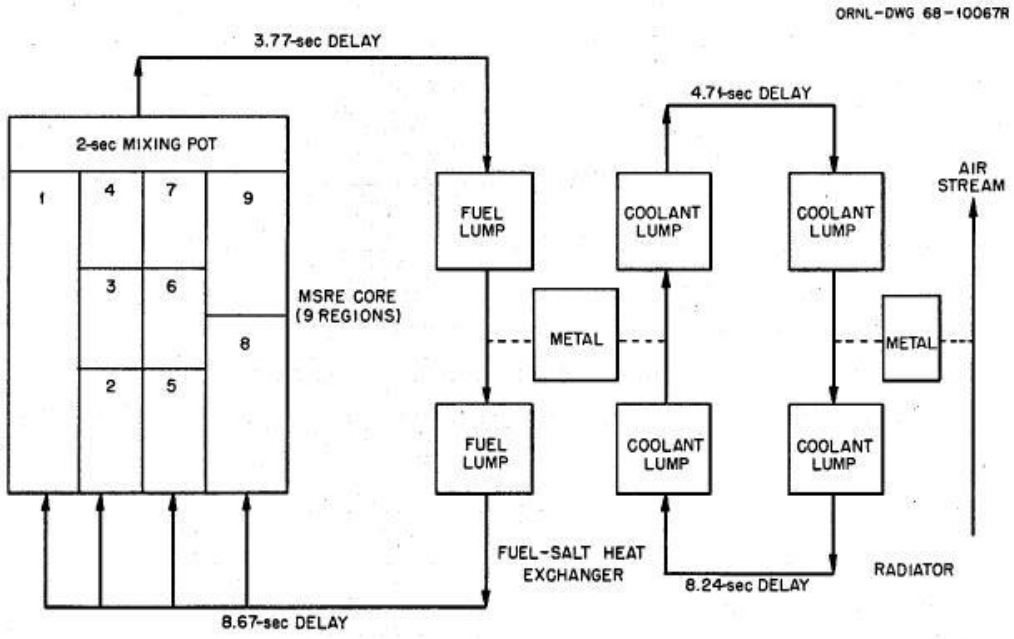

Figure 3.15: Schematic drawing of the MSRE model adopted by ORNL

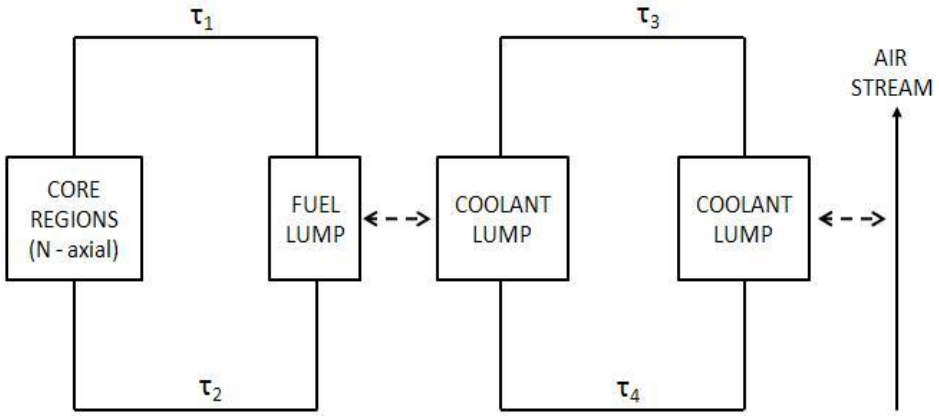

Figure 3.16: Schematic drawing of the MSRE model developed in this thesis work

Chapter 4

Analysis of simulations results

In this chapter, the results obtained through the Simulink simulations are reported. At first, the frequency analysis of the model is performed and compared to ORNL data. Also, the dynamic behaviour of the plant is discussed in the light of the magnitude and phase response obtained at various power levels. Then the steady state behaviour at various power levels is briefly shown and discussed. Further on, simulations of transient-behaviour of the system are illustrated and analysed. These simulations are organized in two sections: in the first one the transients during normal operation of the system will be analysed, while the transients during accidental conditions will be treated in the second one.

It will be shown a comparison between the different models developed in the previous chapter and a preliminary sensitivity analysis on the number of core-regions used to discretize the core in the one-dimensional model. All simulations will be carried out both for fuel type A (U-233) and C (U-235). The dynamic behaviours of the two fuel types will be compared and the differences will be then discussed. In case that experimental data are available, the simulation results will be compared to them. Also, some results will be compared to results obtained with different simulation tools, found in the MSRE bibliography [4] [24].

All the results are analysed and discussed in the light of the prefixed goal, which is to characterize and describe the dynamic behaviour of the MSRE. Merits and defects of the models will be pointed out. Eventual lacks or failures will be analysed and it will be tried to explain them, justifying whether they are accettable or not.

4.1 Frequency analysis of the models

The frequency analysis and the study of the zero-pole map will be reported in this section. They both will be carried out through the *Simulink linearization tool* [25], which allows to obtain either Bode or Nyquist diagram, step response or pole-zero map.

The Bode magnitude and phase responses of the one-dimensional model with a 100 core-regions discretization will be compared with the responses given in MSRE Oak-Ridge reports. The magnitude and phase diagrams are graphed for several power level of the plant working with fuel type A (U-233), in the range from full power (8 MW) to the lower limit of validity of the developed model (1 MW). Fewer phase curves are shown in order to avoid cluttering the plot. The Bode magnitude frequency response obtained from the one-dimensional model is plotted in Figure 4.1 and the Bode phase frequency response is shown in Figure 4.3.

Both the magnitude and phase response obtained from the model developed in this chapter result similar to the ones obtained with the model elaborated at Oak Ridge National Laboratory, which was obatained through a calibration with experimental data. The magnitude and frequency responses of ORNL complete model are reported in Figure 4.2 and 4.4 respectively. They are taken from report ORNL-TM-1070 [19], which deals with reactor stability.

Several observations can be based on the information contained in the the magnitude and phase responses curves. First, the main peak of the magnitude curves gets taller and sharper and moves towards lower frequencies as power decreases. For what concerns the amplitude curve, knowing that high narrow peaks indicate that the system is less damped than is indicated by low broader peaks, it can be observed that the system is less damped at low power. Since the system is self-stabilizing at higher power, it would not tend to run away. For what concerns frequency, since the frequency at which the magnitude curve has a peak approximately corresponds to the frequency at which the system will naturally oscillate in responce to a disturbance [19], the low-power oscillations are much lower in frequency than the full-power ones.

A resonance at about 0.25 rad/s can be noticed in both the magnitude and phase diagram. This dip is due to the fuel circulation time in the primary loop (which is about 25 seconds):

$$\frac{2\,\pi\left[\frac{rad}{cycle}\right]}{25\left[\frac{s}{cycle}\right]} \;=\; 0.25\left[\frac{rad}{s}\right] \tag{4.1}$$

The resonance dip of the magnitude and phase curves are lower than the resonance dips found in ORNL model magnitude curve. This can perhaps be explained considering that in the models developed in this chapter the radial dimension does not appear ever, and the fuel mixing is not modelled, neither the temperature feedback is weighed with position.

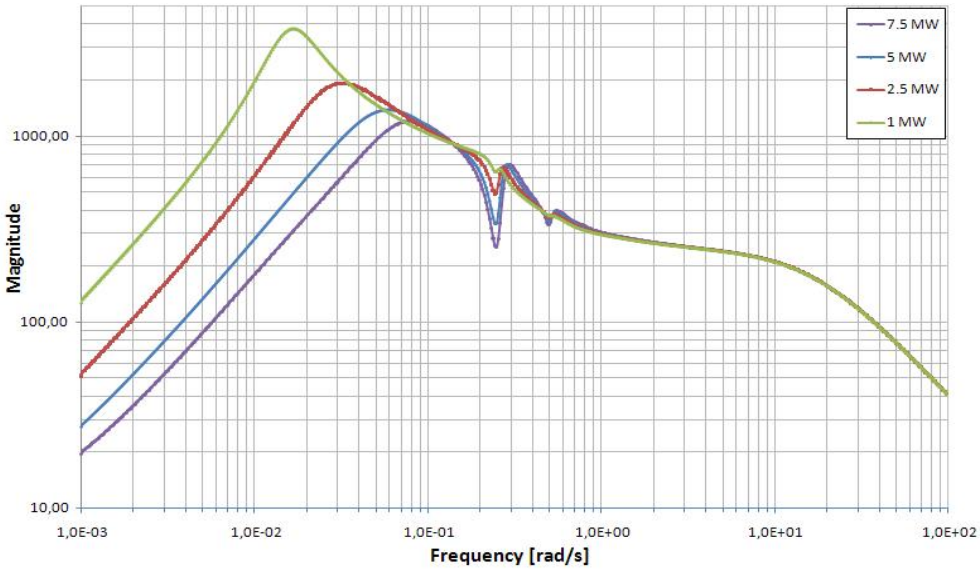

Figure 4.1: Frequency response (magnitude curve) of the one-dimensional discritized model for several power levels

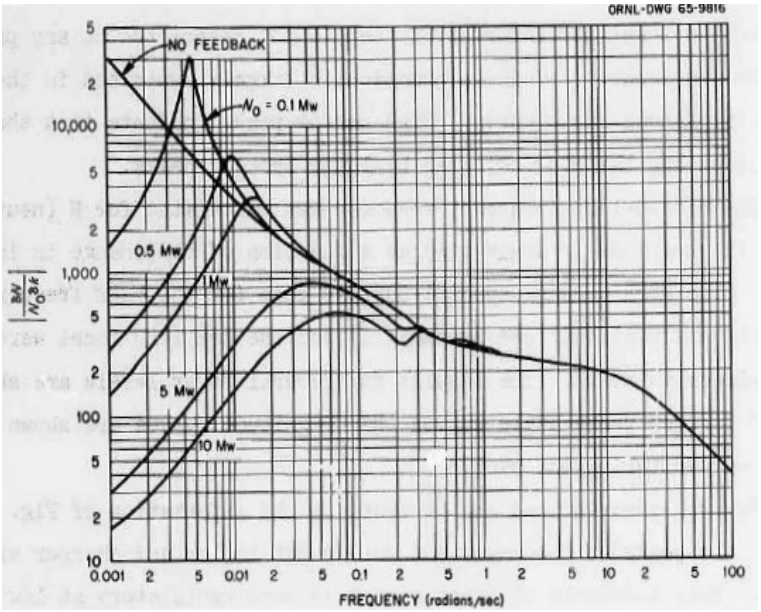

Figure 4.2: Frequency response (magnitude curve) of the ORNL model for several power levels

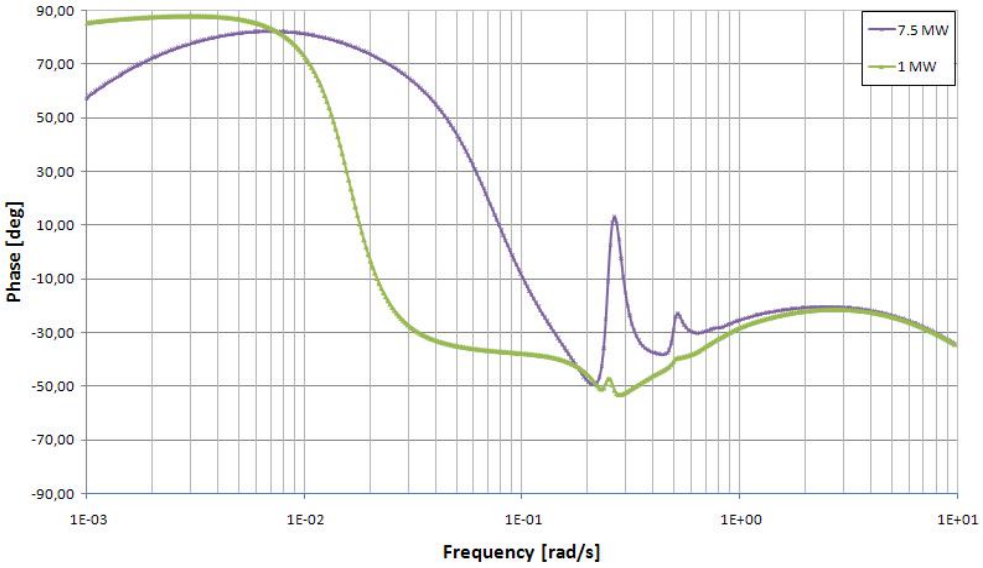

Figure 4.3: Frequency response (phase curve) of the one-dimensional discritized model for several power levels

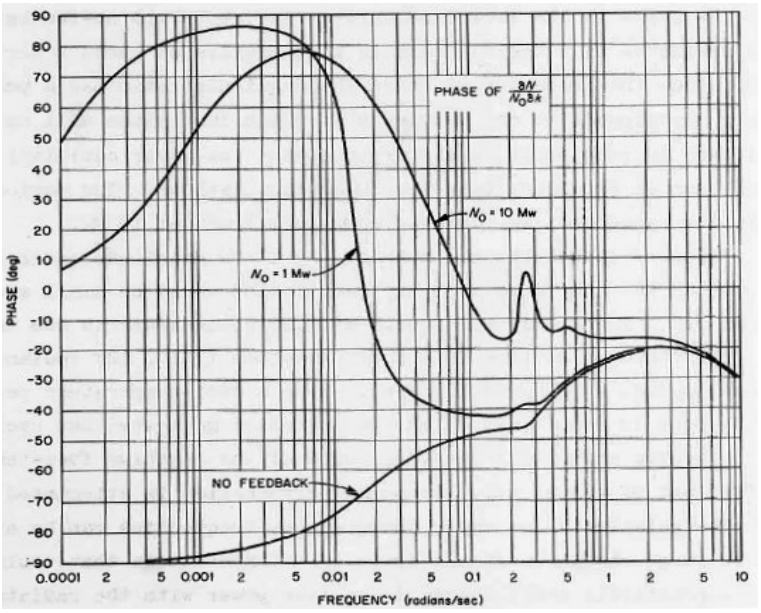

Figure 4.4: Frequency response (phase curve) of the ORNL model for several power levels

Discussing the general dynamic behaviour of the plant, it is noteworthy that the MSRE has a large ratio of heat capacity to power production. This inidicates that temperatures will change slowly with power changes. It also suggests that the effects of the negative temperature coefficients will appear slowly, and the system will be sluggish, even if the values of temperature coefficients are high.

Another factor that contributes to the sluggish time response is thermal resistance, particularly the one of the heat sink (the air radiator) [19]. A qualitative idea of the system time constant for heating and cooling the entire primary and secondary systems can be found considering the equivalent electric circuit of MSRE. A very simple scheme is shown in Figure 4.5. where power is considered an independent

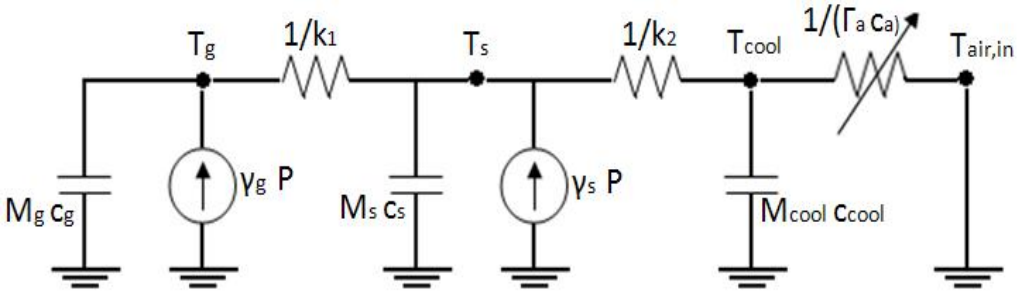

Figure 4.5: MSRE equivalent electric circuit

variable, heat capacities and two thermal resistances (between graphite and fuel salt and between fuel salt and coolant salt) are assumed to be constant, while the radiator thermal resistance varies with air flow. Since at lower power the air flow is lower, this thermal resistance is higher at low power. In general, a time constant (which is not exact solution of the circuit reported in Fig. 4.5) of a R C circuit assumes the form:

$$\tau = C \cdot R$$

where C is the heat capacity of the system and R its thermal resistance. Being the heat capacity considered constant, it was observed that the thermal resitance changes with power, particularly it increases as power decreases. Therefore, the time response changes with power and at lower power it is slower. It is clear that the period of the system is longer at low power.

Finally, the zero-pole map of the one-dimensional discretized model is reported in Figure 4.6. As expected, the transfer function representing the power responce to a reactivity input is constituted of poles and zeros which are all negative. This confirms that the system is stable. The zero-pole map was obtained with the *linearization tool* of Simulink. In this work, for the exponential representing time delays, a third order Padè approximation was adopted.

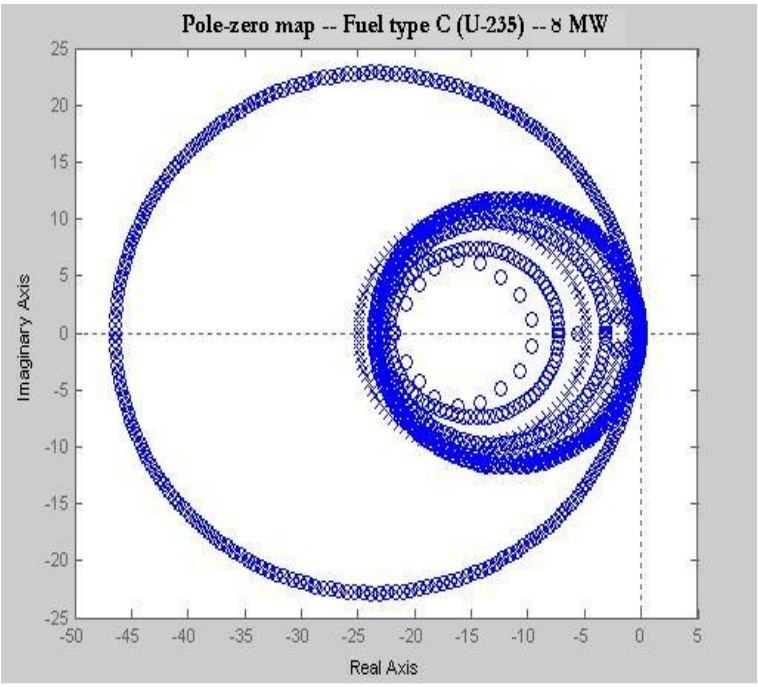

Figure 4.6: Zero-pole map of the one-dimensional discritized model at full power (with fuel type C)

Concluding, it can be stated that there are two important aspects of the MSRE's inherent stability characteristics.

- The reactor tends to increase the relative amplitude of its power variation at lower power, as expected.
- The time response is very long and increases with lower power.

4.2 Steady-state results

In this section some steady-state results are shown. No external control is present. The results concern the precursor distribution, the reactivity loss due to precursor drift, the axial temperature profile of graphite and fuel salt in the core region, and the trend of the plant significative temperatures as the power level changes.

Comparing the zero-dimensional model to the one-dimensional model discretized with N core-regions, it is significant to compare the value of loss of rectivity obtained in the two cases. In Table 4.1 the values of reactivity, which is necessary to compensate for, are reported both for fuel type A (U-233) and C (U-235). One of the main differences between operation with ^{233}U and ^{235}U is the smaller fraction of delayed neutrons with the ^{233}U, as can be seen comparing values of βs.

Reactivity Losses [pcm]		
	U-235	U-233
Model Type	(β=0.666%)	(β= 0.264%)
Zero-dimensional	245.92	111.70
One-dimensional - 2 core-regions	265.16	119.52
One-dimensional - 10 core-regions	272.07	123.50
One-dimensional - 200 core-regions	273.23	124.41

Table 4.1: Comparison between different models of reactivity loss due to precursor drift

Also, a preliminary analysis of sensitivity on the core-regions number used in the discretization ensues from reported results. For instance, at nominal power (8 MW) it is found that for a 200 core-regions the total loss of reactivity with fuel of type C (based on U-235) is $\rho_0 = 273\ pcm$, while, with a zero-dimensional modelling of neutronics the total loss of reactivity was $\rho_0 = 246\ pcm$ (see Eqn. 3.9). The difference between the two estimates, which is quantifiable in about 10%, is due to the different precursors distribution in the two modelling approaches. In 1D-1D model a precursor build up is present in the top regions of the core (see next page), while in the 0D-0D model it is implicitly assumed a uniform distribution through the core region.

Indeed, having developed a N core-regions approximation, and therefore having taken into account the axial distribution of neutron popolation, enables to obtain a more realistic distribution of precursors through the core height (see figures 4.7 and 4.8).
In defining precursor population three phenomena are in competition: formation of precursors, which is proportional to the neutron population of the region through the coefficients β_i, precursor drift due to fuel circulation and decaying of precursors themselves according to their own decay constant λ_i. Investigating Figure 4.7 it can be observed that for precursors groups 1 and 2 the build-up is dominating, since half-lives ($T_1^{1/2}$= 55.01 s and $T_2^{1/2}$= 20.57 s) are much higher than the core transit time

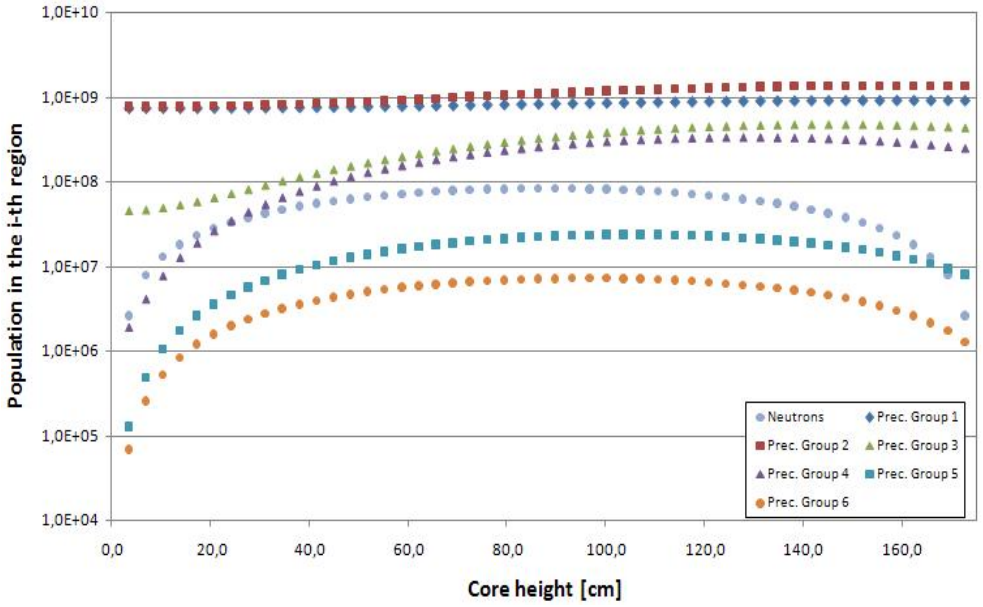

Figure 4.7: Neutrons and precursor population versus core height - 50 core regions (reactor working with Fuel A at 8 MW)

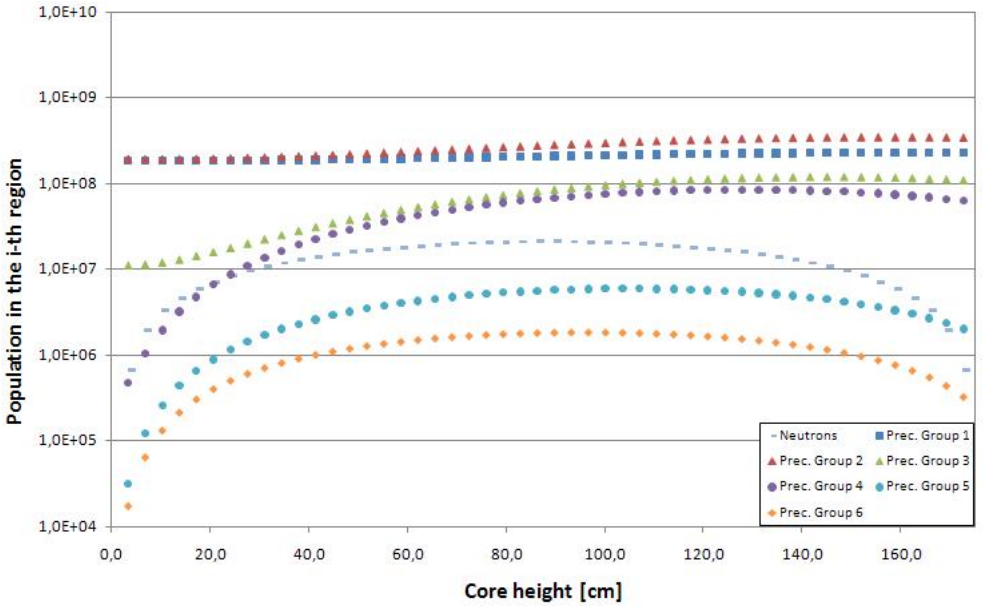

Figure 4.8: Neutrons and precursor population versus core height - 50 core-regions (reactor working with Fuel A at 2 MW)

(τ_c= 8.46 s). Viceversa, precursor population of groups 5 and 6 has the same distribution of neutron populations (axial profile like a cosine), since half-lives ($T_5^{1/2}$= 0.61 s and $T_6^{1/2}$= 0.28 s) are much lower than the core transit time and precursors substantially decay where they have been generated.

Also, it can be observed that precursor population of group 2 is higher than that of group 1, although $T_1^{1/2} > T_2^{1/2}$, because the yield fraction of group 1 is almost one fourth of the yield fraction of group 2 (β_1= 22.8 pcm and β_2= 78.8 pcm). Finally, comparing Figure 4.7 to Figure 4.8, it can be observed that, when the reactor is working at lower power, the ratio between precursor population and neutron population is the same (as expected from zero-dimensional model), while, as obvious, their absolute value are proportionately lower.

For what concerns the control of the MSRE, as mentioned in chapter 2, one of the main requirements is that salts temperatures have to stay above 450 °C so that salt remains molten. This requirement is satisfied in the MSRE by helding constant the core outlet temperature of fuel salt as power is reduced. Its value is fixed at about 660 °C. This implies that average fuel salt temperature, and coolant salt temperature also, increase as power level decreases. (This control strategy is adopted in the power range between 8 MW and 1 MW, while below this power level a "power imposed" control strategy is adopted.) The trend of fuel salt, coolant salt and air temperatures versus the power level is shown in Figure 4.9.

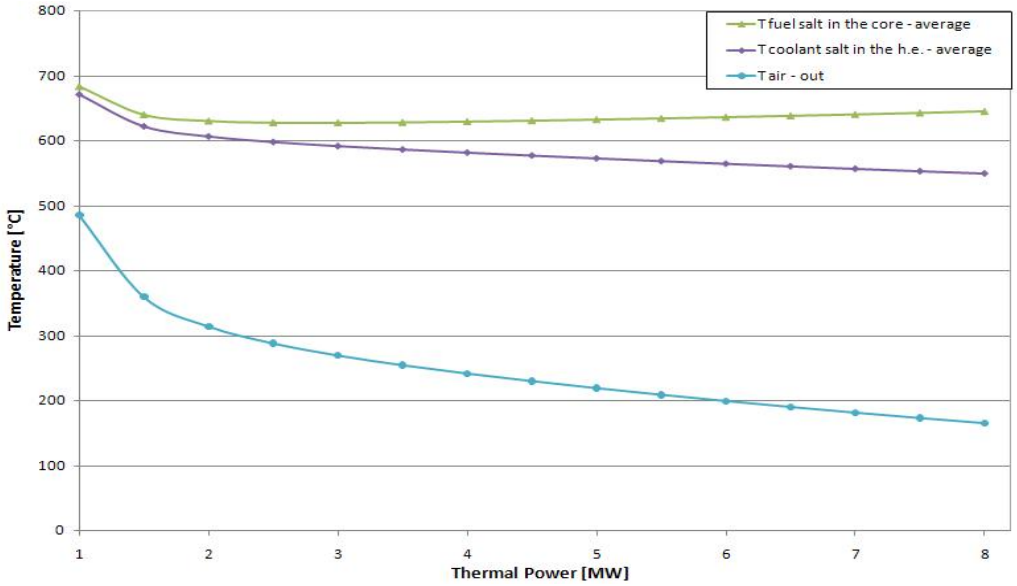

Figure 4.9: Fuel salt, coolant salt and air temperatures versus thermal power

Moreover, for what regards the validity of the model, it is worth reminding (it was anticipated in chapter 3) that the effects of poisoning due to neutron absorbers build-up and to fuel burnup are not modelled [1]. It follows that the model is not capable to reproduce the long-term effects due, for example, to Xenon poisoning, which would imply a compensation through the two shim control rods.

Through the one-dimensional (N regions) model it is possible to observe the axial temperature profile of the fuel salt and the graphite. No data regarding the axial

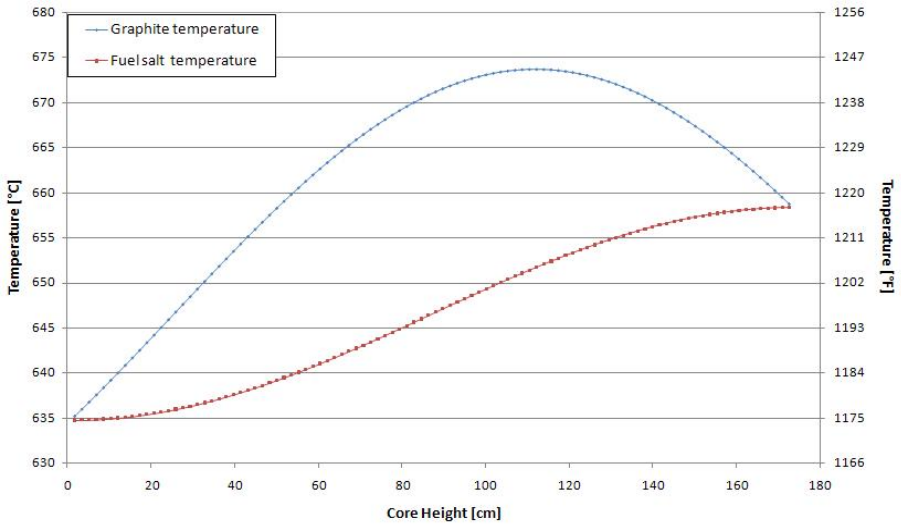

Figure 4.10: Axial profile of fuel salt and graphite temperatures in the core region (8 MW)

temperature profile of an average channel are available in ORNL reports, however it is reported a *hot channel* analysis with axial temperature profile of fuel salt and of the adjacent graphite stringer (see Figure 4.11, taken from [8]). Of course, these data are not comparable for what concerns the values of temperature, but only for what concerns the axial temperature profiles. Finally, it is worth noticing that in the ORNL model graph the graphite and fuel temperature do not "touch" at the core inlet and outlet, while they do in the 1D-1D model simulations. This is due to the fact that, in 1D-1D model, the power axial profile assumes a cosine shape where extrapolated lenghts are not taken into account.

[1] However, it is worth noting that the negative reactivity effect due to build-up of stable fission products, which depends primarily on integrated power, is compensated by periodic additions of U-235. However, the transient effects, such as those due to ^{135}Xe and ^{149}Sm, are compensated by control rod manipulation.

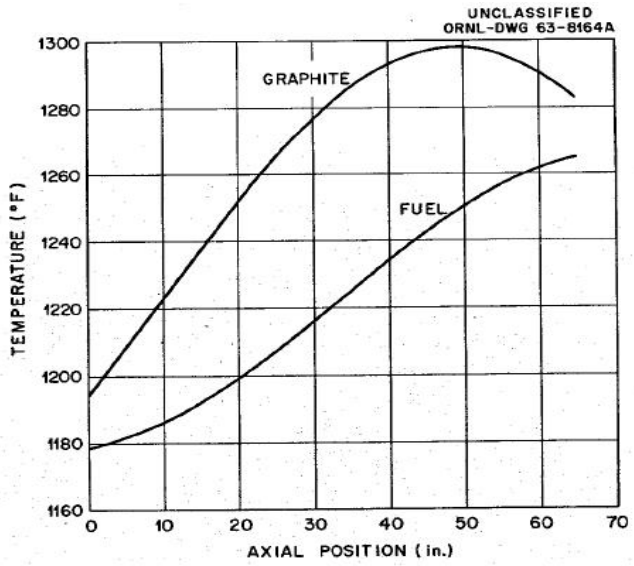

Figure 4.11: Axial temperature profiles in the *hot channel* and adjacent graphite stringer

4.3 Transient-behaviour analysis of the system during normal operation without external controller

In this section will be analysed some of the transients which occur during normal operation of the reactor. First, a general discussion on the MSRE dynamical behaviour is brought on. Then, some control rods insertions and withdraw transients will be simulated. As mentioned, a comparison between different models and experimental data, where available, will be shown. Finally, some variations on air mass flow going into radiator will be simulated. This is the actual way power was changed in the MSRE: as mentioned in section 2.6, it is a "reactor follows" control strategy. In the following sections the developed models will be referred as follows:

- 0D-0D: Zero-dimensional model (see Section 3.1)
- 1D-0D: One-dimensional model of the core (N regions) for what concerns thermo-hydraulics, zero-dimensional as regards the equation of precursors (see Section 66)
- 1D-1D: One-dimensional model of the core (N regions) for what concerns both thermo-hydraulics and the equation of precursors (see Section 68)

Speaking about the MSRE dynamics the first observation is that, whenever the reactor power is raised, temperatures of the fuel and graphite throughout the core

must increase. In the following pages it is meant to describe and analyze these inherent characteristics of the reactor, not including any external control in any of the simulations.

Dynamically, the two most important characteristics of the MSRE are that the core is heterogenous and that the fuel circulates. The fuel circulation acts to reduce the effective delayed-neutron fraction, to reduce the rate of the fuel temperature change during a power change, and to introduce delayed fuel-temperature and delayed neutron-production effects. The heterogeneity introduces a slow feedback effect due to graphite temperature changes [19].

Also, the MSRE has a large ratio of heat capacity to power production. As it was shown in section 4.1, the time constant of the system depends on the thermal resistance, which in turn depends on the air mass flow. As power decreases, the air mass flow decreases, the thermal resistance increases and, finally, the time response of the system becomes slower.

Since in the model developed in the previous chapter the effects due to fuel burnup, buildup of stable fission products, and poisons creation, are not included, it follows that these model can be used only for simulation whose duration is short (on the order of hundreds of seconds). Also, it can be predicted that the inertia of the whole system will be slightly lower in the developed model than what it was in MSRE. This is due to the fact that structural materials such as all metal constituting the heat exchanger, the radiator, all piping structure and so on, was not taken into account in these models. It is also worth reminding that heat losses, which occur throughout all the primary and secondary loop, were not modelled.

4.3.1 Reactivity insertion

In the following pages the transients of power for ^{235}U-fueled MSRE and ^{233}U-fueled MSRE will be obtained and compared with ORNL results. The control rods step Δh is not directly simulated since a representative value of the coefficient α_h is not available. It follows that, in the equation 3.10, it is operated the substitution:

$$\alpha_h \, \Delta h = \Delta \rho_h$$

In Figures 4.12 and 4.13 the power transients following a step insertion of 10 pcm are reported for the various developed models. The initial power level is 8 MW.

In both the cases of ^{235}U-fuel and ^{233}U-fuel it can be observed that in all models the power peak and the undershoot reach about the same value. However, it can be noticed that the shapes of the 1D-1D curves (both with 10 and 100 regions) are slightly different than the 0D-0D and 1D-0D models. Indeed in the 1D-1D model the power peak is reached earlier (the rise is steeper) and also the power decreases earlier. This happens because in a case the modelling of neutronics keeps into account the axial distribution of precursors and their convection due to the salt motion and in the other it does not. Considering the precursor distribution through the core introduces an

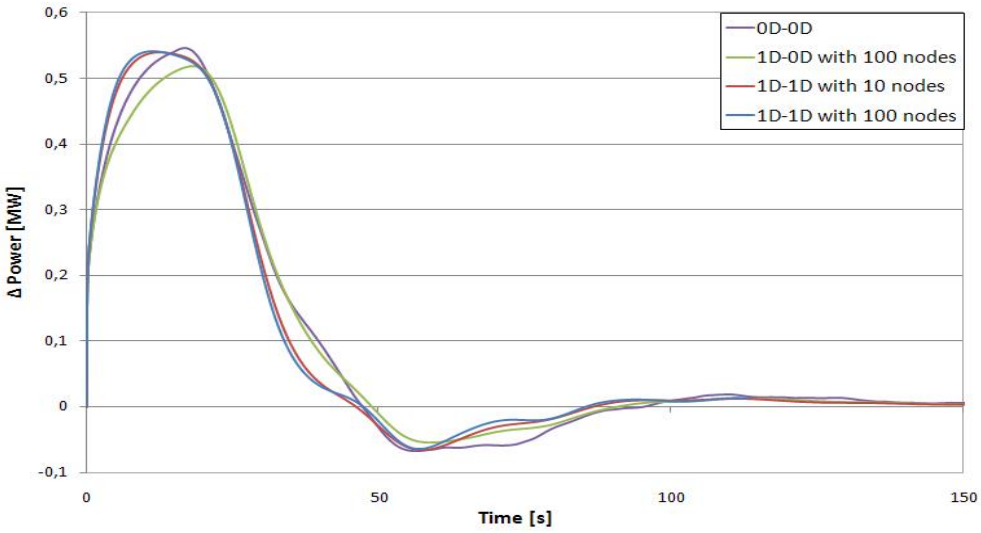

Figure 4.12: Comparison of the power response of the ^{235}U-fueled MSRE of various developed models to an insertion of 10 pcm

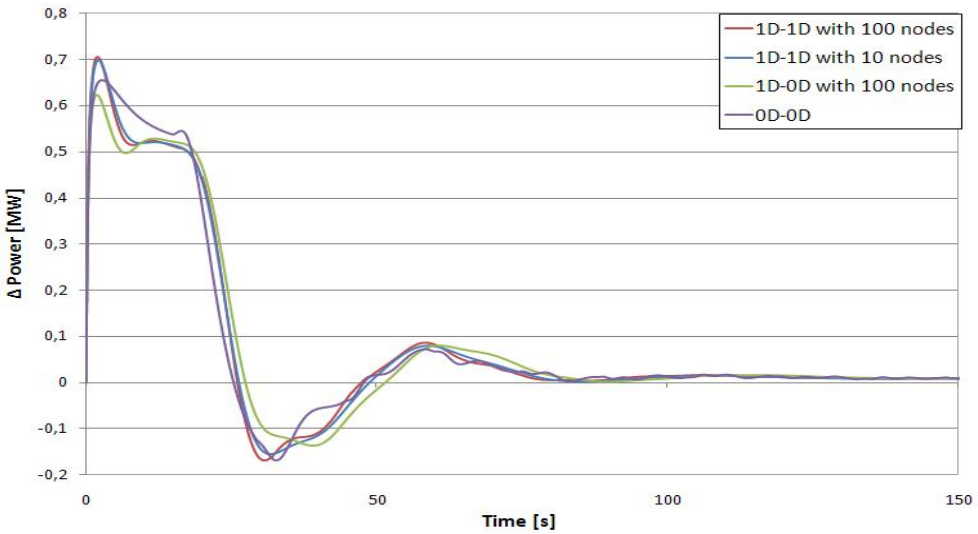

Figure 4.13: Comparison of the power response of the ^{233}U-fueled MSRE of various developed models to an insertion of 10 pcm

effect of buildup which is clearly evident: the long-living precursors do not assume the typical cosine axial distribution and their number increases until the top of the core (see Figures 4.7 and 4.8).

On the contrary, in the 0D-0D and 1D-0D models the differential equation describing the quantity of precursors (see Eqn. 3.8) does not take into account their distribution through the core region, but only their total quantity. Indeed, when expressing the number of precursors leaving the core just through a time constant (time of renewal), as it is typical of a zero-dimensional modelling approach, it is implicitly assumed that they are uniformly distributed. For what concerns the transients, it

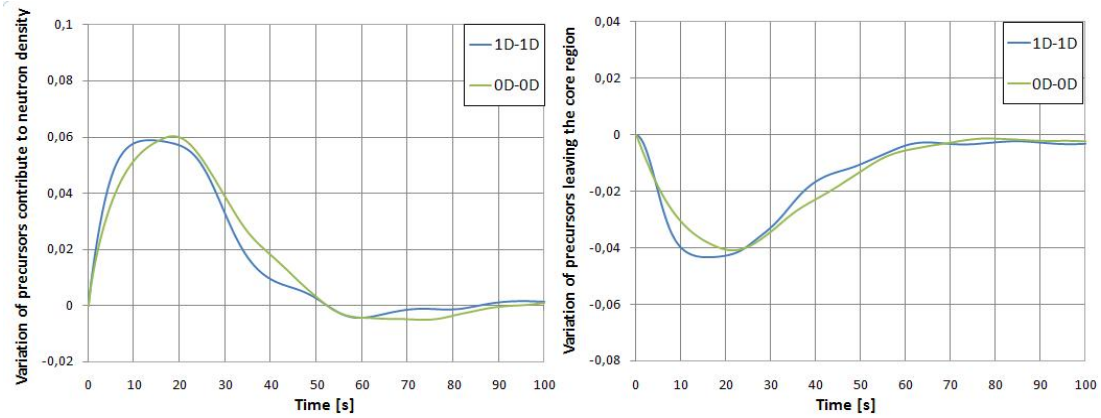

Figure 4.14: Following a reactivity step of 10 pcm in ^{235}U-fueled MSRE it is obtained: variation of the term "contribute of decaying precursors to neutron density" in the differential equation of neutrons (on the left) and variation of the term "precursors leaving the core" in the differential equation of presursors (on the right)

is observable that, since power increases earlier in the one-dimensional model, also the number of precursors increases earlier than in case of zero-dimensional neutronics. This could be explained in the following way. when the neutron density is increased through a reactivity insertion, it adds a *cosine distributed* source of precursors to a non-cosine distribution (see Figure 4.7). This makes the contribute of decaying precursor to neutron generation relatively higher than what it would have been if precursors were uniformly distributed. This might explain why the power peak is reached earlier in 1D-1D models.

On the other hand, having more precursors in the top region of the core affects the fraction of precursors leaving the core [2]. This explains the earlier decrease of power in 1D-1D model. Summarizing, following a positive reactivity insertion:

- The term (in neutron equation) which keeps into account for the delayed neutrons increases earlier in the 1D-1D model than in the 1D-0D and 0D-0D models (see

[2]This is true in a steady-state too, see Table 4.1.

Figure 4.14), therefore the peak is reached earlier.

- The term (in precursor equation) which keeps into account for precursors leaving the core becomes bigger earlier in the 1D-1D model than in the 1D-0D and 0D-0D models, therefore the number of precursors decreases earlier and so does the number of neutrons (see Figure 4.14).

It can be stated that the modelling of precursors distribution affects the neutron and precursors dynamics and makes it more realistic. The 1D-1D model is effectively capable of simulating more accurately the transient behaviour of the core.

Anyhow, for what was seen so far, it seems not justify the necessity to improve the model and adopting a more complex model than the 0D-0D. Indeed, it seems capable of simulating the plant transient behaviour just like the 1D-0D model. However, as already mentioned in the previous chapter (see page 57), if the results on temperature variations are considered, it can be noticed that the zero-dimensional model reproduces unaccetable variations on the temperatures (all the ones that are not state variables). Looking at Figure 4.15 it is evident that the oscillation of outlet temperature given by

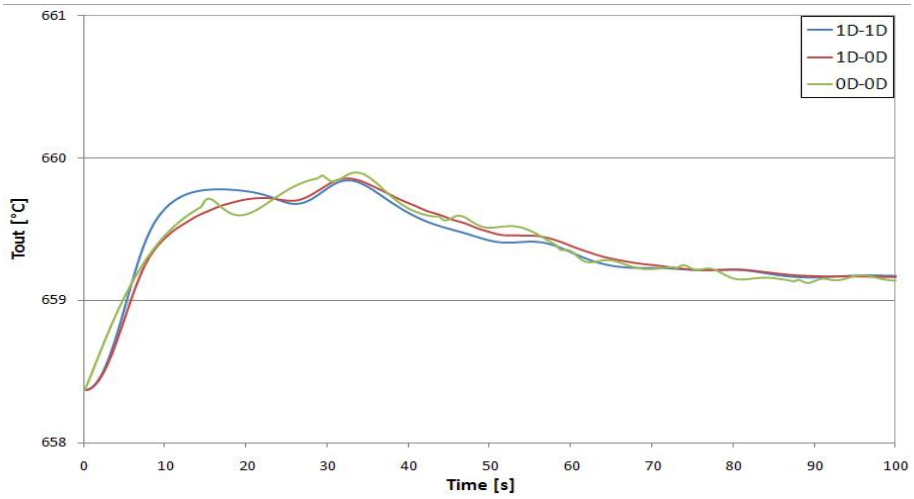

Figure 4.15: Comparison of the fuel-salt outlet temperature response of the ^{235}U-fueled MSRE of various developed models to an insertion of 10 pcm

the 0D-0D model is not physical but only due to the modelling approach. Indeed it is not present in the other models.

It is also interesting to compare the dynamic behaviour of MSRE when ^{235}U-fueled and ^{233}U-fueled. The power response of the plant to the usual 10 pcm (0.01% dK/K [3] reactivity step is given for the two fuel types in Figure 4.16. The difference in the value

[3] k is the effective neutron multiplication factor (see page 53).

of power reached by the peak can be explained through neutronics considerations. Reporting the differential equation (see 3.7) describing the neutron population written in this way:

$$\frac{dn(t)}{dt} = \frac{\Delta\rho(t) + \rho_0 - \beta}{\Lambda} n(t) + \sum_{i=1}^{6} \lambda_i \, c_i(t)$$

it can be seen that both ρ_0 and β are constant. Now, defining an effective fraction of delayed neutron β_{eff}[4] as the difference between the total delayed neutron fraction β and the "compensation reactivity" ρ_0, it is found (using the 1D-1D model with a 100 core regions discretization):

$$\beta_{eff}^{235} = \beta^{235} - \rho_0^{235} = 420.2pcm$$
$$\beta_{eff}^{233} = \beta^{233} - \rho_0^{233} = 152.3pcm$$

Hence, an insertion of 10 pcm of reactivity assumes a different weight for the two fuel types:

$$\frac{\Delta\rho}{\beta_{eff}^{235}} < \frac{\Delta\rho}{\beta_{eff}^{233}}$$

It follows that the same insertion of reactivity causes a higher power peak in the

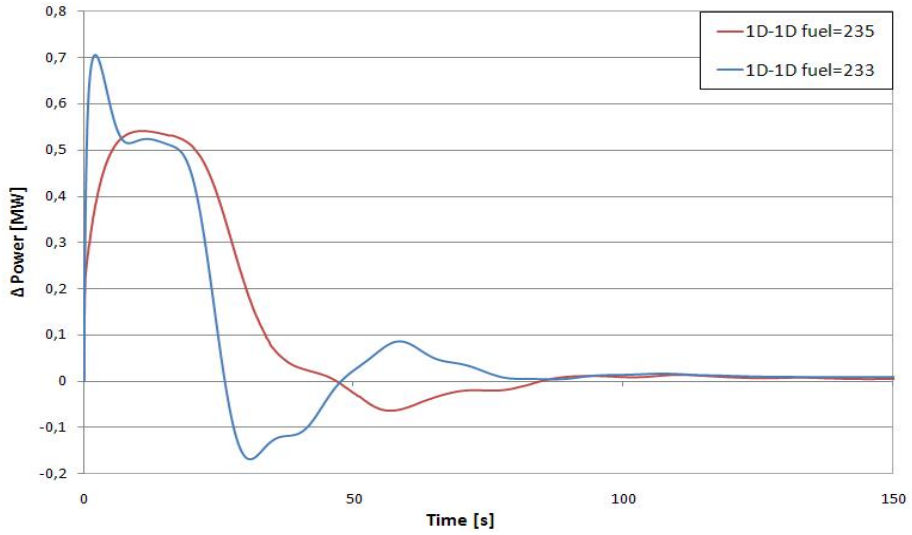

Figure 4.16: Power response of the ^{235}U-fueled MSRE versus power response of the ^{233}U-fueled MSRE of 1D-1D model to an insertion of reactivity (0.01% dk/k)

^{233}U-fueled MSRE than in the ^{235}U-fueled MSRE, as the last is closer to a situation of prompt-criticality. Still, looking at Figure 4.15, it is clear that the deeper undershoot which is present in case of ^{233}U-fueled reactor is a consequence of the peak height: the

[4]It is the effective contribute of delayed neutrons to the core criticality

thermal feedback due to the effect of the power peak on the fuel salt temperature is more relevant since in this case the temperature rise is larger.

Finally, it is worth noticing that the reactivity insertion is almost completely recovered: when the transient is exhausted, the new steady-state value of power is practically the same as it was initially. This is due to the high feedback coefficients.

In the following pages the transients in the simulation obtained calculated by different models are illustrated. In Figure 4.17 and 4.18 the power transients which follow a step insertion of reactivity in the ^{235}U-fueled MSRE are shown for the 1D-1D model and the ORNL model respectively. The inserted reactivity $\Delta\rho$ is equivalent to a 0.01% δk/k step.

In Figure 4.19 and 4.20 the power transients which follow a step insertion of reactivity in the ^{233}U-fueled MSRE are shown for the 1D-1D model and the ORNL model respectively. The inserted reactivity $\Delta\rho$ is equivalent to a 0.02% δk/k step. Some observation, regarding both the ^{235}U-fueled MSRE and the ^{233}U-fueled MSRE, can be made.

- The power peak obtained with the 1D-1D model (the best available in this work) is always higher than the peak obtained with the ORNL model, which was characterized and calibrated through experimental data. At low power the difference on the power peak value is smaller.

- The undershoots which result from 1D-1D model simulations are not present in ORNL simulations except for low power levels. This is strictly connected to the previous obsevation on the power peak: indeed as the power peak is higher, the rise of fuel salt temperature is larger, and consequently the thermal feedback, which appears after the primary loop transit time (about 25 seconds), is more relevant.

- For what concerns the period of oscillation, the duration and the trend of the transients is very similar in the two model, mostly at a low power level.

It is interesting to hypothesize an explanation for the mismatch which is found on the peak values and the amplitudes of the undershoots. It is reasonable to assume that the explanation is a combination of the following causes:

1. The models developed in this work are at most one-dimensional. It follows that the radial effects on power density distribution and mass flow distribution can not be modelled and reproduced. For instance, if the power density was not uniformely distributed in the radial direction (as it is implicitly assumed in these models), but it was higher in the central region, it would happen that the fuel going through those channel would warm up more and faster. The thermal feedback would affect earlier the neutronics, avoiding a so high power peak and consequently a so low undershoot.

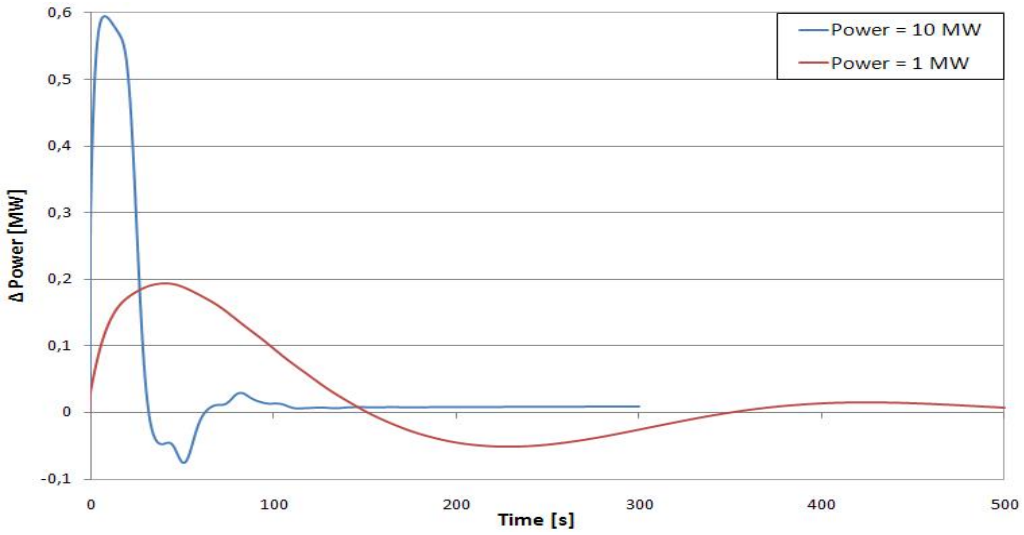

Figure 4.17: Power response of the ^{235}U-fueled MSRE to a 0.01% δk/k step reactivity at various power levels with 1D-1D model with 100 core-regions

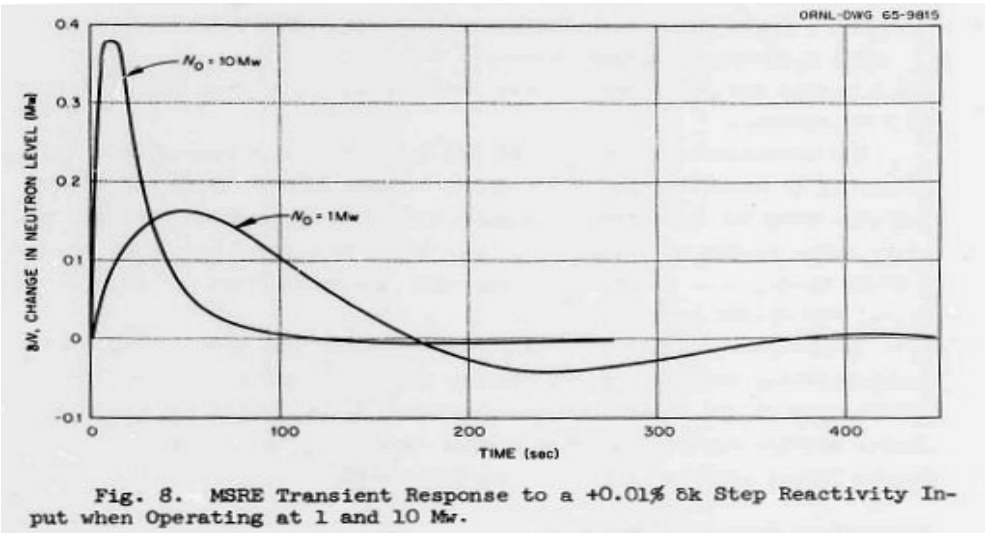

Figure 4.18: Power response of the ^{235}U-fueled MSRE to a 0.01% δk/k step reactivity at various power levels with ORNL model

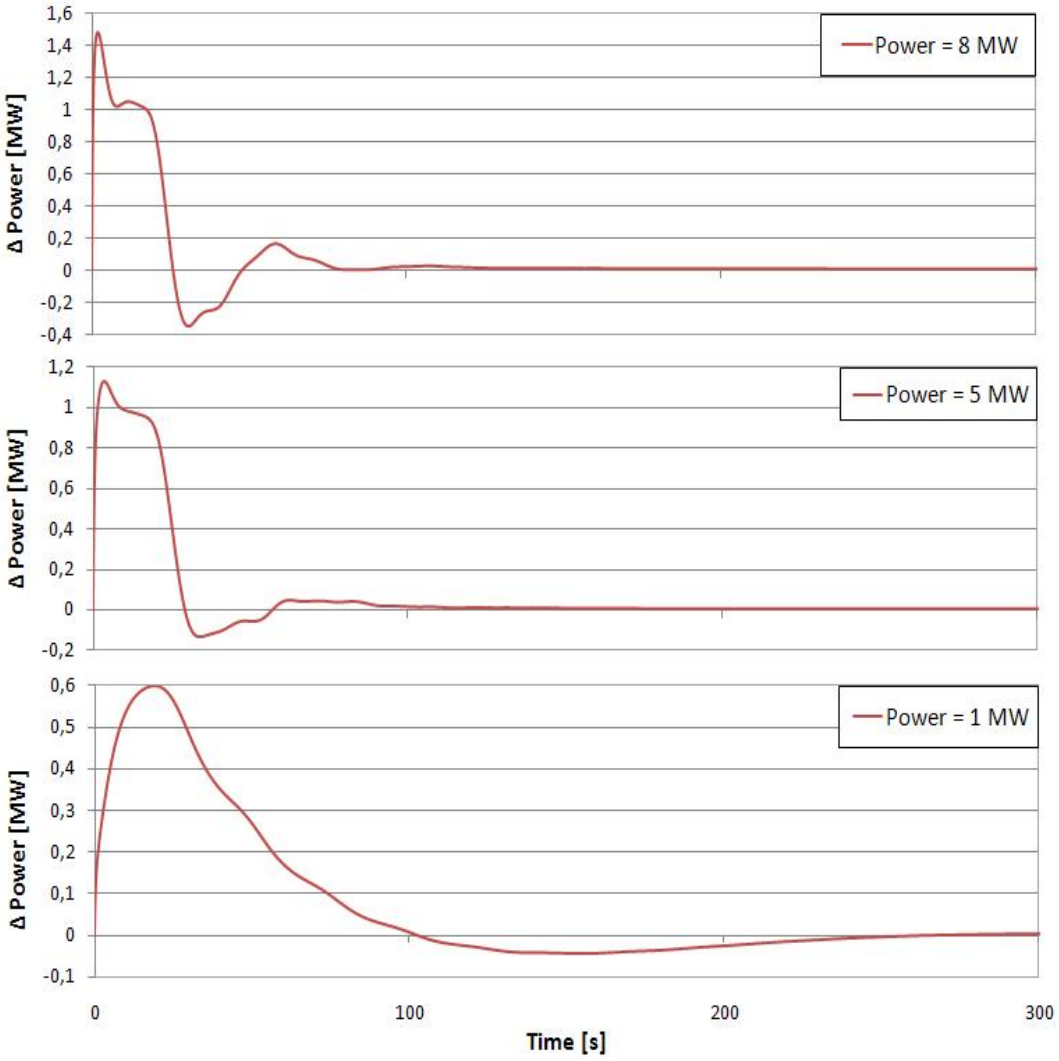

Figure 4.19: Power response of the ^{233}U-fueled MSRE to a 0.02% δk/k step reactivity at various power levels with 1D-1D model with 100 core-regions

2. It can be noticed that, in the ORNL model of the MSRE, the thermal feedback is weighed with the core height. Indeed the feedback coefficient is higher towards the top of the core. Some hypothesis can be made: it might be due to a variation of the thermal feedback coefficents with varying temperature, while in the models developed in this work they are assumed to be constant with temperature. Otherwise, it could be due to the fact that actually a fraction of the thermal power is released out of the core region, while in all the models thermal power is totally lumped in the core region and, in order minimize this approximation, it could have been given more weight to the regions close to the top of the core. Finally, it could be due to the precursors distribution, shaped differently than a cosine, which affects the neutron population distribution through the emission of delayed neutrons.

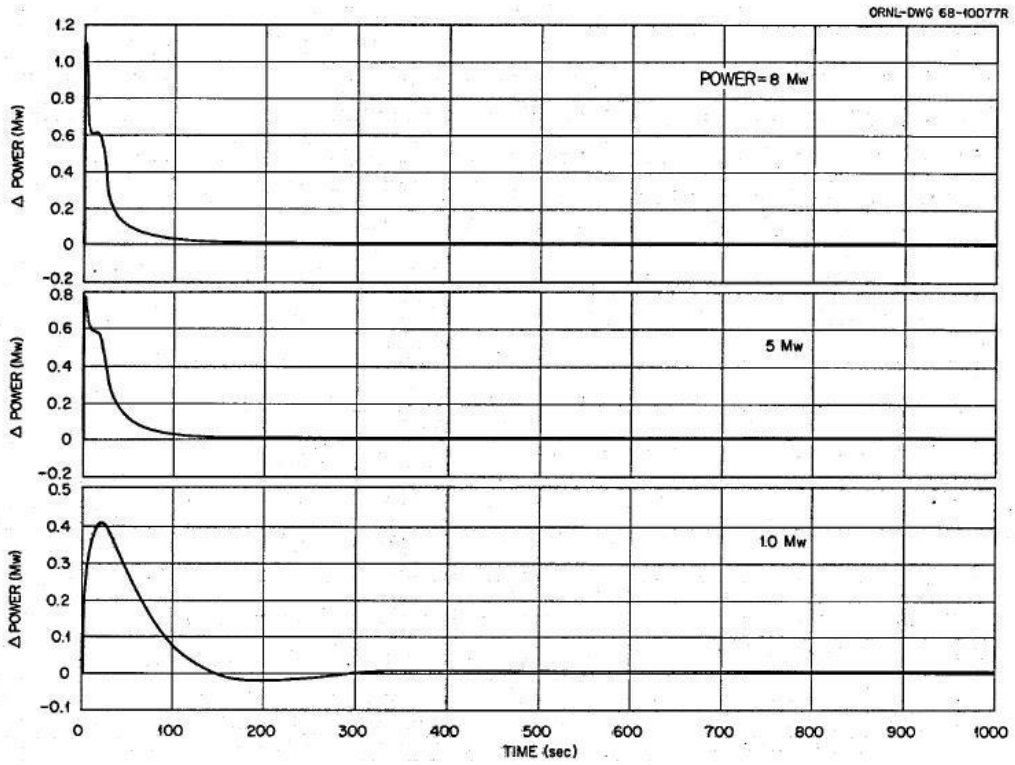

Figure 4.20: Power response of the ^{233}U-fueled MSRE to a 0.02% δk/k step reactivity at various power levels with ORNL model

3. In this work the thermal inertia due to structural materials is not considered. It is realistic to think that, because of these effects, the temperature of fuel reentering the core after having gone through the primary loop is lower, being the other terms equal, than what is predicted in the developed models.

In order to validate the second of these hypothesis (it was chosen the second as it was the simplest to proof) it has been tried to reproduce the effect of the different weighs given to the temperatures in evaluating the thermal feedback. This was done distributing the thermal feeback coefficients giving them a higher value towards the top of the core, but not changing their integral value. The implemented scheme gives the chance to leave a fraction of the feedback coefficents uniformly distributed and the complementary fraction linearly distributed (with values increasing with the height).

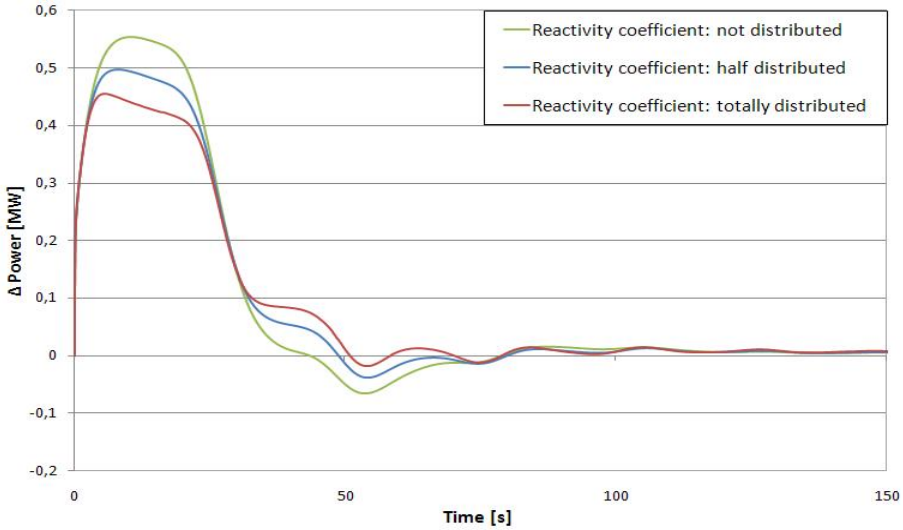

Figure 4.21: Power response of the ^{235}U-fueled MSRE of 1D-1D model to an insertion of 10 pcm when the reactivity coefficient is not uniform all over the core region

In Figure 4.21, three curves are shown for the power responce (1D-1D model of ^{235}U-fueled reactor) to a reactivity step of 10 pcm. The reactor is initially working at full power (8 MW). The yellow curve represents the power response when feedback coefficients are completely uniformly distributed. The blue curve represents the power response when feedback coefficients are half uniformly distributed and half linerly distributed. Finally, the red curve represents the power response when feedback coefficients that are totally linerly distributed over the height.

It appears immediately that the distribution of the thermal feedback (giving more weight towards the top of the core) lowers the peak as it was predicted. This happens because the thermal feedback operates faster. However, since a detailed analysis of neutronics is not available, it was considered not justified to introduce a certain distribution of the feedback weights. Moreover, it would not be available any criterion in order to choose the shape of the eventual distribution.

4.3.2 Step on air mass flow at the radiator

In the following pages it will be illustrated the way the reactor was normally operated in case a change in thermal power was required. As mentioned in chapter 2, this is done through a change in load demand at the radiator.

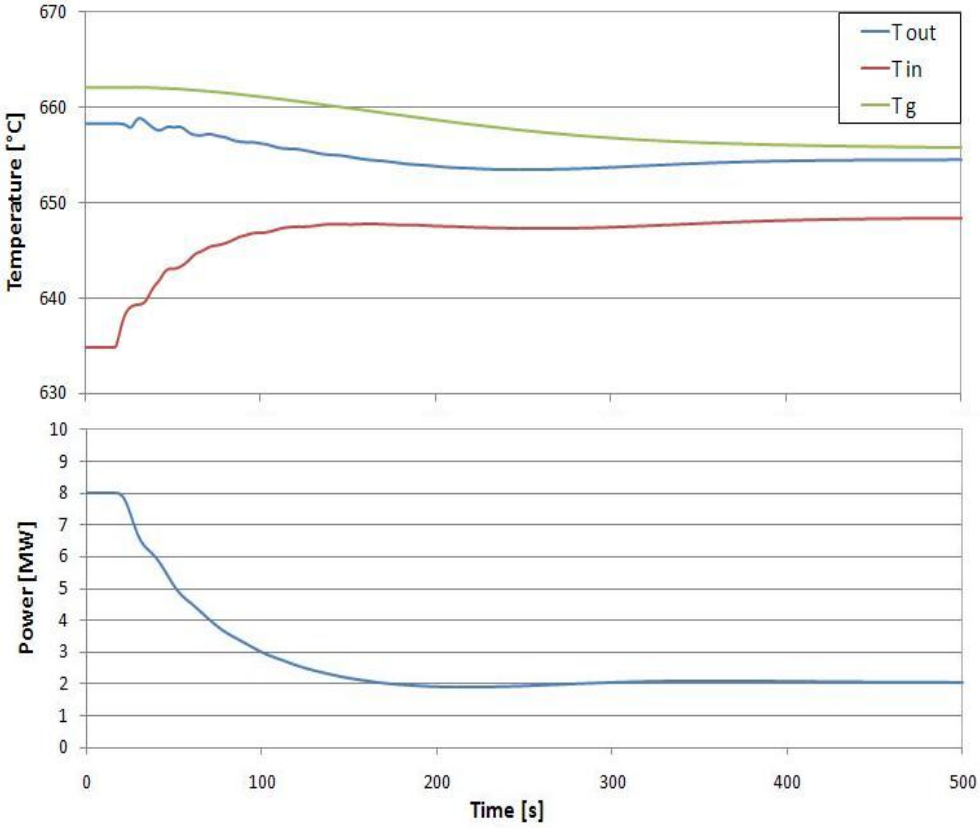

Figure 4.22: Response to a decrease in power demand through a variation of air mass flow at the radiator: the plant goes from 8 MW (full power) to 2 MW

Figures 4.22 and 4.24 show the results of 1D-1D model for the system response to changes in load demand at the radiator. Figures 4.23 and 4.25 show the same results for ORNL model calculations. All simulations were performed in the absence of external reactivity control. Both in case of increase and decrease in load demand, the changes were started at zero time, and the temperature and power response of the reactor were recorded. It is evident how the core starts feeling a change not immediately, because, if the change is put into effect at the radiator, it will take a certain time (dependant of the characteristic circulation time of fuel and coolant salt) to be felt by the core reactor.

It is also evident that the reactor is self-regualting during normal operation because

of the negative temperature coefficients of both the fuel and the graphite. As the load demand decreases , air mass flow at the radiator is decreased , the coolant salt temperature increases and so does the fuel salt temperature, and its feedback on reactivity is negative. Viceversa, as the load demand increases , air mass flow at the radiator is increased , the coolant salt temperature decreases and so does the fuel salt temperature, and its feedback on reactivity is positive (negative temperature coefficient times negative temperature variation).

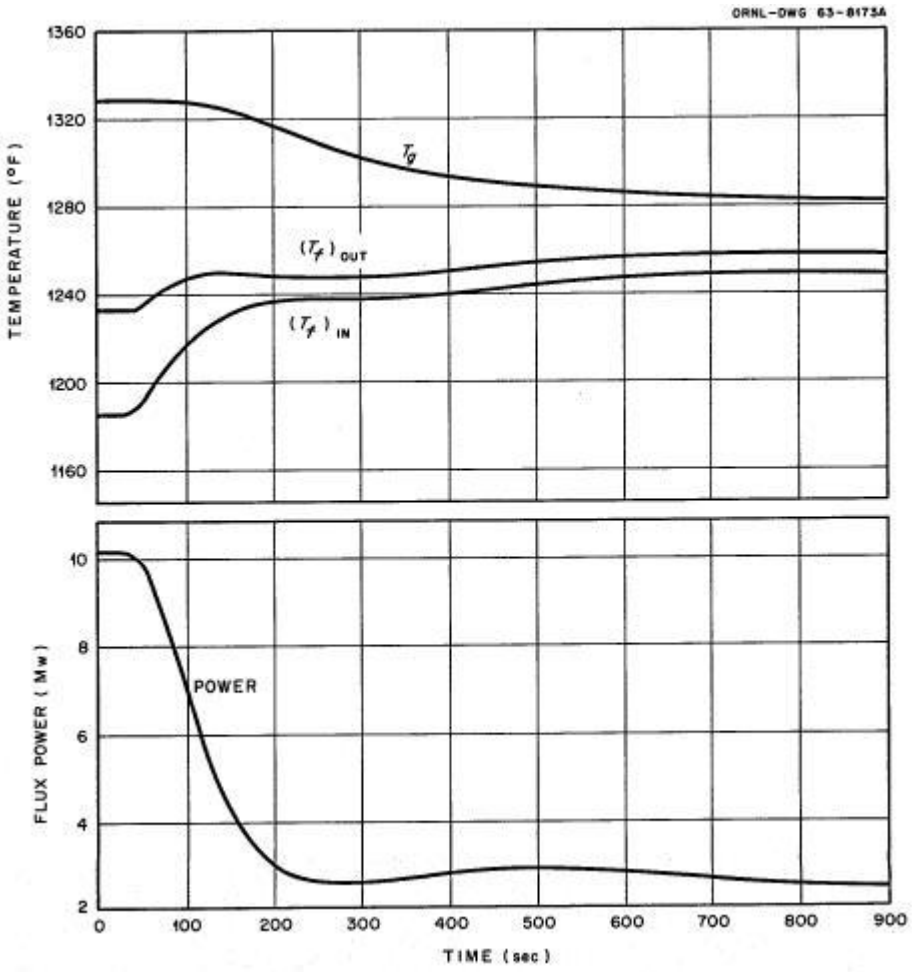

Figure 4.23: Response of ORNL model to a decrease in power demand

The quickness of self regulation depends on the power level (see page 81) and is rather sluggish even at full power. A number of factor contributes to the slow response of the system.

These include [8]:

1. Low power density in the core;
2. High heat capacities of the fuel and graphite;
3. Low heat-transfer rate between fuel and graphite;
4. Low heat production in the graphite;
5. Long loop delay times between the heat sink at the radiator and the heat source in the core.

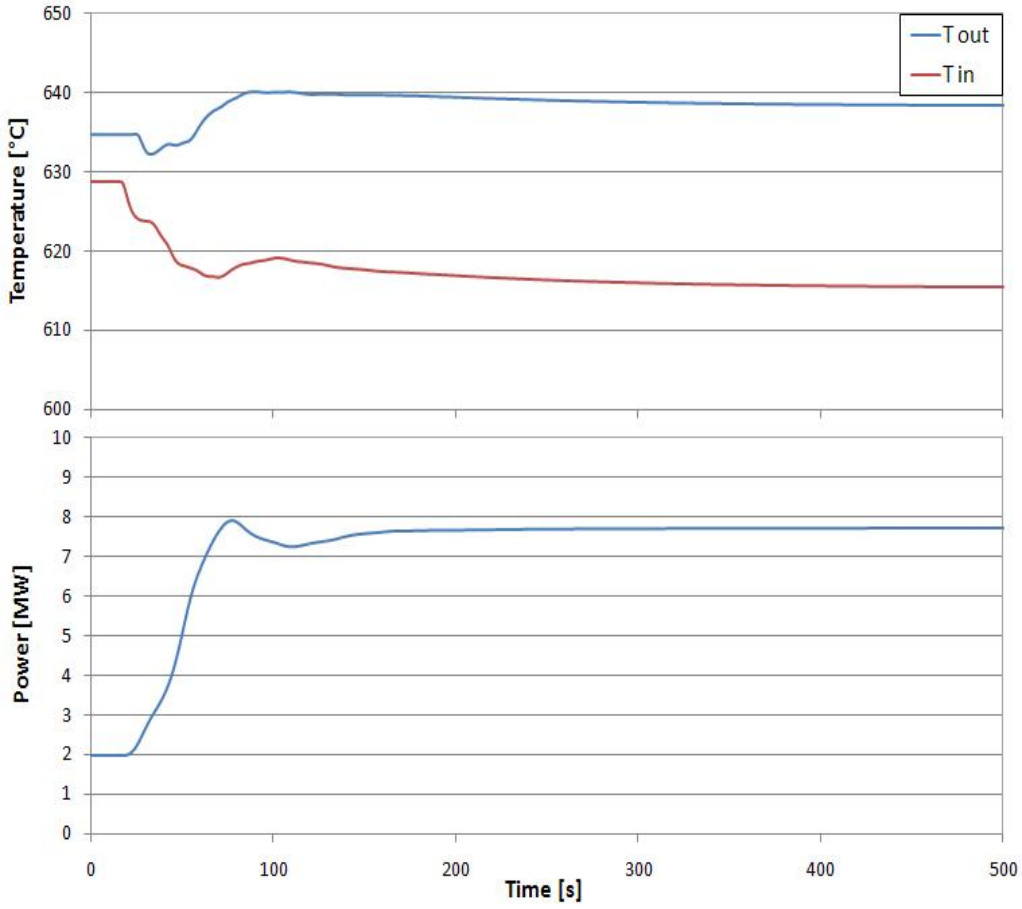

Figure 4.24: Response to an increase in power demand through a variation of air mass flow at the radiator: the plant goes from 2 MW to 8 MW (full power)

Analysing the power and temperature trends, it can be seen (after 200 seconds) a slow decrease in fuel temperature after the increase in power and an increase in fuel temperature after the power reduction. These trends reflect the attainment of the steady-state temperature distribution in the graphite. Moreover, after a decrease in load demand (Figures 4.23 and 4.24), it can be noticed a slow oscillation of power at low power, which was noticed in all simulations and appears to be an inherent characteristic of the system [8].

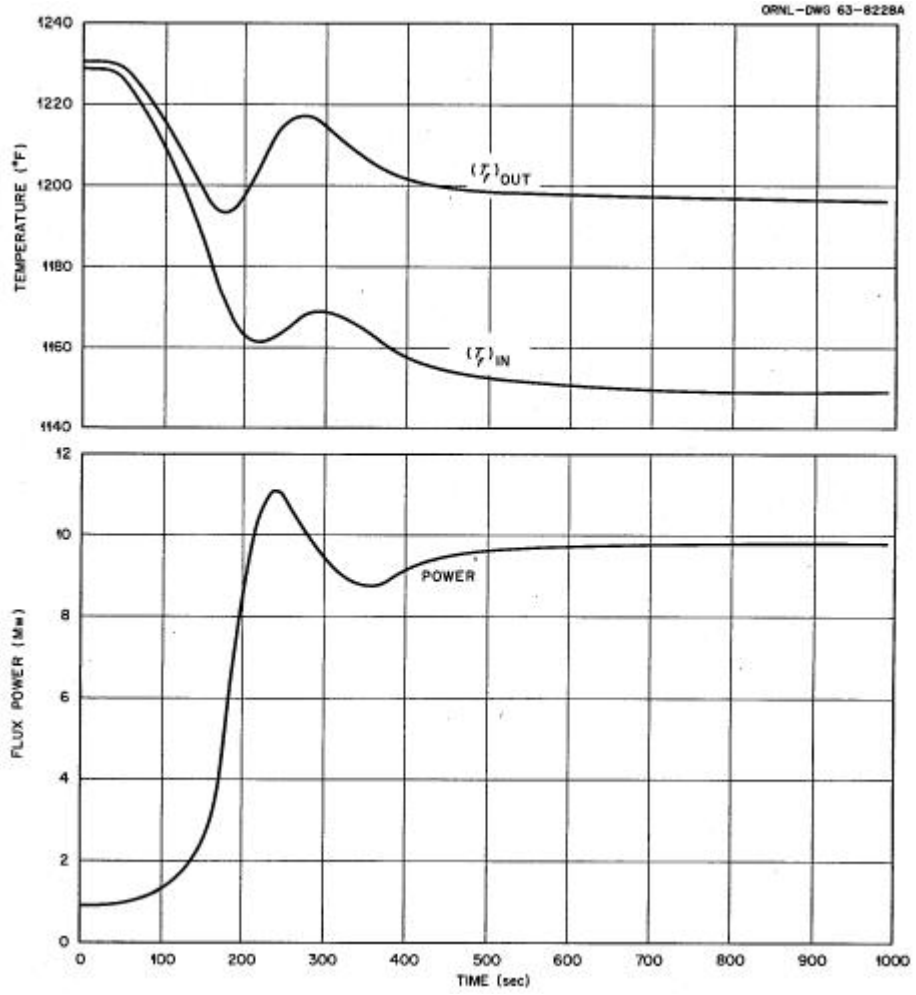

Figure 4.25: Response of ORNL model to an increase in power demand

Finally, it is can be observed that the transient following an increase in load demand is faster in 1D-1D model than in the ORNL model, while the transients following a decrease in load demand does not present this temporal difference. This could be partially explained in this way: in the 1D-1D model the air mass flow is changed

through a step variation (because the air blowers characteristic time is not known) both when increasing and decreasing load demand. On the contrary, it is reasonable to think that in the plant the air mass flow is changed with a step variation when decreasing (the quick-closing doors movement can be represented as a step variation on air mass flow), but it will certainy follow a different pattern when increasing (being one of the two air blowers off when the power is below 5 MW, when turned on it will have a certain inertia during acceleration before reaching its nominal functioning).

However, it is more realistic to think that is due to the control strategy adopted at ORNL. Knowing that power is normally raised through an increase of the heat sink cooling performance, it is reasonable to think that it was set a limit on the rate of increase of air mass flow. Indeed, it is to be considered the risk of freezing the coolant salt at the radiator, since the coolant salt keeps circulating through the secondary loop and being cooled as it was asporting a full thermal power of 8 MW, while in the core the change of power demand has not been felt yet.

4.4 Abnormal transient and accident analysis of the system

In this section typical accidents and abnormal transients will be simulated. The simulations will be simplified, and not capable of reproducing some the phenomena following any of these undesired transients (for instance the change of physical properties and heat exchange parameters, which should be kept into account in case of substantial change of conditions [5]).

The consequences of some highly abnormal incidents/transients are examined in order obtain a preliminary characterization of the inherent safety of the system. The excursions associated with reactivity accidents are inherently self-limiting by virtue of the negative temperature coefficient of reactivity of the fuel. The negative temperature coefficient of the graphite is of little importance during a rapid excursion because of its long reaction time. Altough in this work no external control is present in any of the simulated transient, the action of the safety system is required to prevent equipment damage in the most severe cases [8]. The simulated transients are the following:

- Unprotected rod insertion: simultaneous insertion of all three control rods is postulated.
- Uncontrolled rod withdrawal: simultaneous withdrawal of all three control rods is postulated.
- Loss of fuel circulation: failure of the power supply to the fuel circulating pump (unprotected). The onset of natural circulation is not considered.
- Overcooling: the fuel salt re-enters the core at a temperature lower than its steady state value.
- Loss of load: instantaneous loss of all heat-removal capability at the radiator is assumed.

These simulations where performed both with ^{235}U-fueled and ^{233}U-fueled MSRE: where significative differences between the two fuel types are found, the transients of both are presented and compared. Otherwise, one of the two fuels is chosen, and simulations are performed only with that fuel type.

It is worth noticing that simulations regarding the loss of fuel circulation have been obtained using a *1 region* core (see page 62). This is due to the fact that matrix calculus, which would be required in case of exploitation of 1D-1D model, is not directly appliable since one of the parameters changes (fuel mass flow is a function of time) and this would involve great changes in the Matlab code.

Finally, it is important to underline that no attempt was made to any risk assessment regard the simulated accidents. Through the following simulations it is only

[5] It is worth clarifying that natural circulation does not originate

meant to make a preliminary assessment of the plant dynamic behaviour during undesired/abnormal transients.

4.4.1 Unprotected control rods insertion

It is here reported the plant response to a SCRAM operated through a control rod insertion [6]. The 1D-1D model with a 100 core-regions discretization is employed. In Figure 4.26 the power and temperature response following an unprotected insertion of all three control rods is shown.

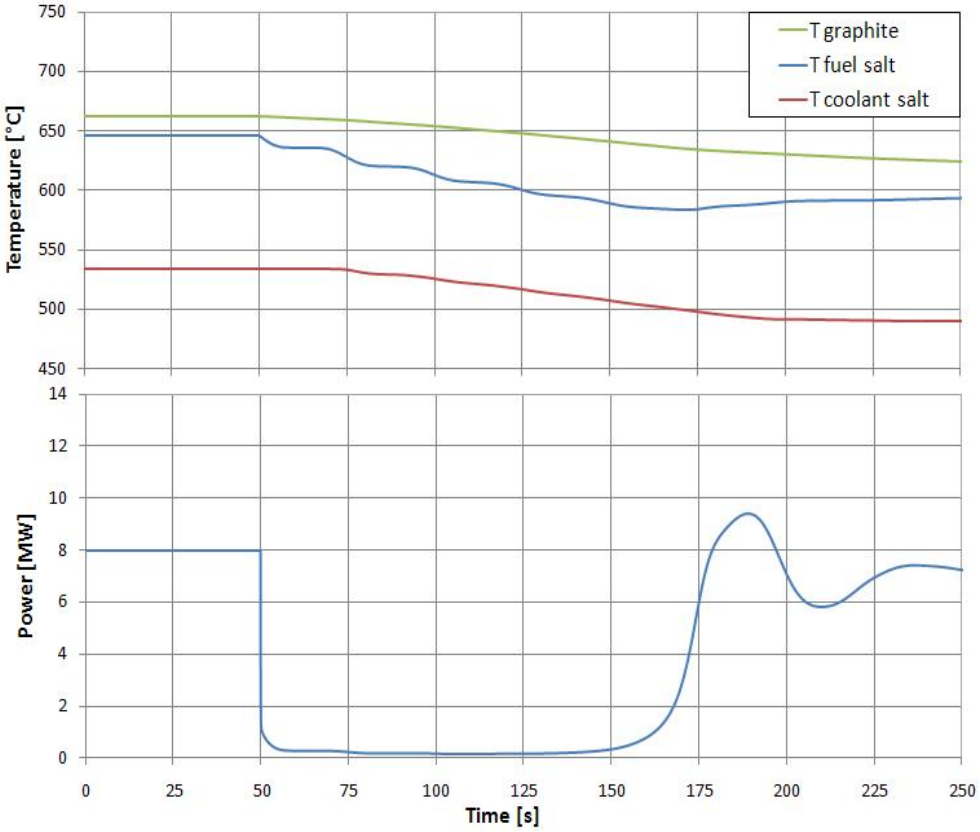

Figure 4.26: Power and temperature response to a reactivity insertion of -800 pcm of ^{233}U-fueled MSRE

The reactor is initially working at full power and is ^{233}U-fueled. (The result obained for ^{235}-fueled reactor is very similar to this one.) At the time t = 50 s a step insertion of rectivity is given (the value of -800 pcm was considered reasonable). No other

[6] No comparison has been taken into account since ORNL data regarding this kind of transient were not available.

parameters except reactivity are changed. It is worth noticing that a step insertion (the value of reactivity undergoes an instantaneous change of 800 pcm) is not completely faithful to reality since a certain velocity of control rods should be kept into account.

As expected, following a power abrupt decrease, graphite, fuel salt and coolant salt temperatures start decreasing. Analysing the trend of fuel salt temperature it appears clearly the influence of primary loop transit time (25 seconds). It can also be noticed that the load demand at the radiator should be lowered, coherently with the negative reactivity insertion in the core. Otherwise, the coolant salt temperature reaches values close to its freezing temperature (about 450 °C). Moreover, if a decrease in load demand is not operated, graphite and fuel salt temperatures keep decreasing until, after about 100 seconds from the SCRAM, their positive feedback makes reactivity positive and the power starts increasing again. This shows that the power can be lowered permanently only allowing temperatures to increase.

4.4.2 Uncontrolled rod withdrawal

In this section the plant response to an unprotected insertion of positive reactivity is shown. All three control rods are simultaneously withdrawn: a reasanoble value of inserted reactivity was considered 600 pcm. As just mentioned, the reactivity is inserted as a step and the rods velocity is not kept into account.

All simulations are carried out through the 1D-1D model with a 100 core-regions discretization. Power and temperature responses are given both for ^{235}U-fueled (fuel C) and ^{233}U-fueled (fuel A) MSRE. For what concerns the former, results of the 1D-1D model are compared with the ORNL model response (Figures 4.27 and 4.28). For what concerns the latter, results are compared with data obtained by DYN3D-MSR code [4], (Figures 4.29 and 4.30). The DYN3D-MSR code was used since no ORNL data regarding uncontrolled withdrawal in case of ^{233}U-fueled MSRE are available. It is a code for molten salts reactor which has been included in the MOST project (see note at page 1. Comparing figures 4.27 and 4.28, which consider a ^{235}U-fueled reactor, it must be preliminary observed that temperature data can be compared only for what concerns average temperatures, as a *hot channel* analysis is not available in the present work.

It can be seen that fuel and graphite temperatures have the same trend in both graphs, even if the difference between the two temperatures in 1D-1D model is about half that in ORNL. (This is coherent with the fact that the peak value results higher in response to a reactivity insertion, see section 4.3.1.) Even for what concerns the power response, the trend is the same in both models, altough the value of power reached at the end of transient in 1D-1D model is almost half of what it is in ORNL model. This can be explained considering the different way of calculating the thermal feedback: in ORNL model the temperature coefficients assume different values according to the core zone they are referred to (and the core is subdivided in axial and radial regions), while, in the model developed in the previous chapter, an average value for both graphite

and fuel salt temperatures is taken. Finally, it can be noticed that transients given by 1D-1D model seem to be slightly slower than ORNLmodel.

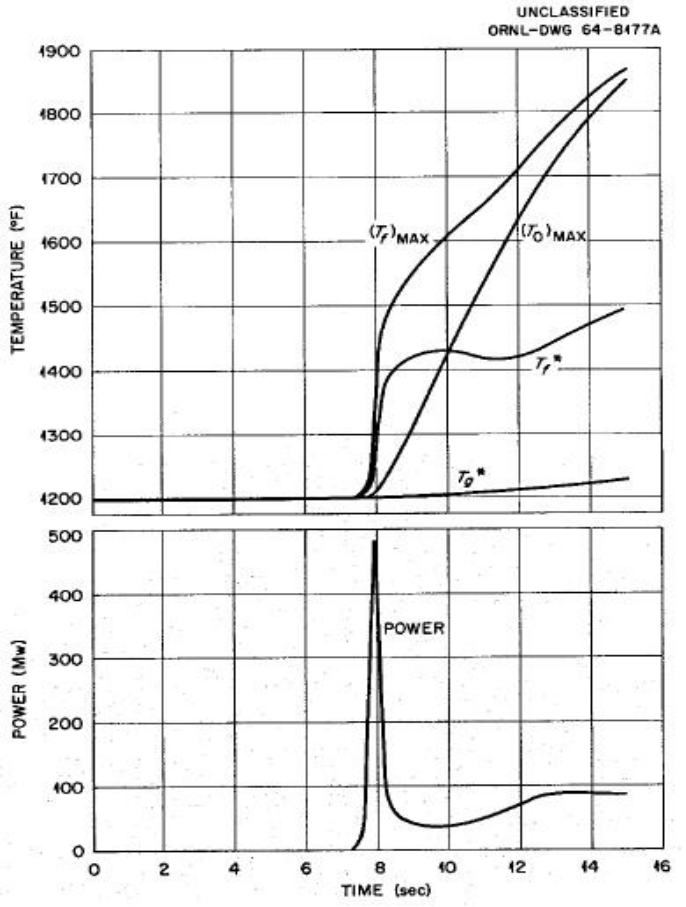

Figure 4.27: ORNL model response: power and temperature transients produced by uncontrolled rod withdrawal, fuel C

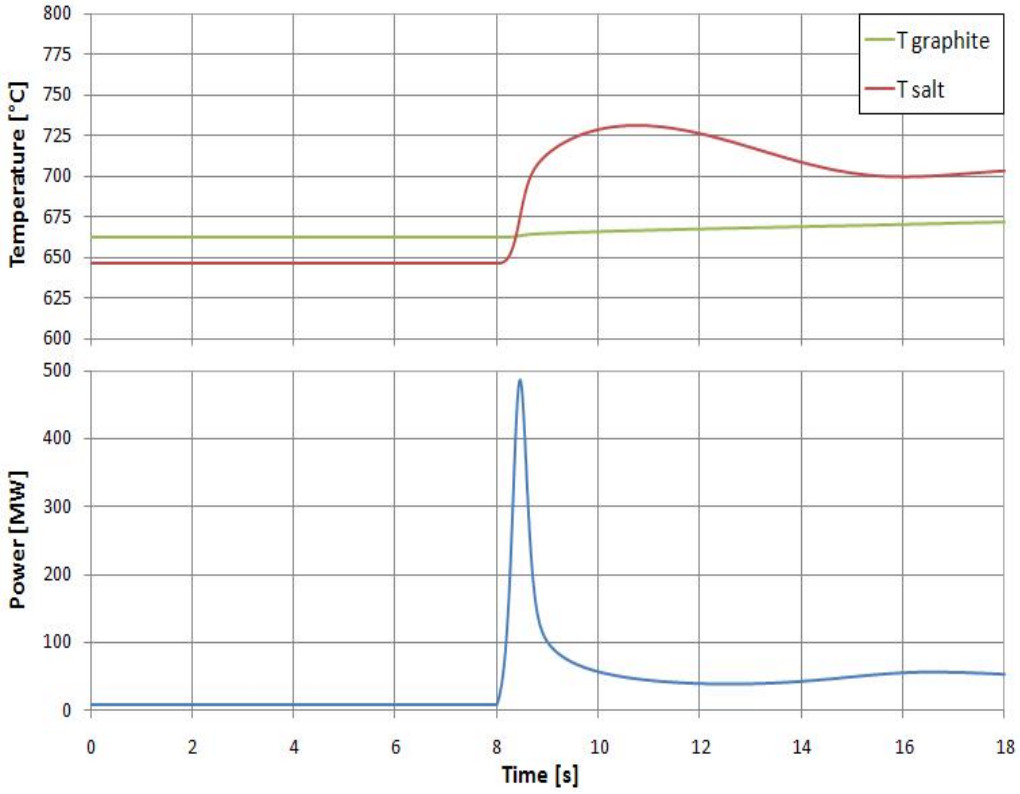

Figure 4.28: 1D-1D model (100 core regions) response: power and temperature transients produced by uncontrolled rod withdrawal, fuel C

In Figures 4.29 and 4.30, it is shown the response of ^{233}U-fueled MSRE to the reactivity insertion with several reactivity levels at nominal power calculated respectively with the DYN3D-MSR code and 1D-1D code (100 core-regions discretized). The power (top) is shown for all reactivity levels; the temperatures (bottom) represent only 300 pcm results.

It is worth noticing that DYN3D-MSR is a tri-dimensional model for what concerns both thermal-hydraulics and neutronics modelling (neutron diffusion is modelled). Therefore, it is a much more complex model than the ones developed in this work. On the other hand, DYN3D-MSR is a model of the reactor core only, and not of the entire plant as the 1D-1D model used for comparison in this case. Indeed, reported simulation of DYN3D-MSR (see Figure 4.29) can describe only the first 16 seconds of the transient because, after that time, the re-entering of the fuel salt which has gone through the primary loop should be considered.

Analysing the power transient, it can be observed a difference in the power peak value, as it was noticed for normal reactor operations (see page 93 for comparison between 1D-1D model and the ORNL model). However, when transient is ended,

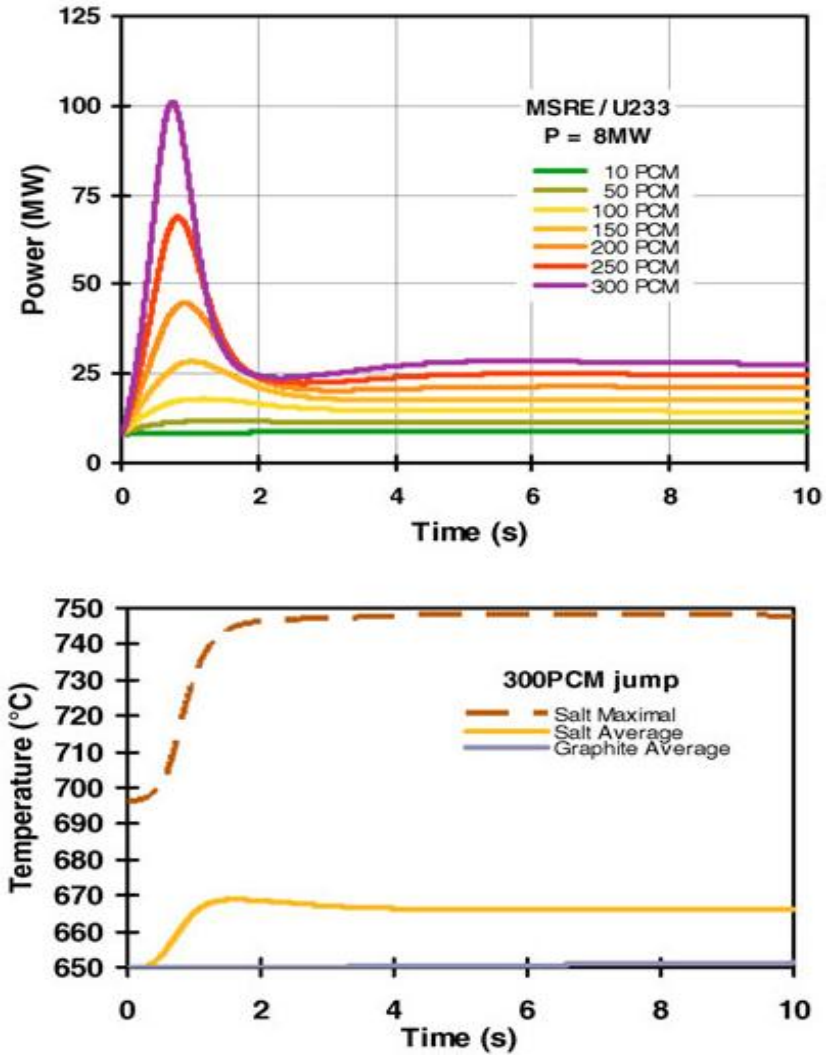

Figure 4.29: Response of MSRE with U-233 loading to the reactivity insertion with several reactivity levels calculated by the DYN3D-MSR code.

the values of power calculated by the two models are similar. For what concerns the temperature transient, both trends and final values are slightly different, but this might be due the tri-dimensional modelling of thermal-hydraulics in DYN3D-MSR.

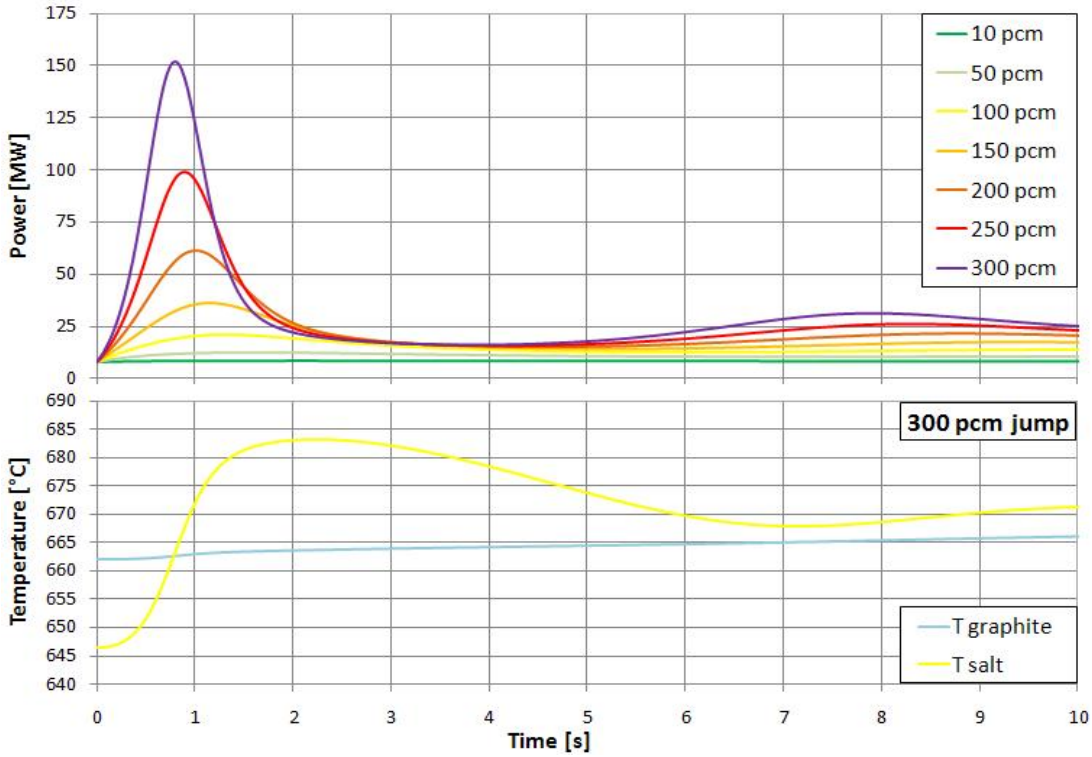

Figure 4.30: Response ^{233}U-fueled MSRE to the reactivity insertion calculated by the 1D-1D model (100 core regions).

4.4.3 Loss of fuel circulation

In the following paragraphs some transients following either a pump coast-down or a departure from the nominal value of fuel mass flow in the secondary loop are reported. In all simulations the coolant salt mass flow maintains its nominal value, and so does the air flow at the radiator.

In the Simulink files the decrease of the fuel mass flow is simulated with the pattern shown here below (initial value of fuel mass flow, before the break-time, is always equal to the nominal). It is obvious that, consequently to the decrease of the fuel mass flow, transit times in the primary loop increase. After 20 seconds they reach huge values since the pump completely stopped and fuel salt is not moving anymore.

$$\Gamma^s(t) \;=\; \Gamma_0^s\, e^{\frac{-(t-t_0)}{\tau_p}} \quad \text{for } t \geq t_0$$

$$\tau(t) \;=\; \tau_0\, e^{\frac{(t-t_0)}{\tau_p}} \quad \text{for } t \geq t_0$$

where:
$\Gamma^s\,(t)$ = fuel salt mass flow [kg/s]
Γ_0^s = nominal value of fuel mass flow [kg/s]
t_0 = transient starting time [s]
τ_p = characteristic time of the pump [s]
$\tau\,(t)$ = transit time [s]
τ_0 = nominal value of transit time [s]
The pump has been chosen to coast down with a characteristic time (τ_p) of 2.5 seconds, which represents a reasonable value for this kind of pump. In Figure 4.31 it is shown the pump UNPROTECTED coast down, with a pump failure at time t_0=20 s. It can be seen that after 20 seconds the pump completely stops.

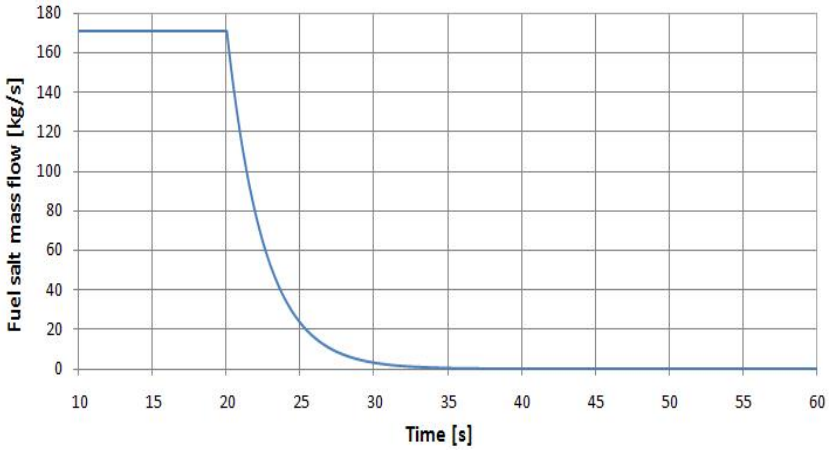

Figure 4.31: Fuel salt mass flow during a pump coast down

In Figure 4.32 it is shown the value of reactivity following a loss of fuel circulation in both cases of ^{235}U-fueled and ^{233}U-fueled MSRE (the different values of initial *compensation reactivity* can be seen). Knowing that no *compensation reactivity* would be nedeed once the fuel salt is not moving since precursor drift is not anymore affecting the neutron moltiplication, it can be seen that the reactor shuts down, since the value of reactivity at the end of the transient is widely negative.

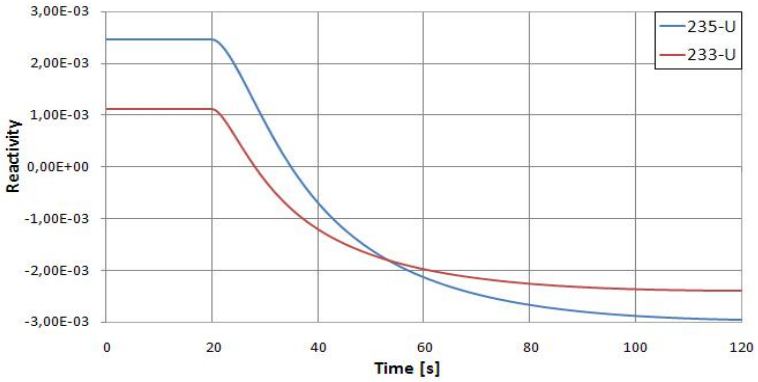

Figure 4.32: Reactivity during a pump coast down for ^{235}U-fueled and ^{233}U-fueled MSRE

In Figures 4.33 and 4.34 the power response is shown. In both cases, as the fuel salt slows down and finally stops, the thermal feedback makes power decresing until the reactor shuts down. However, it can be noticed that the transient starts (at t_0 =20 s) differently according to the fuel type. In case of ^{235}U-fueled MSRE the power initially raises, since the effect of fuel motion (less precursors leaving the core) is initially dominant. On the contrary, in case of ^{233}U-fueled MSRE the power starts decreasing right away. This different behaviour is due to the fuel salt temperature coefficient (see Table 2.18) which is higher (more negative) in case of ^{233}U-fuel.

Coolant salt temperatures are not shown, but it is worth reminding that, in the case of the fuel-pump failure, closure of the radiator doors is required to avoid freezing the coolant salt in the radiator. The system was provided of fuel drain tanks with a cooling system capable of removing fission product decay heat (see section 2.2.3).

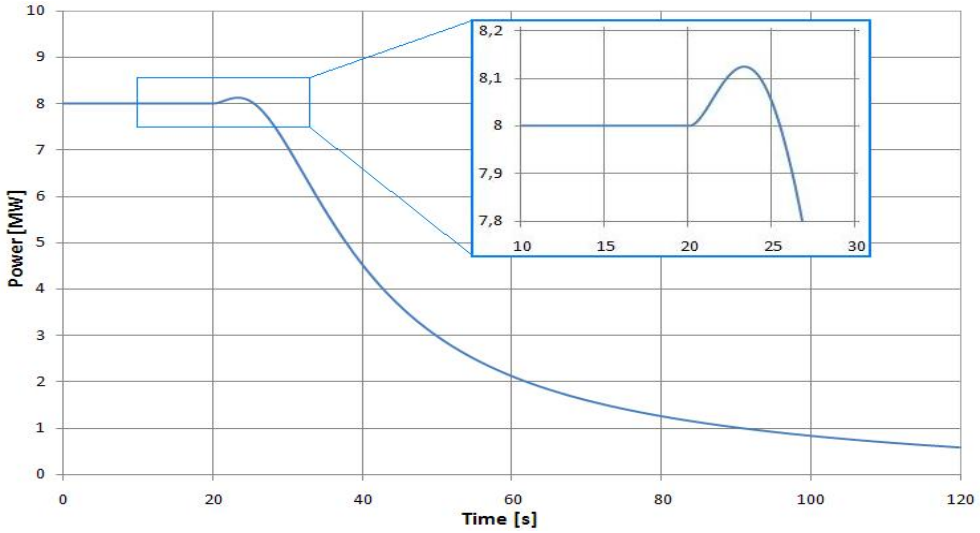

Figure 4.33: Simulation with the zero-dimensional model of the pump break of the ^{235}U-fueled MSRE

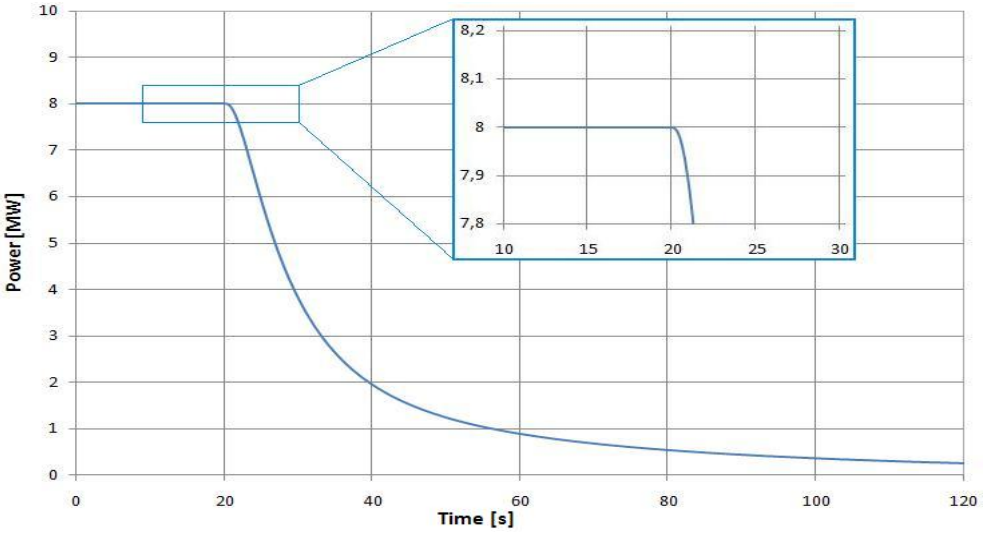

Figure 4.34: Simulation with the zero-dimensional model of the pump break of the ^{233}U-fueled MSRE

4.4.4 Overcooling

It is here shown the power and temperature response to an overcooling of the fuel salt (i.e. the salt re-enters the core much cooler than what it would in normal operation). The simulation is carried out with a 1D-1D *modified* model with a 100 core-regions discretization. The model is modified since only the core is taken into account and fuel salt inlet temperature becomes a controlled variable. Not being modelled the out-of-the-core primary loop, the validity of simulation is restricted to the first 16 seconds of the transient.

The overcooling of the fuel salt simulated in Figure 4.35 is realized in this way: a 10 seconds decreasing ramp is given to the inlet fuel temperature as it can be seen in the graph. The transient starts at t_0 =10 s. ^{233}U-fuel is employed, but the transient is very similar for ^{235}U-fuel, too.

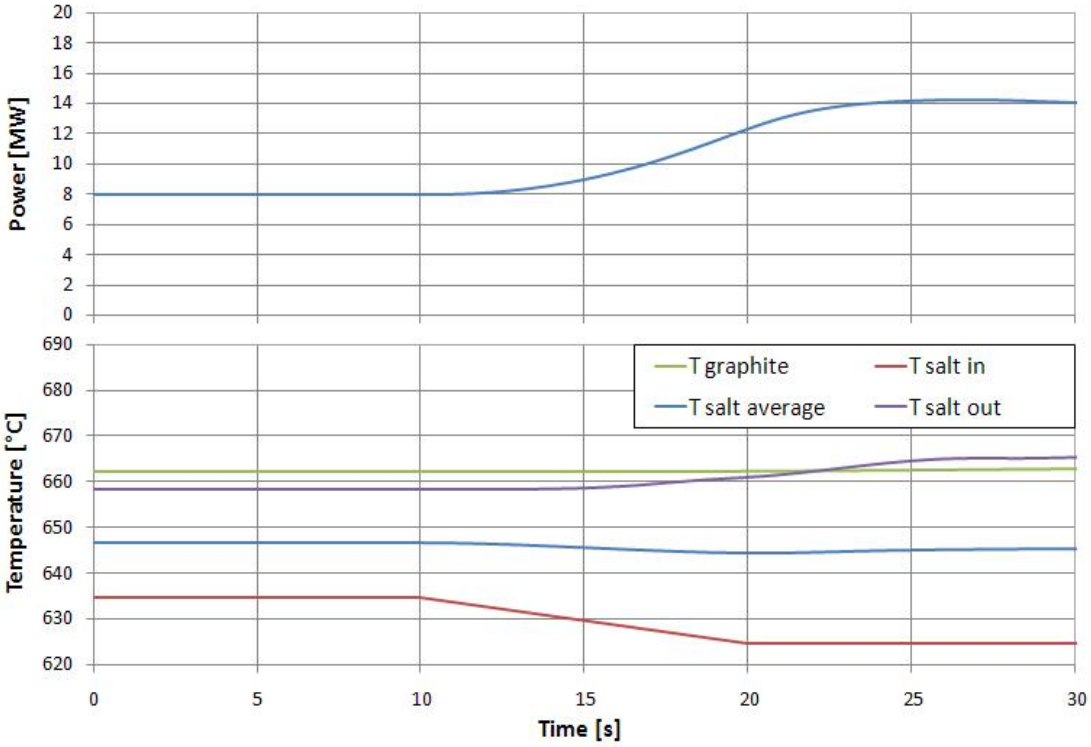

Figure 4.35: Power and temperature response to a 10 °C overcooling of ^{233}U fuel salt. The core is modelled with 100 regions, the rest of the plant is not modelled.

It can be observed that a salt *average* temperature cool-down of 10 °C corresponds to a reactivity insertion of about 100 pcm: indeed the temperature coefficient of ^{233}U-fuel salt is α_s =-11.3 pcm/°C. However, if the power trend following a ramp overcooling of 10 °C is compared with that obtained in Figure 4.30 following a control rods step

insertion of 100 pcm reactivity, the power growth results lower in the first case. This is because the overcooling is on the salt *inlet* temperature: the decrease of the inlet temperature is compensated by the increase of outlet temperature, which is due to the increase of power given by the positive feedback. It can be observed graphite and fuel average temperatures do not undergo relevant changes.

4.4.5 Instantaneous loss of cooling capacity

It is here shown the power and temperature response to a loss of cooling capacity at the radiator. An air blowers break or an undesired radiator doors closure is simulated through an instantaneous change of air mass flow from nominal value to zero is given as input.

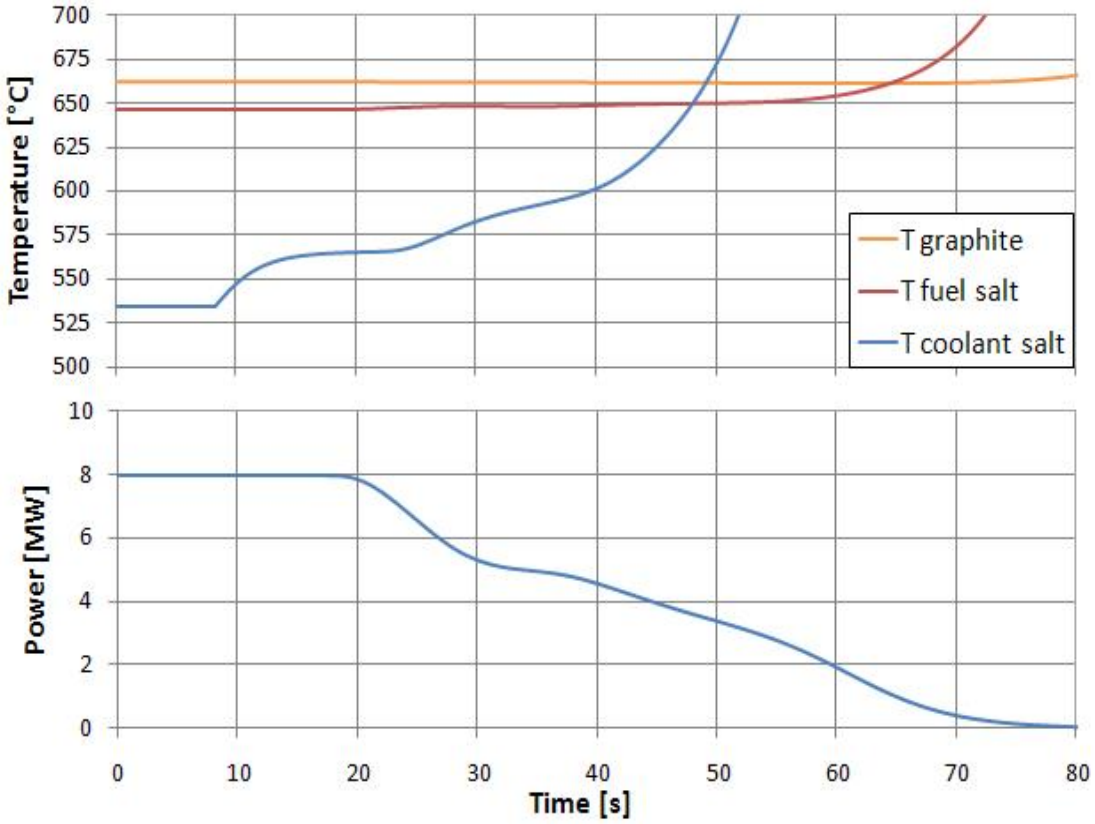

Figure 4.36: Temperature and power response to a loss of cooling capacity at the radiator. The ^{233}U-fueled reactor is modelled through the 1D-1D model with a 100 core-regions discretization.

The simulation is carried out with a 1D-1D model with a 100 core-regions discretization. The transient starts at $t_0 = 0$ s. ^{233}U-fuel is employed, but the transient

is very similar for ^{235}U-fuel, too. As expected, coolant salt temperature increases, and so do the fuel salt and the graphite temperaures: it follows that power decreases consequently to the negative temperature feedback.

It can be observed that coolant salt temperature (measured in the heat exchanger) starts increasing only 8 seconds after the transient started, the fuel salt temperature (measured in the core) after 20 seconds and that the power starts decreasing after 20 seonds too. This is obviously due to the characteristic transit times of the fuel and coolant salt in the system.

Conclusions

The objective of this thesis work has been to develop a numerical model suitable for studying the plant dynamics of a molten salt reactor. The Molten Salt Reactor Experiment (MSRE), an experimental reactor which was operated in the sixties at Oak Ridge National Laboratories, has been chosen as reference because its project data and experimental data (obtained during its operation) are available in the open literature. The MSRE is also used in the frame of the European MOST project for the common benchmark definition.

At first, it is given a brief introduction to the molten salt reactor technology and a description of the molten salt concept. The peculiar features, advantages and disadvantages of this technology have been pointed out.

Subsequently, through an analysis of the public reports regarding design and experimental data, the steady-state condition at various power levels has been characterized. An overview of the control strategy has been given: it has been pointed out that the MSRE was controlled with a "reactor follows" strategy, as it resulted the most convenient. The power level was regulated by varying the power dissipated by a radiator. The control variables which were used to manage the heat removal have been characterized, so that the model could actually work at any power level. The steady state behaviour at various power levels has been shown to be in agreement with a control strategy requiring a fixed core outlet temperature, as actually stated in the ORNL reports. It is notable that in the sixties, as soon as the reactor was put in operation, some design data were found to be uncorrect so that it was necessary to lower the nominal power of the reactor. This variation of power has been properly taken into account in the steady-state characterization here discussed.

Once the static behaviour of the plant has been characterized, the attention has been finally focused on the development of the dynamic model. Numerical models featured by increasing complexity have been developed. With a totally zero-dimensional model some unphysical oscillation of power and temperaures have been found. It has been stated that they were inherent to this modelling approach and that they would have lead to improper values of power and temperatures during transients. Therefore, it has been developed a model whose thermal-hydraulics was discretized in the core region, thus taking into account the convective transport. The values of power and

temperatures have been actually found not to oscillate anymore. Nevertheless, the transients obtained with this approach still have shown a different shape than the ones given in ORNL reports. Therefore, the convective transport of precursors has been included as it was quite clear that the precursor distribution affected the core dynamics. This has been done discretizing the differential equation describing the precursor population. New results have been found for what concerns the "compensation reactivity". Also, the transients showed trends more similar to the ones obtained by the ORNL model.

Using the best available model, the dynamic behaviour of the plant has been characterized. At first, it has been carried out the frequency study of the model. Amplitude and phase responses have shown a good accordance with ORNL data. In general, it can be said that the model response has resulted less damped than the actual reactor response.

Further on, some particular transients of the system have been illustrated and analysed. The normal operation transients taken into account have been: the reactivity insertions and the changes (increase and decrease) in power load at the radiator. The abnormal/incidental conditions transients taken into account have been: unprotected insertion and unprotected withdrawal of control rods, loss of fuel circulation, overcooling of the fuel salt and loss of cooling capacity at the radiator. The model has been found capable of reproducing these transients with a good accordance to the ORNL data (or with other models available in literaure when used).

However, some mismatches were present: for instance, the value of the power peak following a reactivity insertion resulted always higher than expected. Also, at high power an undershoot in power response (to reactivity insertion) was present for both fuel types (^{233}U and ^{235}U), while in ORNL data the undershoot appeared only at low power levels.

The main source of inaccuracy in the developed models has been individuated in the zero-dimensional equation for the neutron population. Indeed, such equation does not properly take into account the nuclear importance and the power density of different core regions. Such drawback could probably be overcome by introducing a radial dimension and by assigning to each core position weighting factors for the temperature feedback and for the power distribution, according to dedicated neutronics computations. The presence of a radial dimension appears fundamental also in order to dump the excessively oscillatory behavior resulting from a single-channel modelling. Improvements and extensions of the model that could be implemented in the future are:

- Radial discretization of the core, in order to take into account the power and mass flow radial distribution;
- Modelling of neutron diffusion or, alternatively, further neutronics studies in order to evaluate the nuclear importance of the various core regions;
- One-dimensional modelling of the heat exchanger.

Appendix

MATLAB CODE

Fixable variables
step=0; %[pcm] TO BE FIXED
P0=8*10E6; %[W] TO BE FIXED
P1=8*10E6; %[W] TO BE FIXED
n=50; % core regions number TO BE FIXED
Theta=1; % TO BE FIXED ($1/2 \leq Theta \leq 1$)
fuel=233; % TO BE FIXED (233 or 235)

Overcooling of fuel salt
Start=10;
Slope=-1; % TO BE FIXED
DecreasingTime=10; % [s] TO BE FIXED
Stop=Start+DecreasingTime;

Calculation of the neutron number at the fixed power
P0s*= 8*10E6; % W
n0s=2.7*10E9;
N0= P0/P01*n0s;

Parameters and phisical properties - nominal values
gammag =0.07;
gammas = 0.93;
k = 0.036*10E6; %W/K
Gs = 171.2; % kg/s
Gcool = 105.7; % kg/s
Mg= 3687; % kg
Cg= 1757; % kg
Msh= 342; % kg
Cs = 1982.5; % J/(kg*K)
Mch= 117.3; % kg

Mcr= 402.6; % kg
Ccool = 2416; % J/(kg*K)
Ma= 25; % kg
Ca = 1015; % J/(kg*K)
Uscool = 82800; % W/K
Ucoola = 2202*(P0/(10E6)) + 233.18; % W/K
Ga = [4.0506*(P0/(10E6))E4 + 49.139*(P0/(10E6))E3 + 334.01*((P0/(10E6))E2) +
9015.7*(P0/(10E6))-4752.9]*4.7195*(10E-4); % kg/s
Tari= 310.93; % K
tau0 = 8.46;
Msc= tau0*Gs;
taushe = Msh*Cs/Uscool;
tau0hes = Msh/Gs;
tauche = Mch*Ccool/Uscool;
tau0hec = Mch/Gcool;
tau0radc = Mcr/Gcool;
tau1= 5.77; % [s] (3.77 + 2 sec di mixing)
tau2= 8.67; % [s]
tau3= 4.71; % [s]
tau4= 8.24; % [s]

Definition of the fuel if fuel==235
as= -4.84*10E(-5)*9/5;
ag= -3.7*10E(-5)*9/5;
lambda=2.4*10E(-4);
lamL= 1/(tau1+tau2+tau0hes);
lamC= 1/tau0;
l1= 0.0124;
l2= 0.0305;
l3= 0.111;
l4= 0.301;
l5= 1.14;
l6= 3.01;
b1= 22.3*10E(-5);
b2= 145.7*10E(-5);
b3= 130.7*10E(-5);
b4= 262.8*10E(-5);
b5= 76.6*10E(-5);
b6= 28*10E(-5);
end
if fuel==233
as= -6.13*10E(-5)*9/5;

ah= +10*10E(-5);
ag= -3.23*10E(-5)*9/5;
lambda=4*10E(-4);
lamL= 1/(tau1+tau2+tau0hes);
lamC= 1/8.46;
l1= 0.0126;
l2= 0.0337;
l3= 0.139;
l4= 0.325;
l5= 1.13;
l6= 2.50;
b1= 22.8*10E(-5);
b2= 78.8*10E(-5);
b3= 66.4*10E(-5);
b4= 73.6*10E(-5);
b5= 13.6*10E(-5);
b6= 8.8*10E(-5);
end
b=[b1,b2,b3,b4,b5,b6];
beta= sum(b)
l=[l1,l2,l3,l4,l5,l6];
expli=[exp(-l1/lamL),exp(-l2/lamL),exp(-l3/lamL),exp(-l4/lamL),exp(-l5/lamL),exp(-l6/lamL)];
rho0= beta-sum ((l.*b)./(1+lamC-lamC*expli));

Matrices for calculation of plant temperatures

A = zeros (15,15);
A (1,1) = -k;
A (1,2) = k;
A (2,1) = k;
A (2,2) = -k;
A (2,3) = -Gs*Cs;
A (2,4) = Gs*Cs;
A (3,2) = 1;
A (3,3) = -1/2;
A (3,4) = -1/2;
A (4,3) = 1;
A (4,6) = -1;
A (5,4) = 1;
A (5,7) = -1;
A (6,5) = Uscool;
A (6,6) = -Gs*Cs;

A (6,7) = Gs*Cs;
A (6,8) = -Uscool;
A (7,5) = 1;
A (7,6) = -1/2;
A (7,7) = -1/2;
A (8,5) = Uscool;
A (8,8) = -Uscool;
A (8,9) = -Gcool*Ccool;
A (8,10)= Gcool*Ccool;
A (9,8) = 1;
A (9,9) = -1/2;
A (9,10)= -1/2;
A (10,9)= -1;
A (10,13)= 1;
A (11,10)= 1;
A (11,12)= -1;
A (12,11)= Ucoola;
A (12,12)= Gcool*Ccool;
A (12,13)= -Gcool*Ccool;
A (12,14)= -Ucoola;
A (13,11)= 1;
A (13,12)= -1/2;
A (13,13)= -1/2;
A (14,11)= Ucoola;
A (14,14)= -Ucoola;
A (14,15)= -Ga*Ca;
A (15,14)= 1;
A (15,15)= -1/2;
B = zeros (15,2);
B (1,1) = gammag;
B (2,1) = gammas;
B (14,2) = Ga*Ca;
B (15,2) = -1/2;
U= zeros (2,1);
U (1,1) = P0;
U (2,1) = Tari;
XK1 = -(A E(-1))*B*U;

Plant steady state temperatures
Tg = XK1(1,1);
Tsc = XK1(2,1);
Tsco = XK1(3,1);

```
Tsci = XK1(4,1);
Tsh = XK1(5,1);
Tshi = XK1(6,1);
Tsho = XK1(7,1);
Tch = XK1(8,1);
Tcho = XK1(9,1);
Tchi = XK1(10,1);
Tcr = XK1(11,1);
Tcro = XK1(12,1);
Tcri = XK1(13,1);
Ta = XK1(14,1);
Taro = XK1(15,1);
for i=1:15
XC1(i,1)=XK1(i,1)-273.15;
end
```

Core discretizetion with Θ-method

```
Msci=Msc/n;
Mgi=Mg/n;
tau0i=tau0/n;
AA=zeros(3*n,3*n);
ki=k/n;
H0=(-(1-Theta)/Theta);
H1=(2-1/Theta);

AA(1,1)=(-ki/(Mgi*Cg));
AA(1,2)=(ki/(Mgi*Cg));
AA(2,1)=(ki/(Gs*Cs*tau0i*Theta));
AA(2,2)=(-2/(tau0i*Theta)-ki/(Gs*Cs*tau0i*Theta));
AA(3,1)=ki/(Gs*Cs*tau0i*Theta)*H1;
AA(3,2)=(2/(tau0i*Theta)*(1/Theta)-ki/(Gs*Cs*tau0i*Theta)*H1);
AA(3,3)=(-2/(tau0i*Theta));
ii=2;
while ii<(n+1)
i=3*ii-2;
AA(i,i)=(-ki/(Mgi*Cg));
AA(i,i+1)=(ki/(Mgi*Cg));
AA(i+1,i-1)=(2/(tau0i*Theta)*1/Theta);
AA(i+1,i)=(ki/(Gs*Cs*tau0i*Theta));
AA(i+1,i+1)=(-2/(tau0i*Theta)-ki/(Gs*Cs*tau0i*Theta));
AA(i+2,i-1)=H0*AA(i+1,i-1);
AA(i+2,i)=(ki/(Gs*Cs*tau0i*Theta)*H1);
```

```
AA(i+2,i+1)=(2/(tau0i*Theta)*(1/Theta)-ki/(Gs*Cs*tau0i*Theta)*H1);
AA(i+2,i+2)=(-2/(tau0i*Theta));
ii=ii+1;
end
ii=2;
while ii<(n+1)
i=3*ii-1;
j=1;
while j<(i-4)
AA(i,j+2)=H0*AA(i-2,j+2);
AA(i+1,j+2)=H0*AA(i,j+2);
j=j+3;
end
j=1;
while j<(i-1)
AA(i,j) = H0*AA(i-2,j);
AA(i,j+1)= H0*AA(i-2,j+1);
AA(i+1,j)=H0*AA(i,j);
AA(i+1,j+1)=H0*AA(i,j+1);
j=j+3;
end
ii=ii+1;
end
BB=zeros(3*n,n+2);
ii=1;
while ii<(n+1)
i=3*ii-2;
BB(i,ii)=(gammag/(Mgi*Cg));
BB(i+1,ii)=(gammas/(Gs*Cs*tau0i*Theta));
BB(i+2,ii)=(gammas/(Gs*Cs*tau0i*Theta))*H1;
ii=ii+1;
end
ii=2;
while ii<(n+1)
i=3*ii-1;
j=1;
while j<(ii)
BB(i,j)=H0*BB(i-2,j);
BB(i+1,j)=H0*BB(i,j);
j=j+1;
end
ii=ii+1;
```

```
end
i=2;
a=0;
while i<(3*n)
BB(i,n+1)=(2/(tau0i*Theta))*H0 E(a);
BB(i+1,n+1)=(2/(tau0i*Theta))*H0 E(a+1);
a=a+1;
BB(i,n+2)=H0 E(a);
BB(i+1,n+2)=H0 E(a+1);
a=a+1;
i=i+3;
end
CC=eye(3*n,3*n);
DD=zeros(3*n,n+2);
```

i-th region power - Cosine distribution

```
PowerFraction=zeros(n,1);
for i=1:n
PowerFraction(i,1)=1/2*(-cos(pi*i/n)+cos(pi*(i-1)/n));
end
U01=zeros(n+2,1);
U01(n+1,1)=Tsci;
U01(n+2,1)=0;
i=1;
while i<(n+1)
U01(i,1)=P0*PowerFraction(i,1);
i=i+1;
end
X00 = -(AA E(-1))*BB*U01;
Tfuel=zeros(n,1);
i=2;
j=1;
while i<(3*n)
Tfuel(j,1)=X00(i,1)-273.15;
i=i+3;
j=j+1;
end
Tgraphite=zeros(n,1);
i=1;
j=1;
while i<(3*n)
Tgraphite(j,1)=X0(i,1)-273.15;
```

```
i=i+3;
j=j+1;
end
```

Neutronics

```
N0i=zeros(n,1);
CC1=exp(-l1/lamL);
CC2=exp(-l2/lamL);
CC3=exp(-l3/lamL);
CC4=exp(-l4/lamL);
CC5=exp(-l5/lamL);
CC6=exp(-l6/lamL);
for i=1:n
N0i(i,1)=PowerFraction(i,1)*(N0);
end
```

Precursors steady state values

```
matr11=zeros(n,n);
matr21=zeros(n,n);
matr12=zeros(n,n);
matr22=zeros(n,n);
matr13=zeros(n,n);
matr23=zeros(n,n);
matr14=zeros(n,n);
matr24=zeros(n,n);
matr15=zeros(n,n);
matr25=zeros(n,n);
matr16=zeros(n,n);
matr26=zeros(n,n);

matr11(1,1)=-1;
matr11(1,n)=(n/tau0)*CC1/(n/tau0+l1);
matr21(1,1)=b1/lambda*1/(n/tau0+l1);
for i=2:n
matr11(i,i)=-1;
matr11(i,i-1)=(n/tau0)/(n/tau0+l1);
matr21(i,i)=b1/lambda/(n/tau0+l1);
end

matr12(1,1)=-1;
matr12(1,n)=(n/tau0)*CC2/(n/tau0+l2);
matr22(1,1)=b2/lambda/(n/tau0+l2);
```

```
for i=2:n
matr12(i,i)=-1;
matr12(i,i-1)=(n/tau0)/(n/tau0+l2);
matr22(i,i)=b2/lambda/(n/tau0+l2);
end

matr13(1,1)=-1;
matr13(1,n)=(n/tau0)*CC3/(n/tau0+l3);
matr23(1,1)=b3/lambda/(n/tau0+l3);
for i=2:n
matr13(i,i)=-1;
matr13(i,i-1)=(n/tau0)/(n/tau0+l3);
matr23(i,i)=b3/lambda/(n/tau0+l3);
end

matr14(1,1)=-1;
matr14(1,n)=(n/tau0)*CC4/(n/tau0+l4);
matr24(1,1)=b4/lambda/(n/tau0+l4);
for i=2:n
matr14(i,i)=-1;
matr14(i,i-1)=(n/tau0)/(n/tau0+l4);
matr24(i,i)=b4/lambda/(n/tau0+l4);
end

matr15(1,1)=-1;
matr15(1,n)=(n/tau0)*CC5/(n/tau0+l5);
matr25(1,1)=b5/lambda/(n/tau0+l5);
for i=2:n
matr15(i,i)=-1;
matr15(i,i-1)=(n/tau0)/(n/tau0+l5);
matr25(i,i)=b5/lambda/(n/tau0+l5);
end

matr16(1,1)=-1;
matr16(1,n)=(n/tau0)*CC6/(n/tau0+l6);
matr26(1,1)=b6/lambda/(n/tau0+l6);
for i=2:n
matr16(i,i)=-1;
matr16(i,i-1)=(n/tau0)/(n/tau0+l6);
matr26(i,i)=b6/lambda/(n/tau0+l6);
end
```

```
c10i=-(matr11) E(-1)*matr21*N0i;
c20i=-(matr12) E(-1)*matr22*N0i;
c30i=-(matr13) E(-1)*matr23*N0i;
c40i=-(matr14) E(-1)*matr24*N0i;
c50i=-(matr15) E(-1)*matr25*N0i;
c60i=-(matr16) E(-1)*matr26*N0i;
somma=0;
for i=1:n
somma=somma+(l1*c10i(i,1)+l2*c20i(i,1)+l3*c30i(i,1)+l4*c40i(i,1)+l5*c50i(i,1)+l6*c60i(i,1));
end
rho0=beta-somma*lambda/N0
```

Matrices definition for discretized equation of precursors

```
AAA=zeros(6*n,6*n);
i=1;
while i<7
AAA(i,i)=-n/tau0-l(i);
i=i+1;
end
i=7;
while i<(6*n)
AAA(i,i-6)=n/tau0;
AAA(i,i)=-n/tau0-l1;
AAA(i+1,i+1-6)=n/tau0;
AAA(i+1,i+1)=-n/tau0-l2;
AAA(i+2,i+2-6)=n/tau0;
AAA(i+2,i+2)=-n/tau0-l3;
AAA(i+3,i+3-6)=n/tau0;
AAA(i+3,i+3)=-n/tau0-l4;
AAA(i+4,i+4-6)=n/tau0;
AAA(i+4,i+4)=-n/tau0-l5;
AAA(i+5,i+5-6)=n/tau0;
AAA(i+5,i+5)=-n/tau0-l6;
i=i+6;
end
BBB=zeros(6*n,7);
i=1;
j=1;
while i<(6*n)
BBB(i,1)=b1/lambda*PowerFraction(j,1);
BBB(i+1,1)=b2/lambda*PowerFraction(j,1);
BBB(i+2,1)=b3/lambda*PowerFraction(j,1);
```

```
BBB(i+3,1)=b4/lambda*PowerFraction(j,1);
BBB(i+4,1)=b5/lambda*PowerFraction(j,1);
BBB(i+5,1)=b6/lambda*PowerFraction(j,1);
i=i+6;
j=j+1;
end
BBB(1,2)=n/tau0*CC1;
BBB(2,3)=n/tau0*CC2;
BBB(3,4)=n/tau0*CC3;
BBB(4,5)=n/tau0*CC4;
BBB(5,6)=n/tau0*CC5;
BBB(6,7)=n/tau0*CC6;
CCC=zeros(8,6*n);
i=1;
while i<6*n
CCC(1,i)=l1;
CCC(1,i+1)=l2;
CCC(1,i+2)=l3;
CCC(1,i+3)=l4;
CCC(1,i+4)=l5;
CCC(1,i+5)=l6;
i=i+6;
end
for i=1:6;
CCC(i+1,6*(n-1)+i)=1;
end
CCC(8,(6*n-1))=1;
CCC(8,(6*n-2))=1;
CCC(8,(6*n-3))=1;
CCC(8,(6*n-4))=1;
CCC(8,(6*n-5))=1;
CCC(8,(6*n-6))=1;
DDD=zeros(8,7);
```

Neutronics steady state values

```
UU0=zeros(7,1);
UU0(1,1)=N0;
UU0(2,1)=c10i(n,1);
UU0(3,1)=c20i(n,1);
UU0(4,1)=c30i(n,1);
UU0(5,1)=c40i(n,1);
UU0(6,1)=c50i(n,1);
```

```
UU0(7,1)=c60i(n,1);
PrecInitial=zeros(6,1);
PrecInitial(1,1)=c10i(n,1);
PrecInitial(2,1)=c20i(n,1);
PrecInitial(3,1)=c30i(n,1);
PrecInitial(4,1)=c40i(n,1);
PrecInitial(5,1)=c50i(n,1);
PrecInitial(6,1)=c60i(n,1);
XX0=-(AAA) E(-1)*BBB*UU0;
```

Matrix of coefficients for obtaining delta reactivity and average graphite temperature

```
Mcoeff=zeros(2,3*n);
j=1;
while j<(3*n)
Mcoeff(1,j)=ag/n;
Mcoeff(1,j+1)=as/n;
Mcoeff(2,j)=1/n;
j=j+3;
end
Mcoeff2=zeros(1,3*n);
j=1;
while j<(3*n)
Mcoeff2(1,j+1)=1/n;
j=j+3;
end
```

Matrix of coefficients for obataining the salt outlet temperature

```
MMcoeff=zeros(1,3*n);
MMcoeff(1,3*n)=1;

FinalValue=Tsci+Slope*DecreasingTime; % [s] for overcooling
```

References

[1] Generation IV International Forum, *A Technology Road Map for Generation IV Nuclear Energy Systems*, GIG-002-00, US DOE Nuclear Energy Research Advisory Commettee and The Generation IV International Forum, 2002

[2] GIF2008, *Generation IV International Forum* - 2008 Annual Report

[3] Delpech M., Dulla S., Garzenne C., Kophazi J., Krepel J., Lebrun C., Lecarpentier D., Mattioda F., Ravetto P., Rineiski A., Schikorr M., Szieberth M.; *Benchmark of Dynamic Simulation Tools for Molten Salt Reactors*, In: Proceedings of the International Conference GLOBAL 2003, New Orleans, LA, pp. 2182-2187, 2003

[4] J. Krepel, U. Rohde, U. Grundmann, F.P. Weiss; *DYN3D-MSR spatial dynamics code for molten salt reactors*, Annals of nuclear energy, Vol. 32, pp. 449-462, 2007

[5] E.S. Bettis, W.B. Cottrell, E.R. Mann, J.L. Meem and G.D. Whitman; *The Aircraft Reactor Experiment-Operation*, Nuclear Science and Engineering, Vol. 2, pp. 841-853, 1957

[6] R. C. Robertson, *MSRE Design and operations report - Part I*, Technical Report ORNL-TM-0728, 1965

[7] Idaho National Laboratory, *FY2005 Ten-Year Program Plan*, Appendix 6.0, Generation IV Nuclear Energy Systems, DOE Nuclear Energy Research Initiative MSR Program Plan, 2005

[8] R. B. Briggs, *Molten-salt reactor program - Semiannual progress report*, Technical Report ORNL-3708, 1964

[9] R. H. Guymon, *MSRE Systems and components performance*, Technical Report ORNL-TM-3039, 1973

[10] H.G. MacPherson, *The Molten Salt Reactor Adventure*, Nuclear Science and Engineering, Vol. 90, pp. 374-380, 1985

[11] H. G. MacPherson, *Molten Salt Reactor program quarterly progress report*, Technical Report ORNL-3014, 1960

[12] C.H. Gabbard, *Reactor power measurement and heat transfer performance in the Molten Salt Reactor Experiment*, Technical Report ORNL-TM-3002, 1970

[13] T.W. Kerlin and S.J. Ball, *Experiment dynamic analysis of the Molten Salt Reactor Experiment*, Technical Report ORNL-TM-1647, 1966

[14] MATLAB® , The MathWorks, Inc., 2007

[15] J. R. Engel and P. N. Haubenreich, *Temperatures in the MSRE core during steady - state power operation*, Technical Report ORNL-0378, 1962

[16] Incropera, De Witt, Bergman, Lavine; *Fundamentals of Heat and Mass Transfer*, 6th ed., Wiley & Sons, 2007

[17] Kays and London, *Compact Heat Exchangers* 3rd ed., McGraw-Hill, New York, 1984

[18] C. Guerrieri, *Dynamics of circulating fuel reactors in the zero-dimensional and three-dimensional approach*, Master Thesis, Politecnico di Milano, 2009

[19] S.J. Ball and T.W. Kerlin, *Stability analysis of the Molten Salt Reactor Experiment*, Technical Report ORNL-TM-1070, Appendix A, 1965

[20] Baker and Graves-Morris, *Padé Approximants*, Cambridge University Press, 1996

[21] Quarteroni, Sacco, Saleri; *Numerical mathematics*, Springer, 2000

[22] J.R. Lamarsh, *Introduction to Nuclear Reactor Theory*, Addison-Wesley Publishing Company, 1966

[23] Todreas, N.E., Kazimi, M.S., *Nuclear Systems I - Thermal Hydraulic Fundamentals*, Taylor & Francis, Levittown, 2003

[24] J. Krepel, U. Rohde, U. Grundmann, F. P. Weiss, *Dynamics of Molten Salt Reactors*, Nuclear Technology, Vol. 164, pp. 34-44, 2008

[25] SIMULINK software, The MathWorks, Inc., 2008